(2)

STUDY OF SIGNAL PROCESSING TECHNIQUES FOR AUTOMATED IDENTIFICATION OF 121.5/243 MHz EMERGENCY BEACONS

COMMUNICATIONS RESEARCH LABORATORY

FACULTY OF ENGINEERING

McMASTER UNIVERSITY

HAMILTON, ONTARIO, CANADA

(2)

STUDY OF SIGNAL PROCESSING TECHNIQUES FOR AUTOMATED IDENTIFICATION OF 121.5/243 MHz EMERGENCY BEACONS

by

C.R. Carter (1) and T. Chung

Communications Research Laboratory

McMaster University

Hamilton, Ontario, Canada

L8S 4K1

March 1985

EXECUTIVE SUMMARY

In the SARSAT signal environment, it is possible to receive many (5 to 20) simultaneous emergency beacon signals, combined with voice and interference of various types, all simultaneously occupying essentially the same frequency-time space. The uplink signals from each of these sources results in doppler curves (used for position location computation) which are interlaced, overlapping, and often segmented due to signal falling below the threshold for parts of the satellite pass.

This report examines: 1) the problem of differentiating between doppler data generated by a modulated 121.5/243 MHz beacon and other signal sources in the band; 2) the signal characterization of ELT signals; and 3) the use of these results to provide data management techniques to reduce position location data proliferation arising from the same ELT being seen on multiple orbits and by different satellites.

The report first provides a survey of the different sources of interference which occur in the 100 to 500 MHz frequency band. It is seen that the interference can be divided into two categories, namely; that due to natural sources (such as atmospheric noise and galactic noise) and man-made noise (such as autombile ignition noise and CB radio interference). It is shown that when it is present, man-made noise dominates and can take on a wide range of different characteristics.

Next, the report examines those sources of interference which enter the 121.5/243 MHz frequency bands of the SARSAT system. It is seen that these sources may be either impulsive or in-band. One simple method of classifying the interference is to separate on the basis of bandwidth, i.e. CW, narrowband and wideband. It is seen that these designators can be useful in identifying the interference which is in fact received in the SARSAT system. Thus, it is possible to provide identifiers which in turn lead to a measure called activity of the pass. The activity of the pass gives a measure of the amount of interference level which is encountered on any particular pass.

The spectral properties of ELT signals are examined in detail. It is shown that the typical ELT signal can be related to one of two different models which accurately predict ELT signal spectrum. Thus, it is possible to identify properties of the ELT signal which can be measured and related to a specific ELT signal. Of course, the usefulness of the measurement is dependent on the quality of the signal being measured.

Finally, these properties of interference and ELT signal characteristics are combined to form a signal identifier which can be used to classify any received signal. This classification can then be used to provide a label which is used on all the different received signals. Signals having the same characteristics fall into the same bin which then provides a significant reduction in data to be handled.

TABLE OF CONTENTS

TABLE OF CONTENTS (continued)

TABLE OF CONTENTS (continued)

1. INTRODUCTION

Existing emergency beacons operating at 121.5 MHz have a distinctive siren-like AM modulation characteristic. Apart from normal production variations in the characteristic of this modulation which is allowed in the specifications, there is no other information incorporated in the signal to differentiate one emergency beacon signal from another.

In the SARSAT signal environment, it is possible to receive many (5 to 25) simultaneous emergency beacon signals, combined with voice signals and interference of various types, all simultaneously occupying essentially the same frequency-time space. The uplink signals from each of these sources results in doppler curves (used for position location computation) which are interlaced, overlapping, and often segmented due to signal falling below the threshold for parts of the satellite pass.

Although the current signal processing software in the SARSAT LUT can cope with this signal situation reasonably well, the present processing algorithm is based solely on comparing the available data against theoretical doppler data which would occur from any position in the LUT coverage area.

Occasions arise when the LUT computes locations using segmented data available from several different signal sources, but still representing an available doppler curve. The location thus computed does not represent the location of any real signal source, and is considered to be a LUT-generated false alarm.

1.1 OBJECTIVES

A study program in the area of ELT signal identification is necessary to determine the feasibility of originating signal processing approaches to perform the following functions:

1) Differentiate between doppler data generated by a modulated 121.5/243 MHz beacon and other signal sources in the band (i.e. CW, voice signals, etc.).

2) Perform signal characterization on each signal to enable differentiation among ELT signals, and thus associate each available doppler data segment with the correct signal source.

3) On the basis of being able to differentiate and distinguish among emergency signals based on signal processing parameters or characteristics, originate data management techniques to reduce position location data proliferation arising from the same ELT being "seen" on multiple orbits and by up to four different satellites.

1.2 OVERVIEW OF REPORT

Section 2 provides a survey of interfering sources in the frequency band from 100 to 500 MHz. These sources include: natural sources such as atmospheric noise, galactic noise, solar flare interference and the like; and man-made interference such as automobile ignition noise, power generating facility interference, scientific and industrial equipment noise, CB radio interference, and so on. Section 3 deals specifically with the effects of interference on the SARSAT system and examines the problems which may occur and how this interference may affect the processing of ELT signals. In addition, examples of interference received by the SARSAT system are examined and a set of parameters is identified which characterize the interference. Section 4 considers the different types of ELT signals which are received and provides models which accurate describe ELT signal. From this, it is possible to select a set of parameters which characterize ELT signals. Section 5 describes how the parameters characterizing interference and ELT signals can be used to develop data management techniques for categorizing received ELT signal emissions. Finally Section 6 provides Conclusions, followed by References.

2. SURVEY OF INTERFERING SOURCES AT

2.1 OVERVIEW

A computer literature search of interfering sources in the frequency band from 100 to 500 MHz has resulted in the listing of approximately 1100 titles of which approximately 100 papers and one textbook have been obtained. These have all been reviewed and a summary of the relevant findings is now presented. In the frequency band from 100 to 500 MHz, there are many different types of background noise and interference. These can be divided into: natural sources such as atmospheric noise, galactic noise, solar flare interference and the like; and man-made interference such as automobile ignition noise, power generating facility interference, scientific and industrial equipment noise, CB radio and amateur radio interference and so on [1-3]. When it is present, man-made interference is often dominant such as in the case of the urban environment where we see that the background is several dB higher than the next highest source, as illustrated in Fig. 2.1 [1, p. 14].

Natural sources of interference may have either a relatively smooth spectrum such as galactic noise or may be impulsive such as atmospheric noise and solar flares. The galactic noise is relatively constant in time whereas the impulsive noise occurs relatively infrequently such as during lightning storms.

Man-made noise can take many different forms such as smooth spectrum due to a large number of automobile ignitions, impulsive noise due to power switching circuits or harmonic interference due to unfiltered power generators or radio transmitters. Some of these sources will now be examined in detail to determine their possible influence on signals in the 100 to 500 MHz frequency band.

2.2 INTERFERENCE AT 121.5/243 MHz

Airborne surveys of interference at 121.5, 243 and 406 MHz were made in 1977 by flying surveillance aircraft over selected regions of the United States [4-7] using receiver

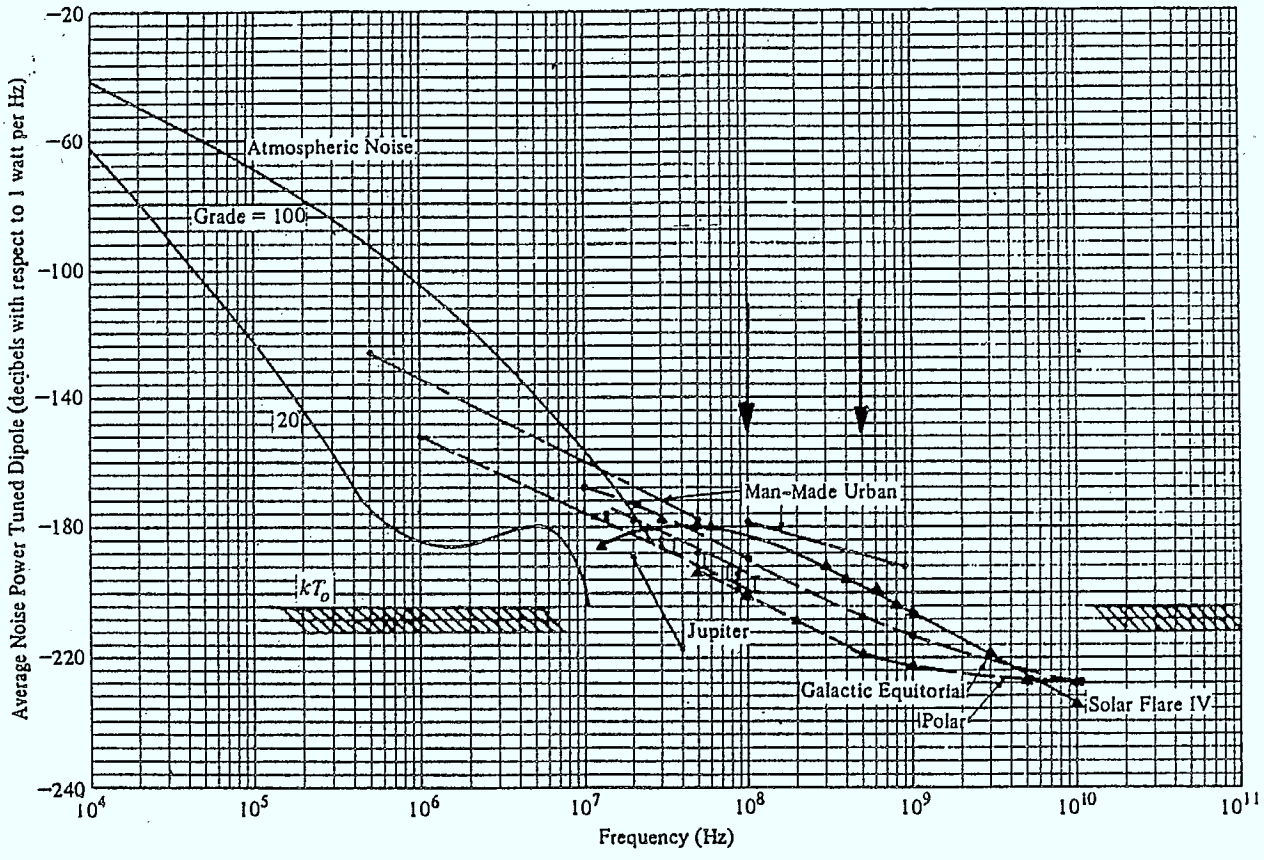

Fig. 2.1 Average power density of natural and man-made radio noise sources observed with a tuned dipole antenna. Note that for the band from 100 to 500 MHz, man-made urban interference exceeds Solar Flare IV noise by 4 to 10 dB and Galactic noise by some 10 to 20 dB. Receiver noise at -204 dBW/Hz provides the lower bound at kT_o.

bandwidths of ± 25 KHz for the 121.5/243 MHz frequencies and ± 50 KHz for the 406 MHz frequency. These measurements were intended to give information as to the degree of background over urban and suburban areas which would be received by search and rescue satellites.

Figures 2.2 and 2.3 illustrate the variation which takes place in interference level when overflying cities of several different populations [5-6]. As expected, the amount of interference increases significantly with the population of cities and the time of day (night) as shown in Fig. 2.3. Regretably, no estimate was attempted to determine the relationship based on number density (number of people per unit area) versus interference level.

Figure 2.4 shows the radiation in the 243 MHz band for essentially the same area as Fig. 2.3. We can thus conclude the following:

1) At 121.5 MHz, the interference varies strongly with population density.

2) At 121.5 MHz, the interference level varies approximately 5 to 10 dB depending on the time of day.

3) At 243 MHz, the interference varies strongly with population density.

4) At 243 MHz, the interference varies with time of day but not as strongly as for the 121.5 MHz band.

5) No clear relation exists between the levels of interference at 121.5 MHz and 243 MHz.

Since these results were conducted in 1977, it is possible that the impact of more recent developments such as the CB craze are not reflected by the measurements.

A more recent set of measurements has shown that the contribution to antenna noise temperature near geostationary orbit using LES-5 and LES-6 data is less than 22°K in the 243 to 260 MHz frequency band [8]. However, since square law relationships exist for range, this translates to antenna temperature of 30,000°–40,000°K at SARSAT satellite altitudes.

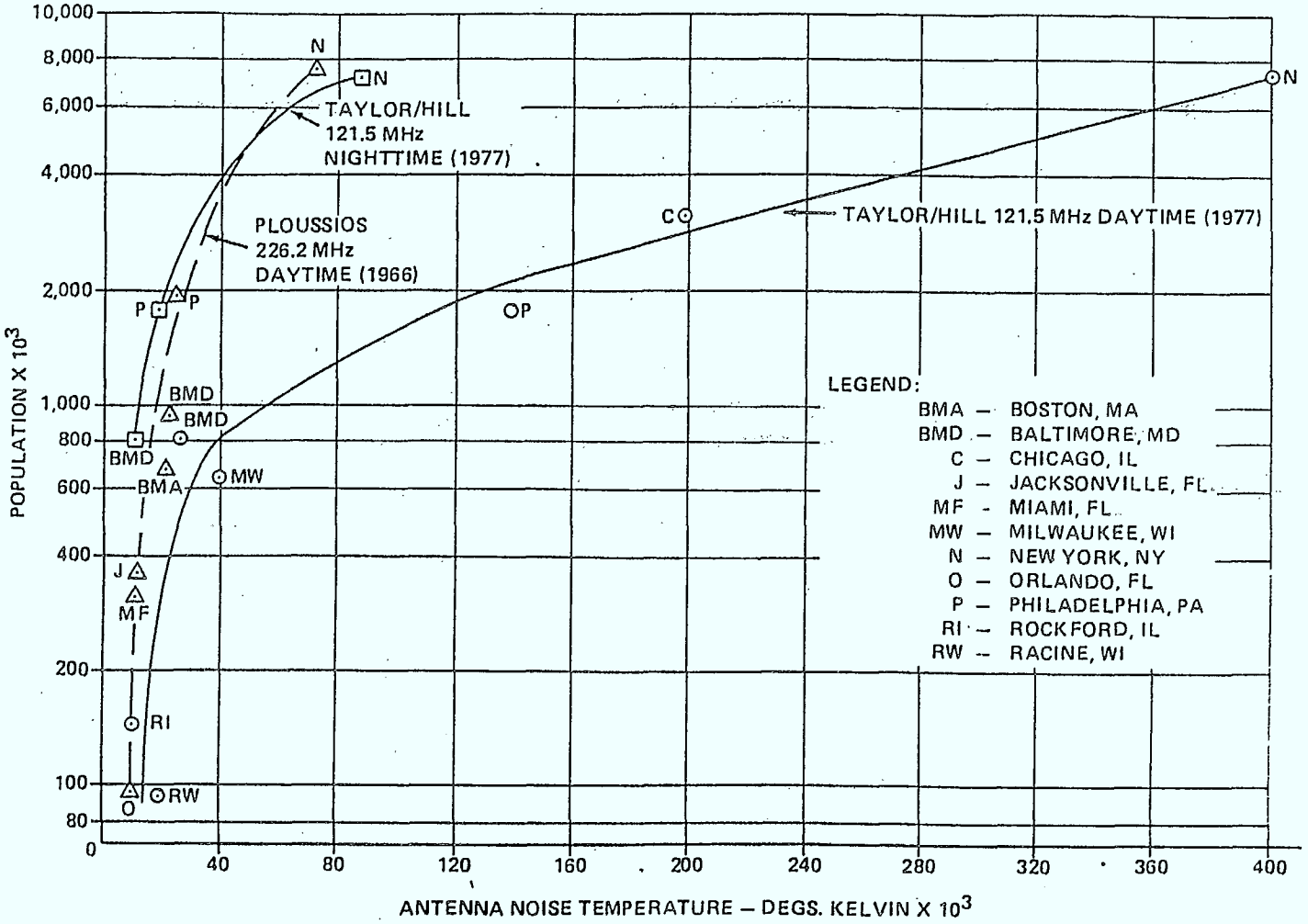

(a)

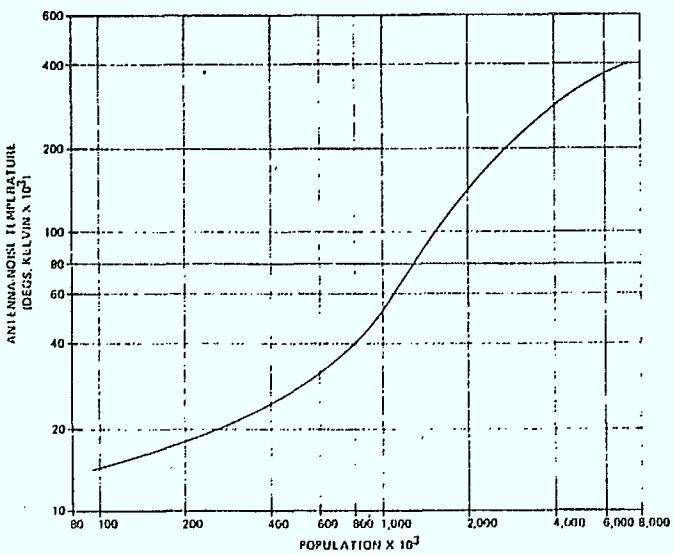

(b)

Fig. 2.2 (a) Relation between antenna noise temperature and population.
(b) Population magnitude versus 121.5 MHz antenna noise temperature (daytime).

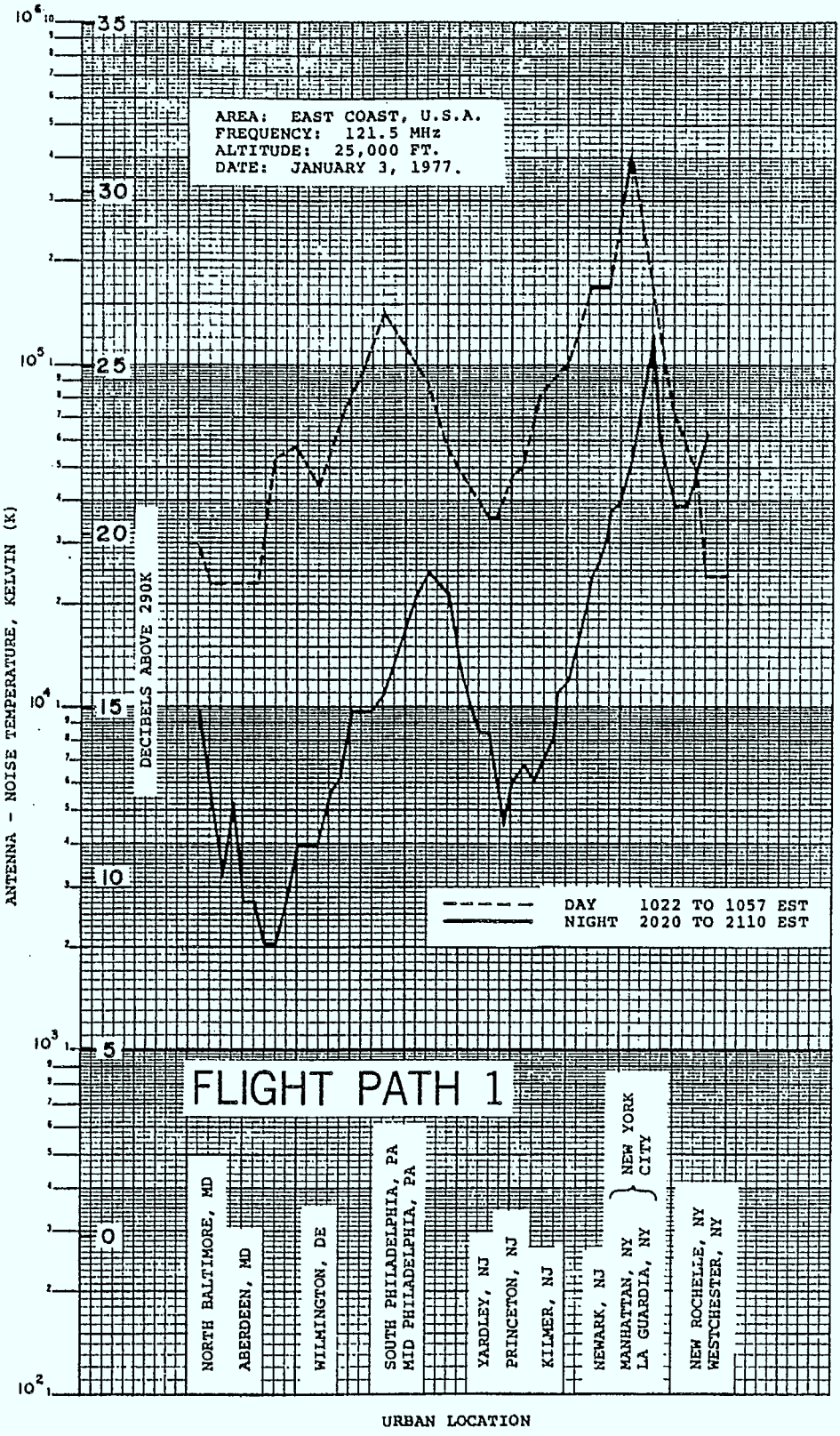

Fig. 2.3 Antenna noise temperature at 121.5 MHz for a flight path over eastern cities of the U. S. A. during the daytime and the nighttime.

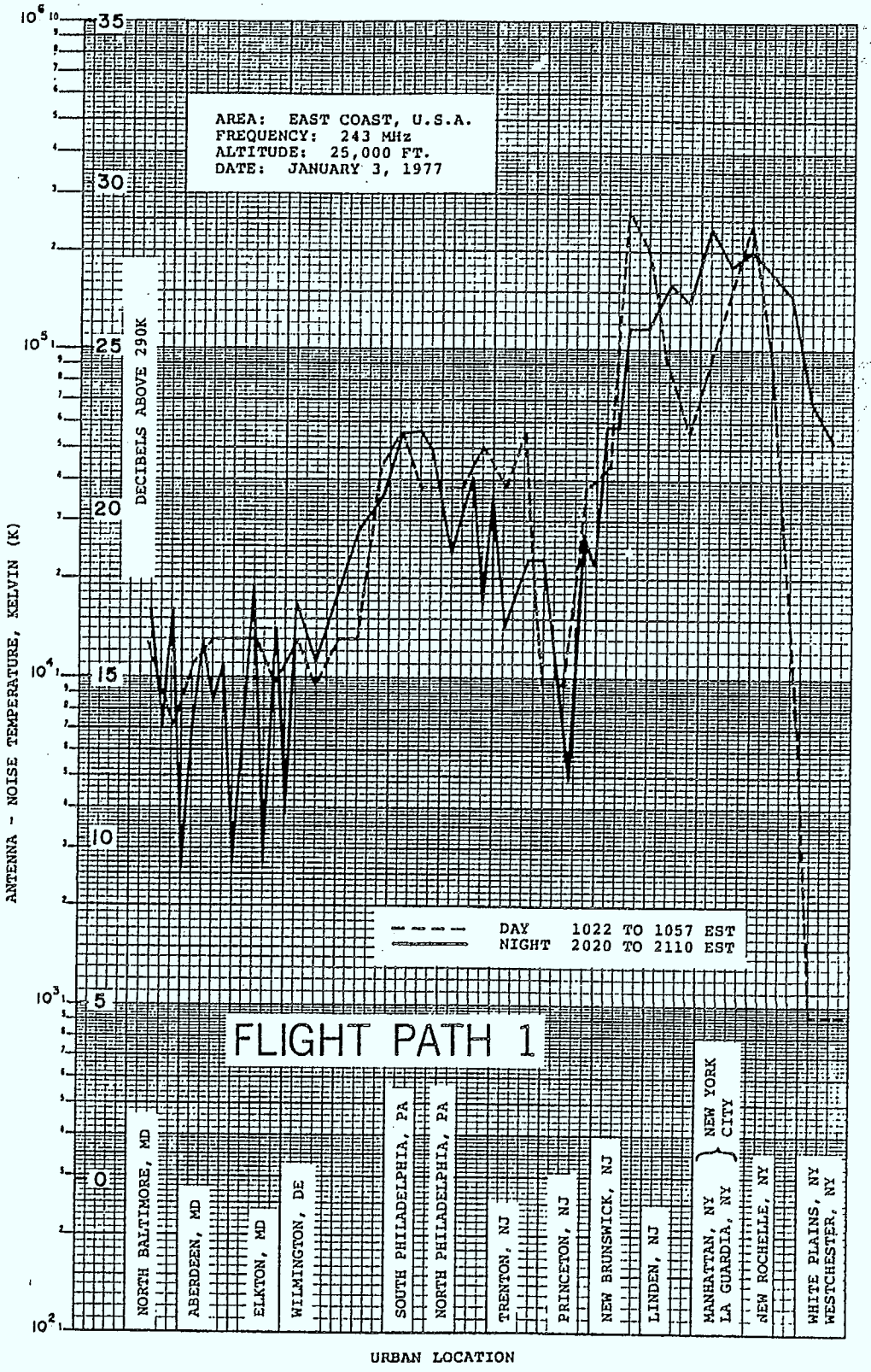

Fig. 2.4 Antenna noise temperature at 243 MHz for a flight path over eastern cities in the U. S. A. during the daytime and the nighttime.

2.3 CB, RADIO AND TELEVISION INTERFERENCE

In the mid-1970's, there was a huge increase in the number of CB radio systems that went into operation and a corresponding increase in the number of interference complaints received [9-11]. The main source of interference was due to the jamming of TV signals at the harmonically related frequencies of 27 MHz although there are other problems such as the jamming of ambulance radio by 6th harmonic at short range [12].

Two problems were found to arise, the first being due to the inadequate filtering at the input to the TV itself, and the second problem being due to the lack of filtering at the output of the CB unit. It was further discovered that the majority of cases belonged to this latter case.

Two different causes for the interference are [9]: the use of high power (24 to 400 W) linear amplifiers which are in fact somewhat non-linear producing harmonics and possibly sub-harmonics; and the use of high gain (4 to 8 dB) antennas which concentrate the nominal 4 W output power of the typical CB unit producing a high effective isotropic radiated power (EIRP). The problem of the high power linear amplifier is further compounded by relatively low cost ($325.00 for an increase from 4W input power up to 85W output power [13]). The combinations of linear power amplifier and high gain antenna also exist and it is estimated that the EIRP can reach 700W.

Of considerable concern is the fact that the 121.5 MHz ELT band is the 9th harmonic of the 2nd subharmonic of 27 MHz and 243 is the 9th harmonic of 27 MHz. It thus appears quite likely that at least some of the interference received by the satellites is due to these harmonics especially from faulty CB rigs with perhaps high power linear amplifiers.

Other possible sources of interference may be due to harmonics of radio and TV transmitters. The list includes [14]:

121.5 MHz – 2nd harmonic of TV channel 3

– 3rd harmonic of fixed and mobile radio

– 5th harmonic of fixed and land mobile radio

– 7th harmonic of maritime mobile radio

– 9th harmonic of fixed mobile radio

– odd order harmonics of amateur radio bands

243 MHz – 2nd harmonic of 121.5 MHz voice channel

– 3rd harmonic of TV channel 5

– 5th harmonic of fixed and mobile radio

– 7th harmonic of fixed and mobile radio

406 MHz – 3rd harmonic of aeronautical mobile radio

– 5th harmonic of TV channel 5

– 7th harmonic of TV channel 2

– 9th harmonic of fixed mobile radio

– 15th harmonic of 27 MHz CB radio

An upcoming and related problem is the development of low power TV which operates with a power level of 10 W for channels 2 to 13 [15]. By late 1982, over 6500 applications had been received.

Another potential problem exists with cable TV since the frequency band covered runs from 5 to 450 MHz. The problems due to leakage from the cable appear to have been recognized in 1977 [16] but regretably no action appears to have been taken as late as March 1984 [17].

2.4 MOTOR VEHICLE IGNITIONS

Impulsive noise from automobiles is generated by the ignition system, the battery charging circuitry, accessory motors, electric warning devices, and starter motors [1, pp. 21-74, and 18-22]. The frequency band of these emissions extends entirely across the band from

100 to 500 MHz (up to a reported 7 GHz [18]) and the spectrum for a large number of vehicles (perhaps hundreds of thousands in a city, for instance) is essentially smooth, not unlike additive white Gaussian noise passing through a simple RC lowpass filter. Almost all vehicles radiate at 50 MHz and 75% are found to be noisy at 150 MHz [18].

2.5 POWER TRANSMISSION LINES AND CONVERTERS

2.5.1 High Voltage AC

There are several different possible sources of interference which can arise from an ac power system, all well documented in [1, pp. 75-134]. These include harmonics of the 60 Hz power frequency, corona (due to the electric field ionizing the surrounding air) and gap breakdown (due to voltage difference between two points and accentuated by the alternating feature of the 60 Hz). Normally, harmonics of the 60 Hz are too small to be a problem in the 100 to 500 MHz frequency range; however, corona and gap breakdown may be detectable.

Measurements on 244, 345, 525 and 735 kV transmissions lines have shown that the corona has a 1/f frequency characteristic extending into the hundreds of megahertz frequency range which depends strongly on weather conditions.

Gap breakdown may produce nanosecond duration pulse widths with frequency components extending into the hundreds of megahertz. Measurements show that in some cases the gap breakdown interference may exceed that due to corona, as shown in Fig. 2.5.

2.5.2 High Voltage DC

Radio interference due to high voltage DC is not so well documented. However, it can be generated from several different mechanisms including corona, station noise, single unit flashover and HVDC converter stations [23-25]. The noise due to corona is well documented and is essentially the same as for HVAC. The corona is again strongly dependent on weather conditions and operating voltage (an increase from 450 kV to 500 kV increases interference by 5 dB [24]) and can be approximated by a $1/f^n$, where $1 < n < 2$, spectral characteristic. For

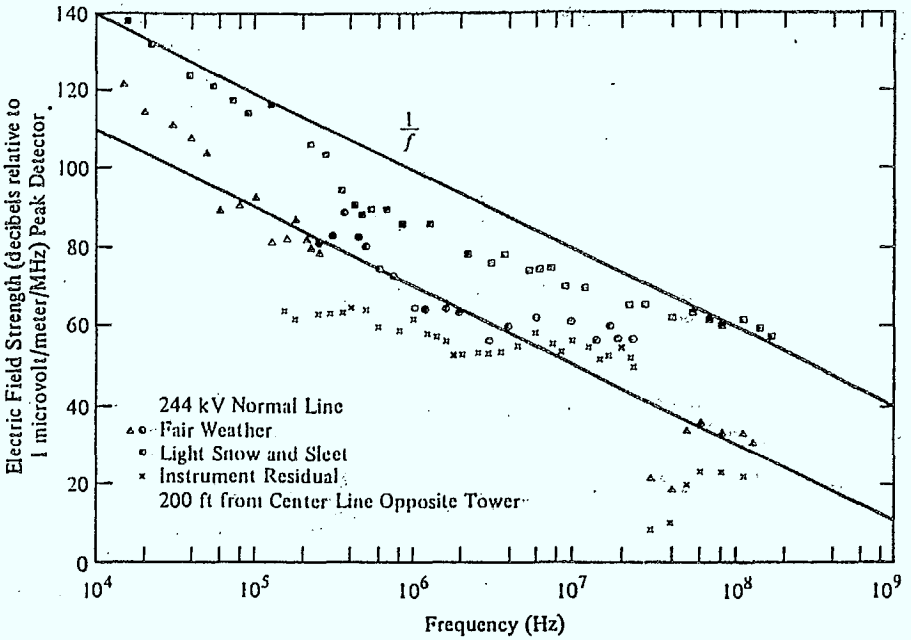

(a)

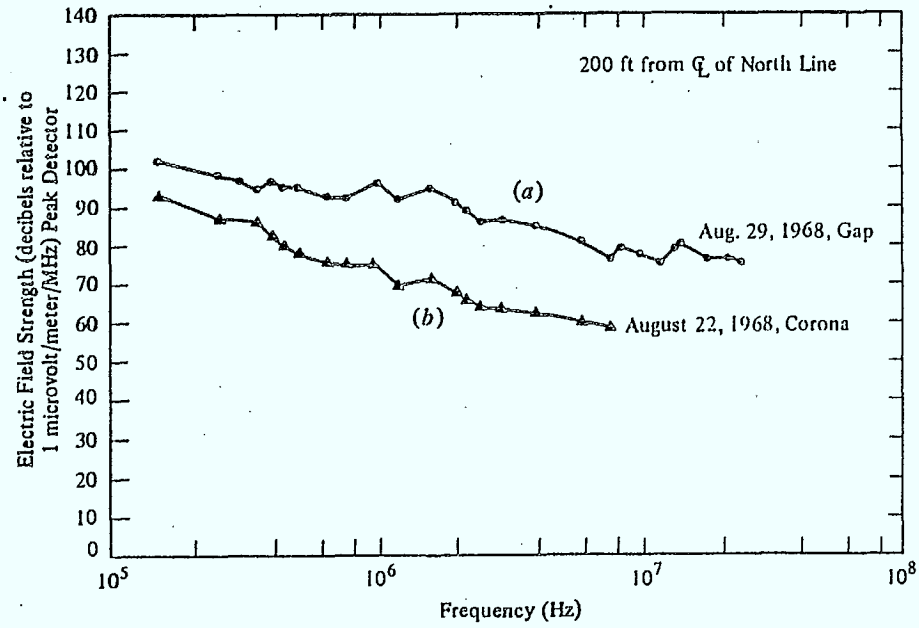

(b)

Fig. 2.5 (a) Peak electric noise field strength for a 244 kV ac transmission line with noise due to corona. Measuring location 200 ft. laterally from the tower [1, p. 104].
(b) Comparison of two radio noise sources [1, p.109].

one particular case on the Nelson River HVDC line, it was found that the data agreed well with this relation [23].

The problems of station generated noise for this system were also investigated at reduced voltage to eliminate corona but it was found that the levels were too low to be accurately detected [25].

Single unit flashover occurs on insulators often due to moisture and other contaminants [26]. Unlike corona noise, the flashover noise is impulsive and has a spectrum that can be detected at 100 MHz using a TVI meter. The repetition rate is low and may vary from one discharge per ms to one discharge in 100 ms. However, the signal is strong enough to be noticeable on a TV screen competing with a TV broadcast signal.

Finally, radio interference can be generated by HVDC converter stations using thyristors to convert the dc into ac [27]. However, the power density appears to drop quickly with frequency and most of the power is confined to the frequency range below 1 MHz.

2.6 ATMOSPHERE AND IONOSPHERE

2.6.1 Atmospheric

One of the main sources of natural noise in the environment is due to lightning flashes [28-31]. The electromagnetic radiation radiated by lightning flashes cover the frequency range from visible light down to a few Hz [29]. It has been determined that for frequencies above 10 KHz, the spectrum varies as 1/f [28] into the hundreds of MHz while at UHF, the spectrum is flat with density of approximately 10^{-15} W/m^2–Hz at a distance of 1 km from the base of the channel [29]. This corresponds to a level of about 50 dB above thermal noise for an antenna of 1 m^2.

Actual measurements have detected this noise at 100 MHz and it has been noted that in the tropics several thunderstorms are normally active within an 1000 km radius [30]. The total number of flashes ranges from 50 to 100 per minute with each flash comprising a 'bunch of submicrosecond pulses' having a total duration in the millisecond range. Naturally, at the

higher latitudes this activity is much less; but, with the wide coverage area of the satellite antenna, there is bound to be some atmospheric disturbance received.

2.6.2 Ionospheric

Ionospheric scintillation can pose a problem for signals at the SARSAT frequencies due to variation in the propagation velocity of the uplink signal and scintillation fades [32-33]. Measurements have shown that a signal propagating through the ionosphere from the Navy Navigation Satellite System may vary by ± 10 dB at 150 MHz and ± 5 dB at 400 MHz for a considerable fraction of the time [32]. As well, the problem of ionospheric scintillation is worst in the north of the auroral zone and near the geomagnetic equator. Fortunately, since signal level is not the parameter being measured by the SARSAT system, these problems of amplitude change are not significant provided that the signal is strong enough to be properly received.

The change in the propagation delay of the uplinked signal for the SARSAT frequencies has been studied and found to produce an error of only approximately several Hz at 121.5 MHz [34].

2.7 MISCELLANEOUS SOURCES

2.7.1 Printed Circuit Boards (PCB) and Computers

Due to the clocking and timing pulses in computers and printed circuit boards in general, there is a significant amount of interference being generated in the frequency band between 10 MHz and 1 GHz [35-37]. Unfortunately, this source of radiation may leak from the cabinets containing the equipment and propagate in all directions. Since clock signals are rich in harmonics, it is quite possible for the third harmonic of a 40.5 MHz oscillator to be significant at 121.5 MHz and similarily the third harmonic of an 81 MHz oscillator to interfere at 243 MHz. Whether this is, in fact, a problem is not clear at this time, however.

2.7.2 Industrial Heating Equipment

A popular operating frequency for dielectric heating applications is 27.12 MHz with a tolerance of ± 0.6% [38]. Unfortunately, the equipment also generates harmonics and quite possibly subharmonics with the result being that the 9th harmonic of the second subharmonic may jam the 121.5 MHz band and the 9th harmonic may jam the 243 MHz band. Again, there seems to be little additional data as to the seriousness of this problem.

2.8 CONCLUDING REMARKS

Except in unusual storm conditions, such as those producing large numbers of lightning flashes, the main sources of interference affecting the SARSAT system will be man-made and in many cases, originate in urban centres. There is a wide array of impulsive noise sources which may coalesce to produce an overall background not unlike Gaussian noise for narrow band systems such as SARSAT, a certain number of unmodulated carrier sources due to harmonic generation and the like, which fall in the SARSAT bands, and modulated carrier sources which are produced by harmonics and subharmonics of CB and other radio sources.

3.0 NOISE AND INTERFERENCE IN THE 121.5/243 MHz FREQUENCY BANDS

3.1 OVERVIEW

In this section, we examine the problem of noise and interference which relate specifically to the 121.5 MHz and 243 MHz SARSAT frequency bands. We note that the 121.5 MHz band is 25 kHz in bandwidth and the 243 MHz band has a 50 kHz bandwidth. The ratio of bandwidth to centre frequency in both cases is 0.02%, indicating that both receivers can be classed as narrowband.

First, we examine the types of interference which can affect the reception of ELT signals. Then, the interfering sources are categorized into CW, narrowband, and wideband. It is shown how the interference can adversely affect SARSAT receiver operation. Some typical examples of interference recorded from pass data are examined and, finally, the activity of the pass is examined. This whole procedure leads to an interference classifier which can be used to evaluate interfering sources and activity of the pass.

3.2 TYPES OF INTERFERENCE

Interference may be thought of as unwanted emanations which compete with desired ELT signals in the frequency bands of interest. Normally, interference is only significant if the strength is sufficiently high to cause a noticeable degradation in the detection of the desired signal. Thus, it is possible to define a threshold level which separates harmful interference from insignificant interference. Specification of this threshold depends on the type of interference encountered.

There are two fundamentally different kinds of interference which affect receivers of the COSPAS-SARSAT type of system. These are impulsive interference and in-band interference.

3.2.1 Impulsive Interference

Impulsive interference is normally thought as being due to:

1) a small number of high power, short duration video pulses or a small number of high power, short duration pulses of carrier which shock excite the receiver;

2) a high power carrier which rapidly sweeps in and out of the receiver passband, again shock exciting the receiver; and

3) a large number (or mix) of low power video pulses, low power pulses of carrier and low power swept carrier sources which add together to form a broadband spectrum of interference.

The first two of these are referred to as Case 1 and Case 2 and described in detail. The third source of interference is considered to be broadband interference and discussed in Section 3.5.

Case 1

The first of these is due to short duration pulses where the pulse duration is small compared to the reciprocal of the bandwidth of the receiver. In this case, the pulse may be either video or modulated carrier. For modulated carrier pulses, the carrier frequency may be inside or outside the bandwidth of the receiver. Essentially, impulsive interference shock excites the 'ringing response' of the receiver every time a pulse reaches the receiver input. The output of the receiver due to such an input pulse can be simplistically represented by [39]

$$r(t) = A \exp[-at] \sin 2\Pi f_R t \qquad (3.1)$$

where

A = amplitude constant

a = damping constant which is a function of the bandwidth and the phase linearity of the receiver.

f_R = centre frequency of the receiver passband (for narrow band systems)

t = time

Normally, this type of interference fills the bandwidth of the receiver and thus appears to be 'wideband interference'. Since 'a' is usually a complicated combination of the overall bandwidth and all phase characteristics of the system, its value is seldom known. However, it can be expected to lie in the range

$$B/20 < a < B/5 \tag{3.2}$$

where B is the 3 dB bandwidth of the receiver.

An estimate of the jamming effectiveness of this impulsive interference can be obtained by noting that the receiver remains jammed whenever the RMS value of r (t) exceeds the RMS value of the desired signal and receiver noise at the output of the receiver. For an array of impulses with random amplitudes, there is an average duration T_I in seconds for which the receiver remains jammed. Since the impulses are normally generated at random times, we define the average number of impulses per second to be N_I. Then, the fraction of the time that the receiver remains jammed is simply

$$J = 1 - N_I T_I \tag{3.3}$$

We note that when $J \leq 0$, the receiver is completely jammed and no signals can be detected. Thus, a threshold can be arbitrarily set, say $J = 0.1$, which indicates that 90% of the time desired ELT signals can be detected.

Case 2

Impulsive interference can also be generated by sweeping a carrier from outside the passband of the receiver through the passband and back outside the passband. This type of interference causes two difficulties. First, there is the interference generated while in the passband. The effects of this are discussed in Section 3.2.2. Second, there is the interference produced in sweeping from in-band to out-of-band or vice versa. If the sweep rate is sufficiently high, the receiver 'ringing response' is excited and the receiver is jammed as in Case 1.

3.2.2 In-band Interference

In-band interference consists of modulated and unmodulated carriers which do not change frequency rapidly. Here, the signals compete in amplitude and bandwidth with the desired signals. Examples of this include CW carrier, harmonics of transmitters, and voice transmissions. In this case, the threshold can be defined on a power density basis with the signal competing directly with the interference. The main factor is the number of false alarms which can be allowed (number of erroneous peaks in the power spectrum for a given threshold setting) and this can be defined by the false alarm rate for a given probability of detection as in radar.

All such sources in the COSPAS-SARSAT system are classed as narrowband since the system bandwidth is very small compared to the carrier frequency i.e., $B << f_R$.

However, within the band we may denote different bandwidths of interference. For instance, unmodulated carrier produces a near line spectrum interference. Voice produces a 5 to 10 KHz bandwidth interference and other sources essentially fill the entire 25 KHz bandwidth. Thus, for the present we will use these classifications:

CW – interference produced by an unmodulated carrier

NB – narrowband such as that produced by voice (5 to 10 KHz)

WB – wideband which fills most of the 25 KHz bandwidth.

3.3 CW INTERFERENCE

CW or unmodulated carrier interference presents three problems to the SARSAT type of system. First, it produces clutter that appears on the frequency plot which increases the complexity of the signal processing strategy. Second, is the problem of reduced dynamic range and thresholding when automatic gain control or limiting is employed. Third, is the problem of FFT dynamic range when a strong CW signal appears with weaker signals and background noise.

Normally, the effect of increased clutter on the frequency plot is not severe since the signal occupies a very narrow band of frequencies. However, the other two problems are far more serious and are examined in detail next.

3.3.1 Automatic Gain Control and Limiting

Automatic gain control and limiting produce essentially the same effect on the signal however the implementations are slightly different. Thus, only the case of AGC will be considered.

Usually, automatic gain control is applied to the analog amplifier stages of the receiver in the form of amplitude control of the time signal. The gain of any AGC amplifier can be written as

$$G = \frac{P_o}{P_I} \tag{3.4}$$

where

P_o = the total output power

P_I = the total input power from N sources

$$= \sum_{j=1}^{N} P_{Ij}$$

Now, if we assume that the output power is constant, which is typical of most AGC systems, then the gain of the amplifier varies inversely as the input power.

Let us assume that one source, namely the ith source of interference, is far stronger than the other sources of signal and background noise, then the gain of the AGC amplifier is given approximately by

$$G = \frac{P_o}{P_{Ii}} \tag{3.5}$$

where P_{Ii} = input power from the ith source.

Then, for the kth signal, which may be an ELT, the signal out of the AGC amplifier is simply given by

$$P_{ok} = G * P_{Ik}$$

$$= \frac{P_o * P_{Ik}}{P_{Ii}} \tag{3.6}$$

Both P_o and P_{Ii} are constant. Therefore, as the power of the ith interfering source increases, the output power of the kth source decreases.

In practice, what this means is that when a strong CW source is received, it 'captures' the AGC or limiter, an effect well known radar receiver systems. Weaker sources and background noise are greatly reduced in level and the output of the receiver is said to be 'quietened'. Naturally, this is highly undesirable since the unwanted high amplitude CW signal is easily received while the desired weaker signals disappear altogether.

A possible method of combatting this type of interference is to use a log-lin type of rf amplifier which has the characteristic gain shown in Fig. 3.1. Normally, the noise background has sufficient level to cause the amplifier to operate at point A, which is just above the logarithmic knee. When strong CW interference causes the output of the AGC amplifier to quieten, the operating point runs down the log amplifier curve which greatly reduces the change in dynamic range. Thus, the background noise and weaker signals are reduced by the logarithm of the strong signal which substantially improves the detection properties of the weak signals.

3.3.2 FFT Dynamic Range

A second problem due to thresholding can arise with the calculation of the FFT, as illustrated in Figures 3.2, 3.3, 3.4 and 3.5 for one second intervals of 13 block averaged 8 K FFT spectral estimates. Here we see that the signal spectrum for orbit C1/860 has been plotted at 9, 10, 11 and 12 minutes into the pass, respectively. At 9 minutes, the spectrum appears reasonably normal with a flat background and several prominent signal peaks. At 10

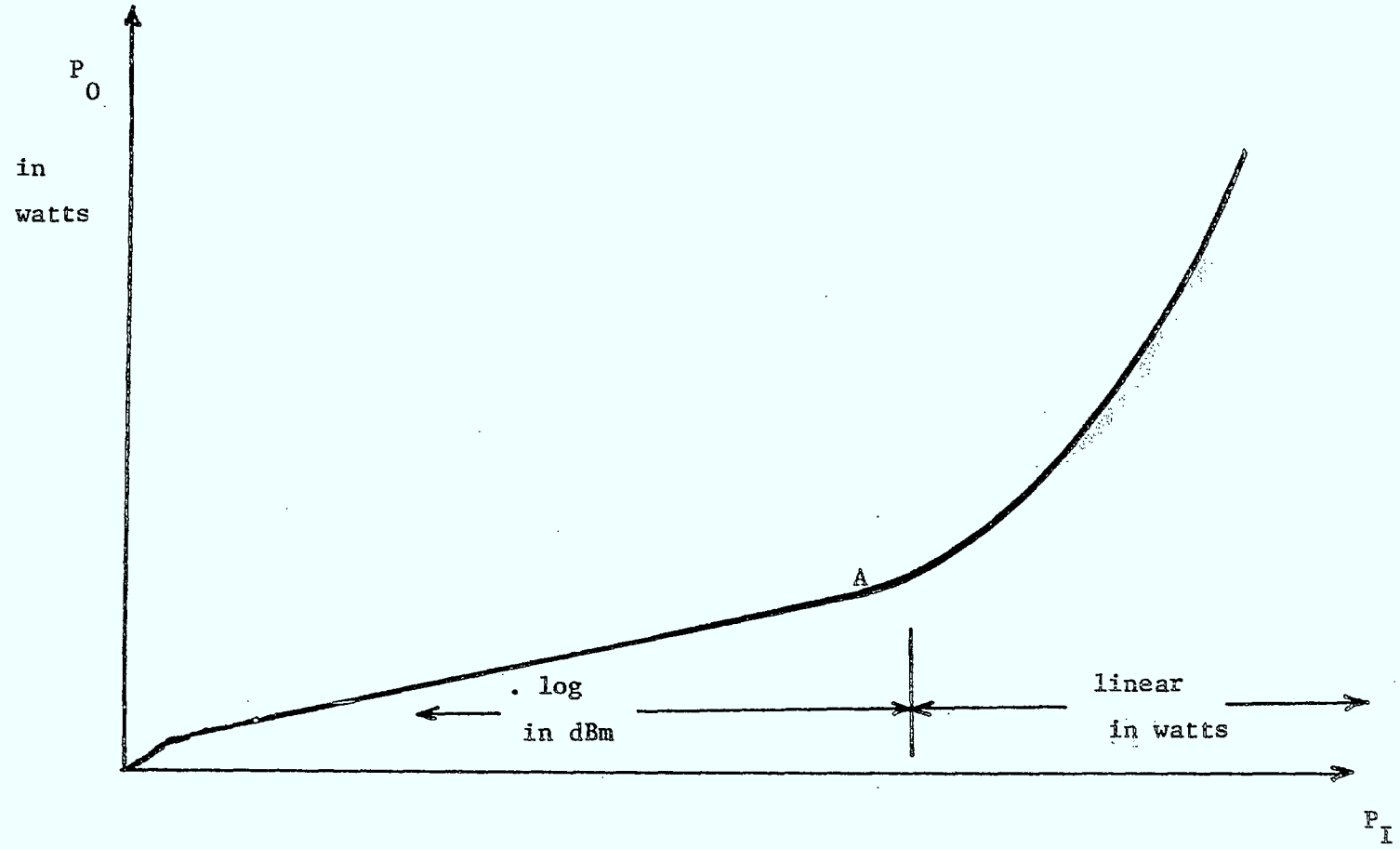

Fig. 3.1 Input-output relationship for a log-lin amplifier.

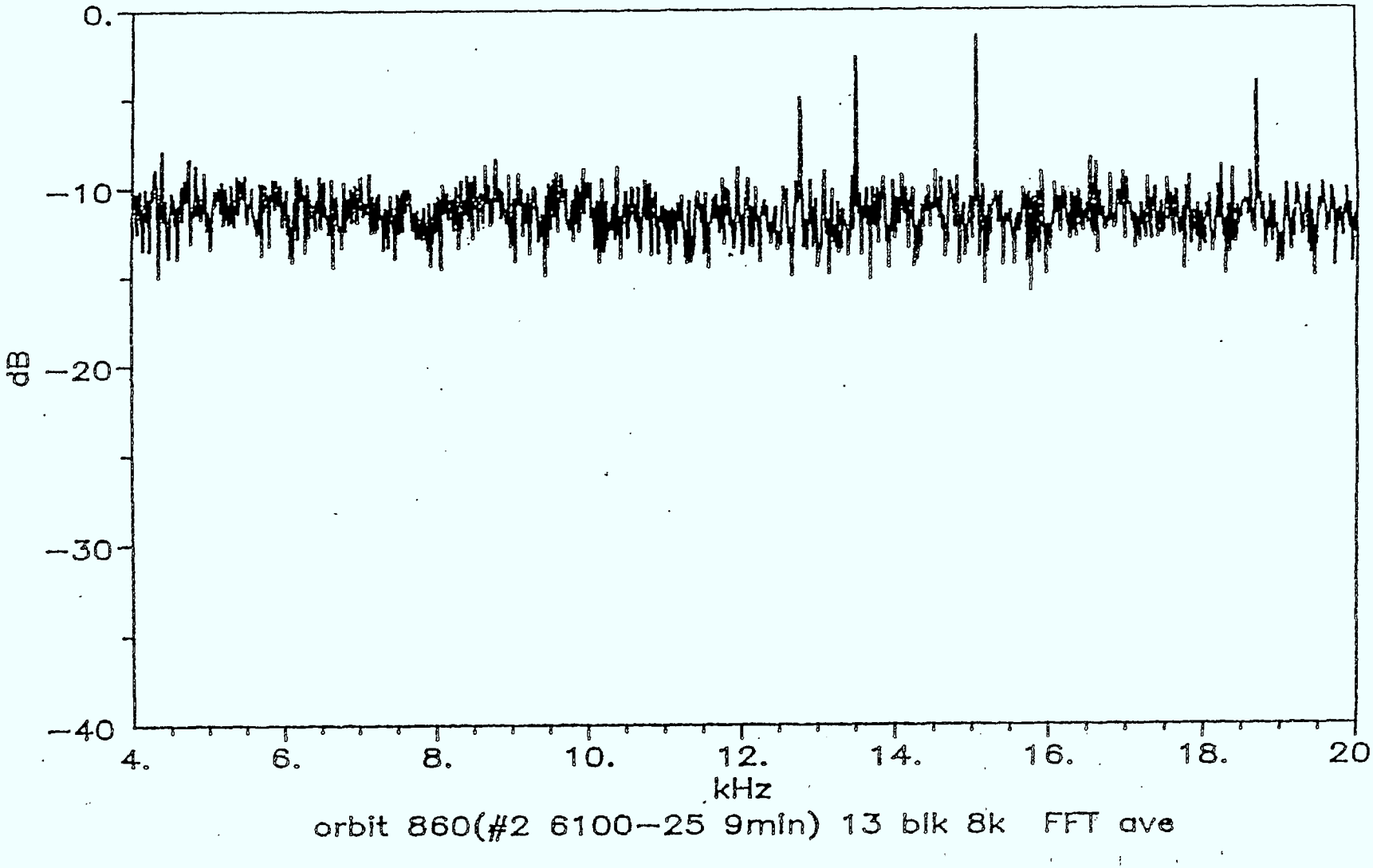

Fig. 3.2 Spectral plot for SARSAT signal with no interfering sources.

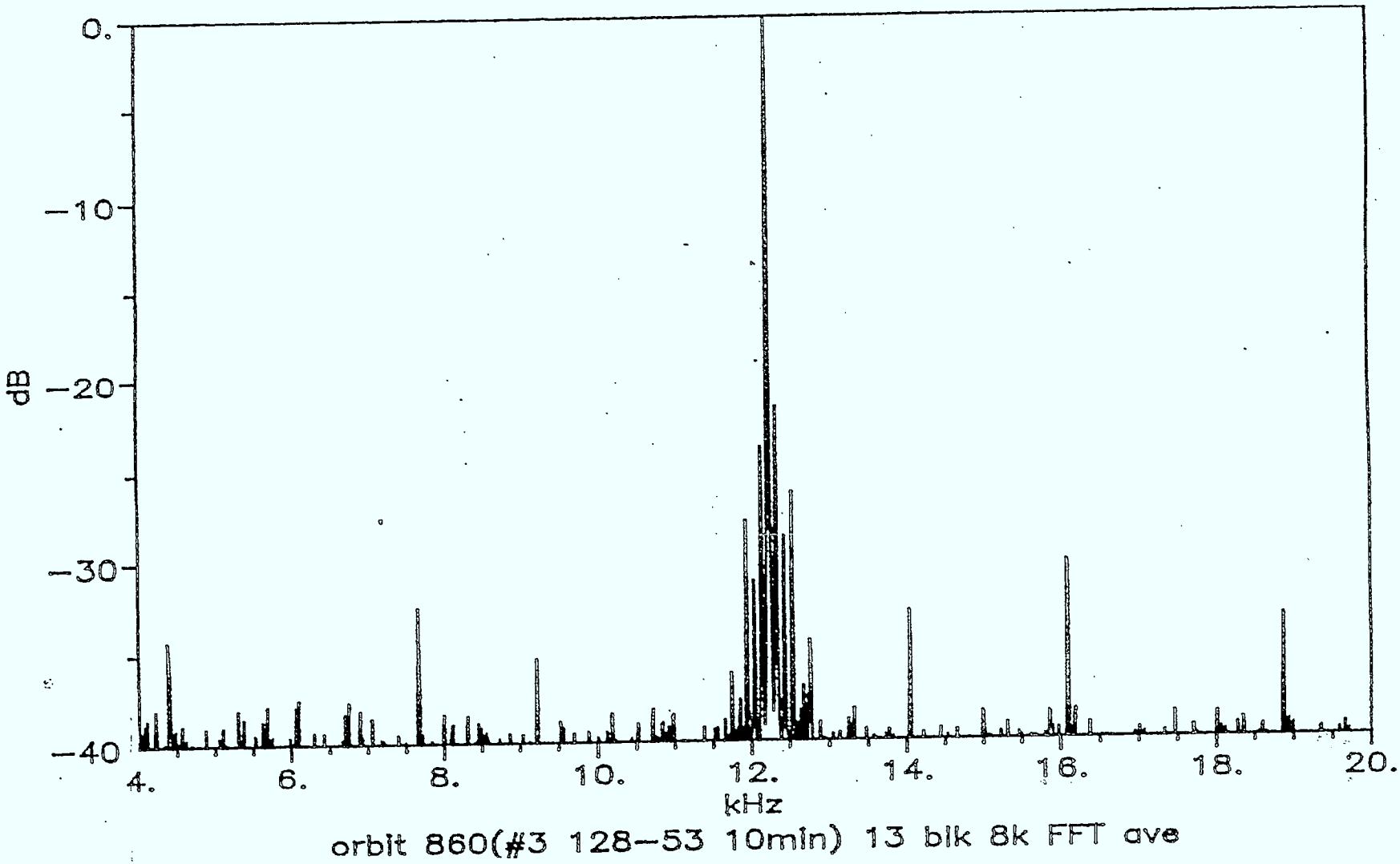

Fig. 3.3 Spectral plot for SARSAT signal with a strong CW interfering signal. Note the sidelobes around the main carrier peak.

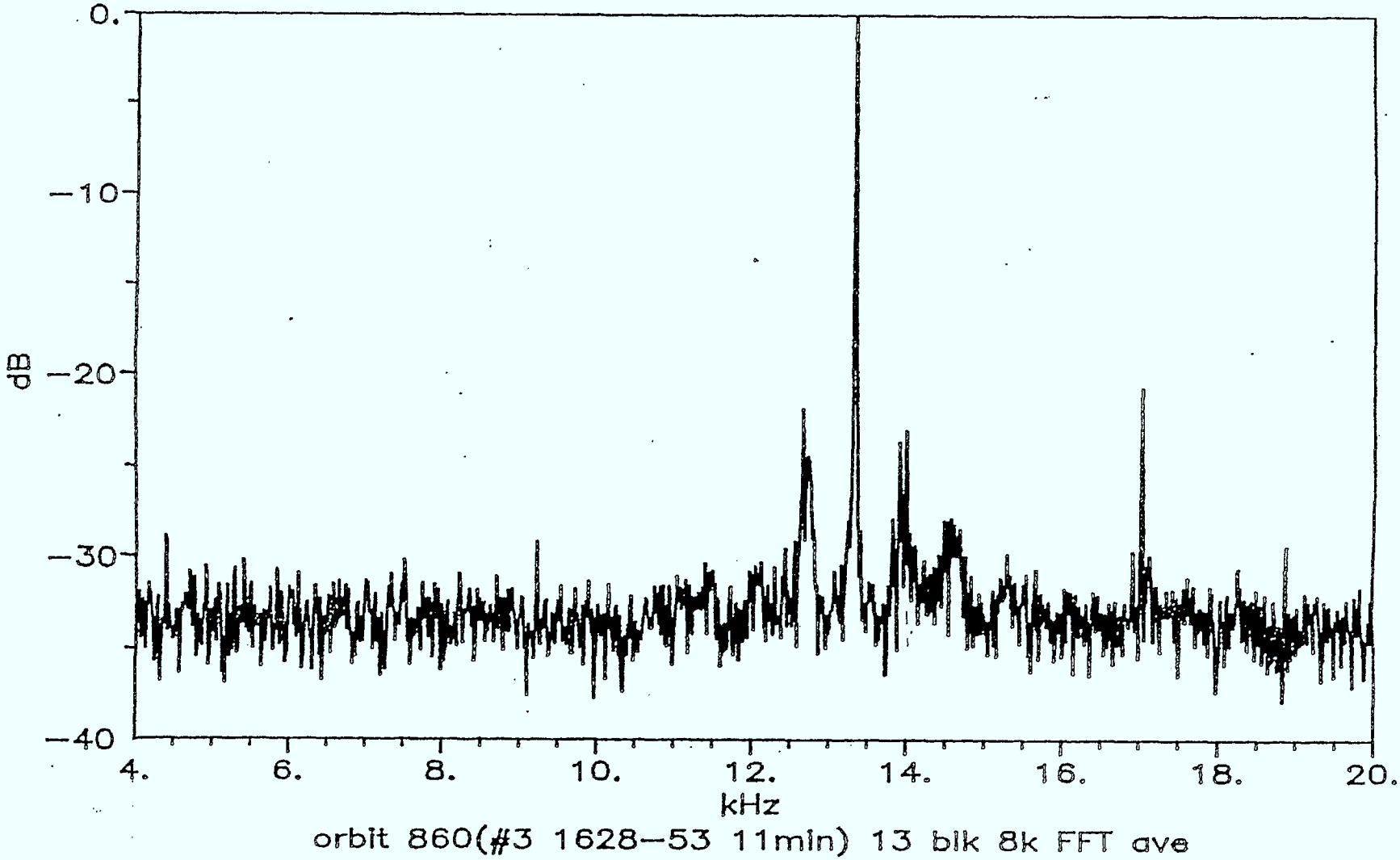

Fig. 3.4 Spectral plot for SARSAT signal with low degree of modulation on the interfering signal.

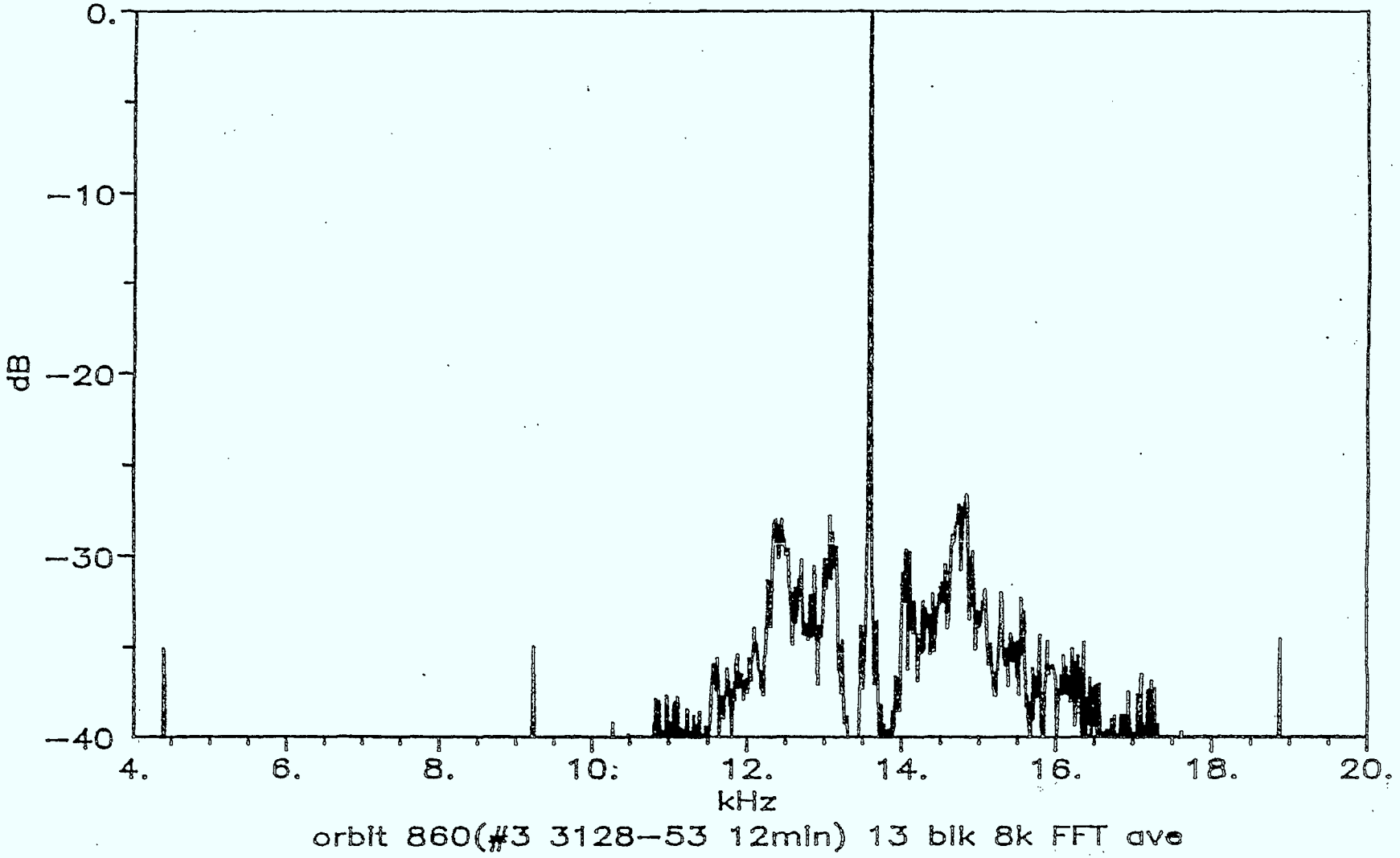

Fig. 3.5 Spectral plot for SARSAT signal with increased degree of modulation on the interfering signal.

minutes, a very strong CW source is received which reduces the background level by some 30 dB. The fact that the signal is CW is demonstrated by the fact the sidelobes of the FFT are clearly visible. At 11 minutes, the signal exhibits modulation sidebands which are further developed by the 12 minute mark where the background has again dropped below the 40 dB down level.

One solution to this problem is to filter the data using a notch filter to remove the CW source. Unfortunately, the FFT would then require recalculation with the filtered data. If the spectral plot has sufficient dynamic range, then a second solution is to simply remove the CW data set from the output spectral plot. In the case documented here, at least 50 dB of dynamic range would be required and in other cases it could easily be more.

3.4 NARROWBAND INTERFERENCE

Narrowband interference refers to interference having a bandwidth which is considerably less than the 25 KHz bandwidth being processed for the 121.5 MHz signal band. Typical sources of interference are shown in the dot plots of Fig. 3.6. This kind of interference can be detected by using a median filter type of averager on the frequency plot as illustrated in Fig. 3.7. In this case, we see that the median filter eliminates all of the sharp peaks due to signals leaving only the background. In this case, the background is due to the receiver noise of the system and the contributions due to the interfering source.

The indication of interference is provided by noting the increase in the level of the output of the median filter as the window sides across the frequency band. With noise alone, the output of the filter is reasonably flat whereas with narrowband interference there will be an increase of several dB in the level which then can be detected by thresholding.

Narrowband interference can be combatted by choosing a processing strategy which has little or no effect on the ELT signal but significant effect on the interference. Such a processor is the 'minimum selection' already investigated as part of the SARSAT program in CRL. Figure 3.8 illustrates the averaged spectra obtained with the overlap of a coherent ELT

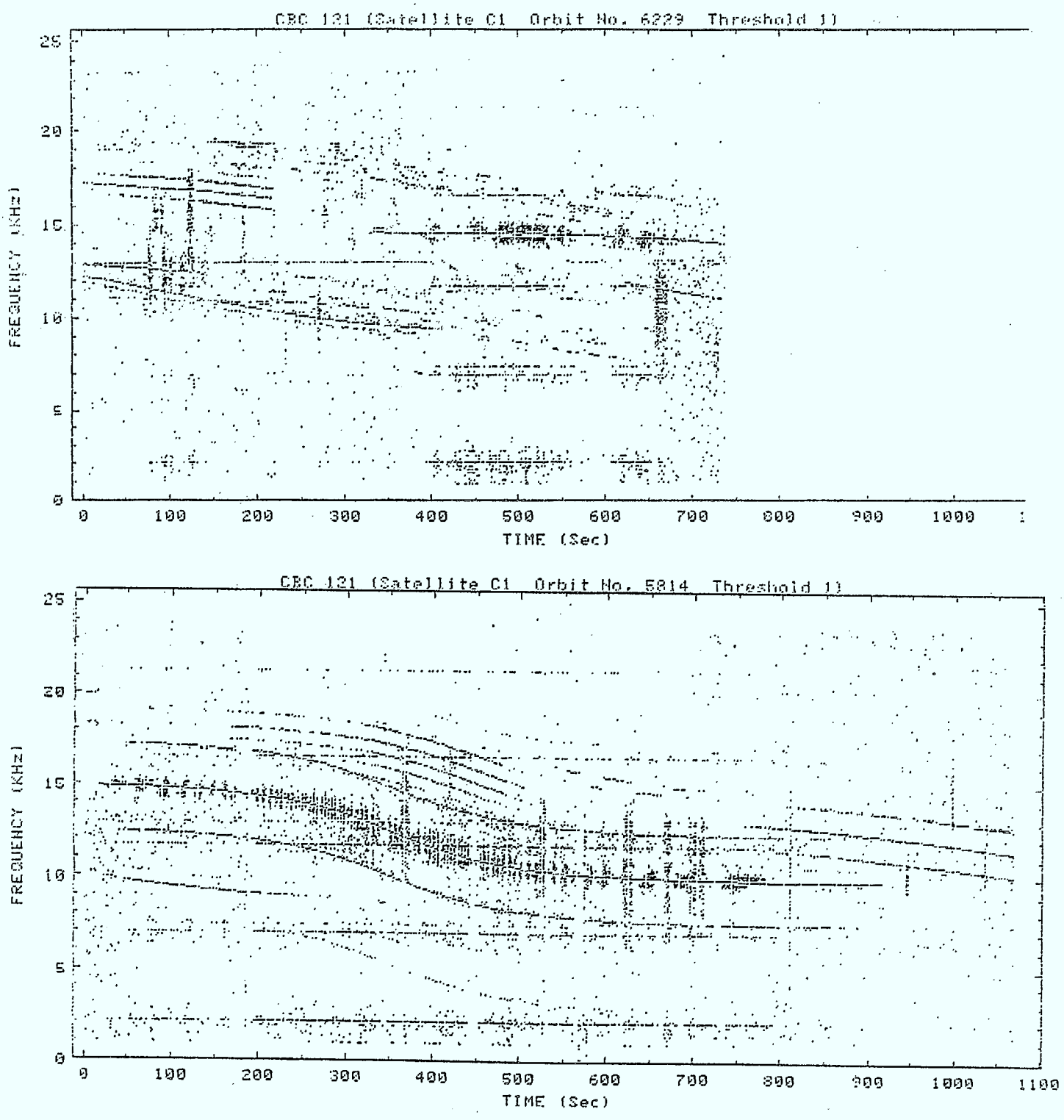

Fig. 3.6 Sample dot plots showing narrowband interference.

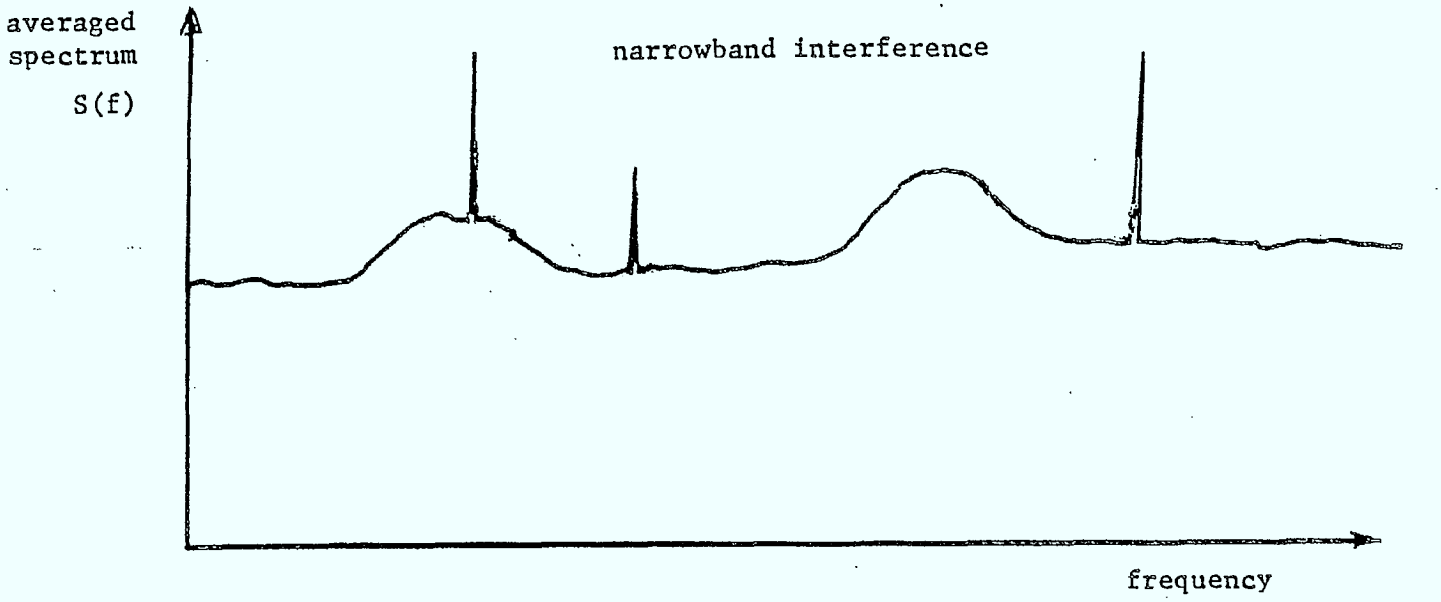

(a)

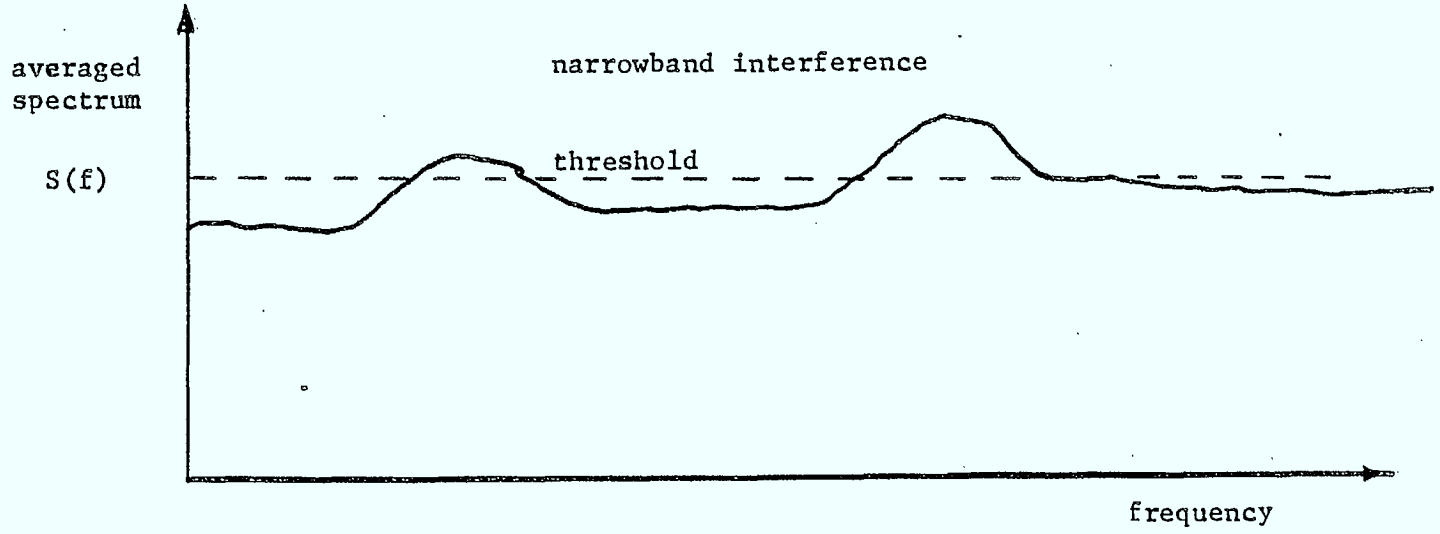

(b)

Fig. 3.7 (a) Averaged spectrum showing signal peaks, narrowband interference and background receiver noise.
(b) Averaged spectrum after median filtering with threshold distinguishing interference from receiver noise.

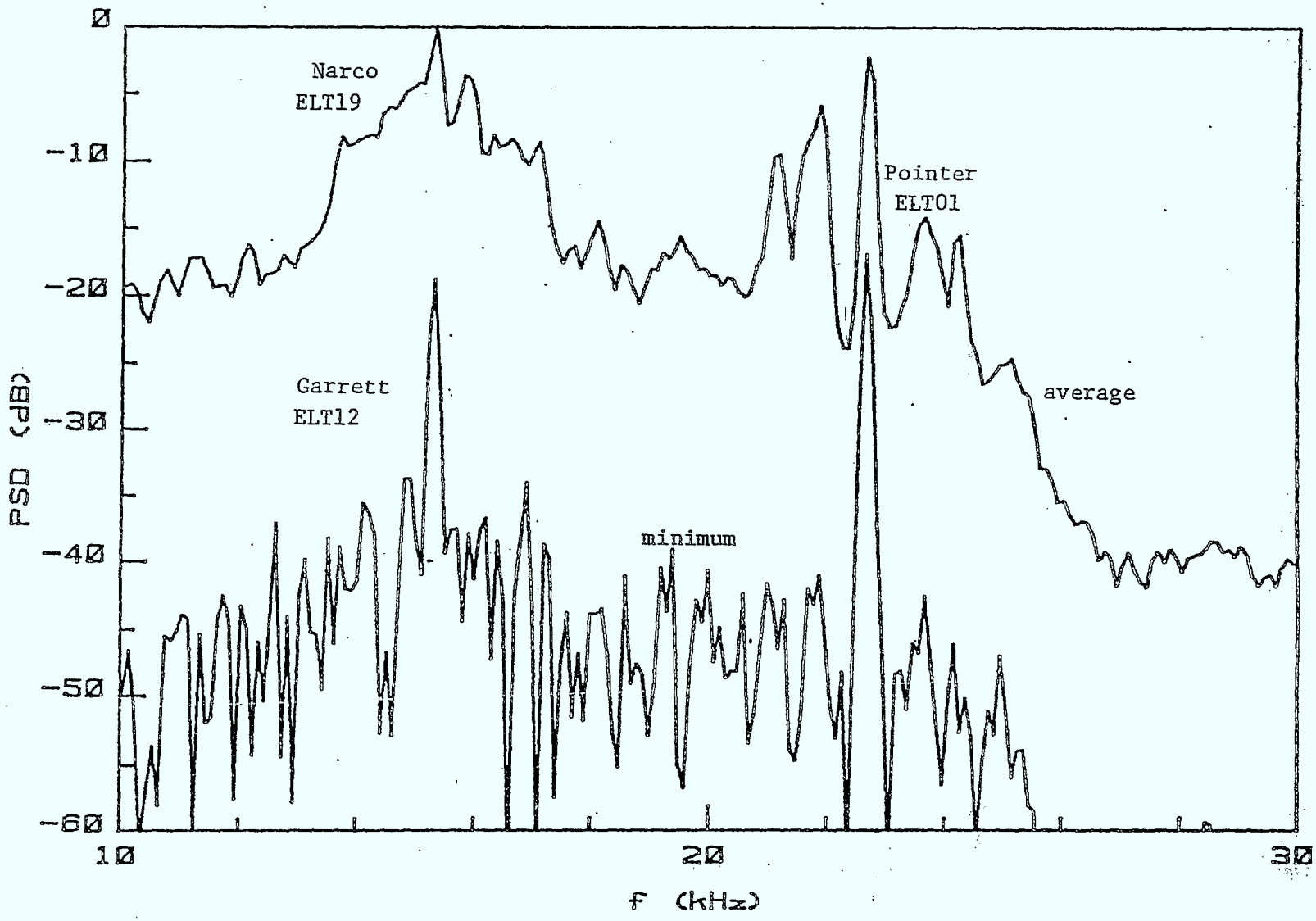

Fig. 3.8 Comparison of the average and minimum spectra for a combination of Pointer and Garrett ELT signals overlapped by the Narco ELT signal. Note that the minimum spectrum simplifies detection of the Garrett ELT signal.

signal and a non-coherent signal. It is clear that the coherent ELT signal is greatly masked by the non-coherent signal. Using the 'minimum selection' technique, we see that much of the effect of the non-coherent ELT signal has been eliminated while the coherent ELT signal has been preserved.

3.5 WIDEBAND INTERFERENCE

Wideband interference can be considered to be interference which covers most of the 25 KHz bandwidth of the ELT band, such as the dot plots examples of Fig. 3.9. In this case, median filtering may or may not be of use in detecting the interference since the level of most of the band may be increased by approximately the same level. However, the overall power of the output signal is increased. This can then be measured by either envelope detecting the signal itself, as described in the next section, or monitoring the AGC control level.

Wideband interference can be produced by several means, including the effects of a large number of low power impulsive sources, the shock excitation produced by a small number of high power impulses or by the wideband modulation of a carrier.

The effect of a small number of high power impulses can be reduced by employing a limiter in the rf amplifier stages of the receiver at the satellite. Essentially, it is necessary to use wide bandwidths prior to the limiter in order that the filter 'ringing response' is not excited. Then, the limiter in effect clips off the high level impulse so that it is no longer able to shock excite the narrowband receiver. Finally, the signal is fed to a narrowband linear-phase characteristic (possibly surface acoustic wave device filter) filter in order to establish the desired bandwidth properties. Note that very little can be done at the earth station to solve the problem once the 'ringing response' at the satellite has occurred.

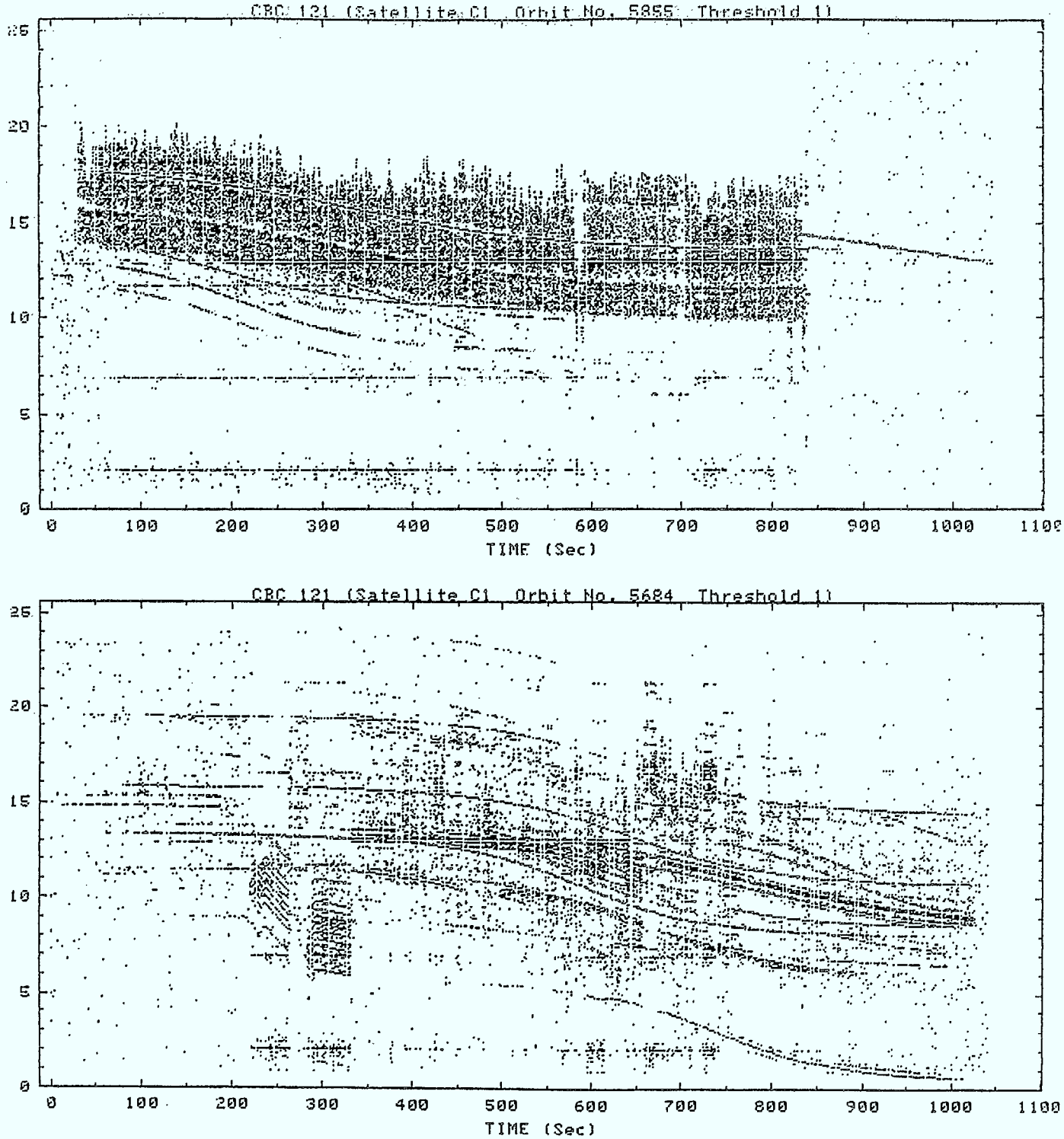

Fig. 3.9 Sample dot plots showing wideband interference.

3.6 ACTIVITY OF THE PASS

3.6.1 Pass Data

Real satellite pass data have been reviewed by considering dot charts. It was found that a small fraction of the passes are nearly free of any significant interference, which leaves a large portion with some degree of interference. The number of dots as presented on the dot charts was arbitrarily divided into eight different levels of activity, as hown in Fig. 3.10. Approximately 100 dot charts were reviewed for each of SARSAT at 121.MHz and 243 MHz, and COSPAS at 121.5 MHz, with each plot being classified in one of the activity levels. A plot of number in each activity level versus the activity level is given in Fig. 3.11. We see that the activity levels for the three curves are all approximately the same with 50% of the charts falling in levels 0, 1 and 2. However, this also shows that about half of the dot charts indicate significant inteference being present. (The activity level of the plots is restricted to a maximum of 122 dots per line. Thus, there may actually be cases of higher level interference which are not recorded.)

3.6.2 Detailed Interference

During a satellite pass, the field of coverage changes considerably as the antenna scans over cities with their many sources of interference, areas containing large numbers of false alarms and other sources of electromagnetic interference. A few sample traces of waveforms received are now examined. From S1/2614, we see a 10 ms duration of signal (Fig. 3.12) which appears to represent the case of normal gaussian noise with the possibility of embedded ELT signals but no significant interference. Figure 3.13 illustrates a strong ELT signal with a small amount of noise in the background.

Contrast these with the traces from C1/6229 (Fig. 3.14) which clearly indicates an interfering PSK modulated source or Fig. 3.15 which is a strong CW interferer. Figure 3.16 could be an example of voice interference. In these last three figures, it is clear that the AGC circuit has considerably reduced the level of background noise and any weak ELT signals by a

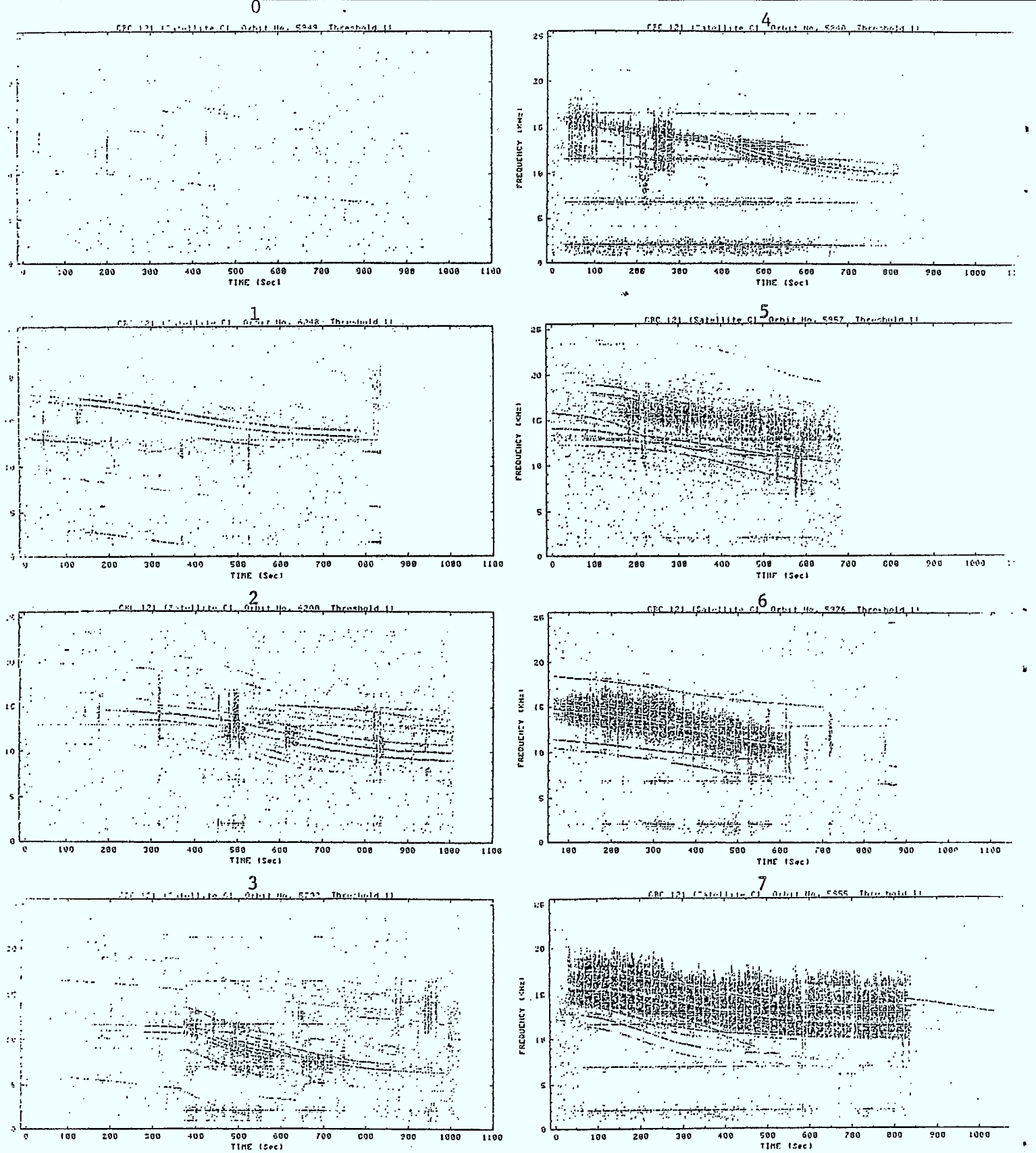

Fig. 3.10 Levels of activity for 8 different backgrounds of interference. Activity level 0 contains almost no interference while activity level 7 contains heavy interference.

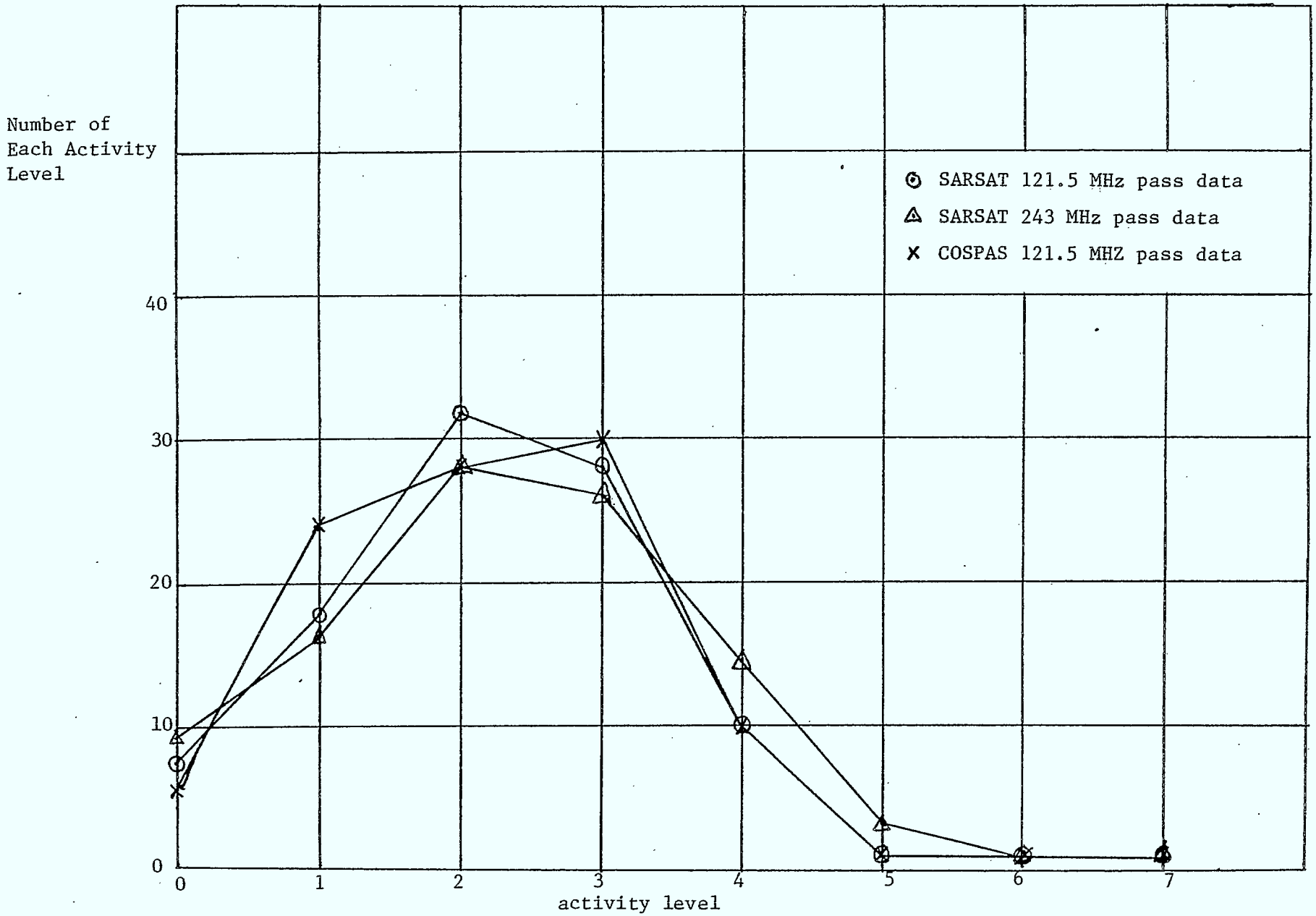

Fig. 3.11 Plots of number of each activity level versus activity level for approximately 100 satellite passes.

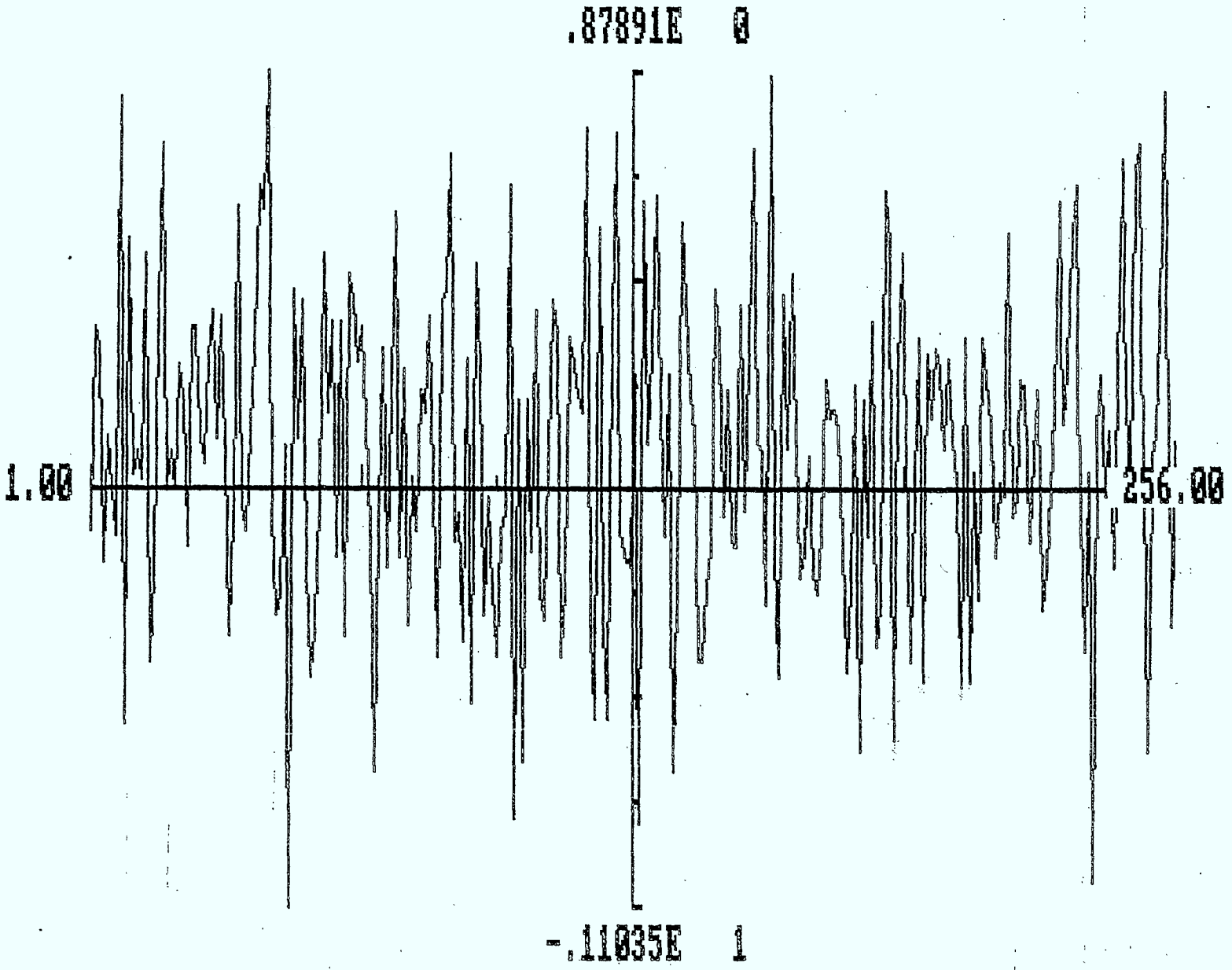

Fig. 3.12 A 10 ms segment of SARSAT signal illustrating receiver noise background.

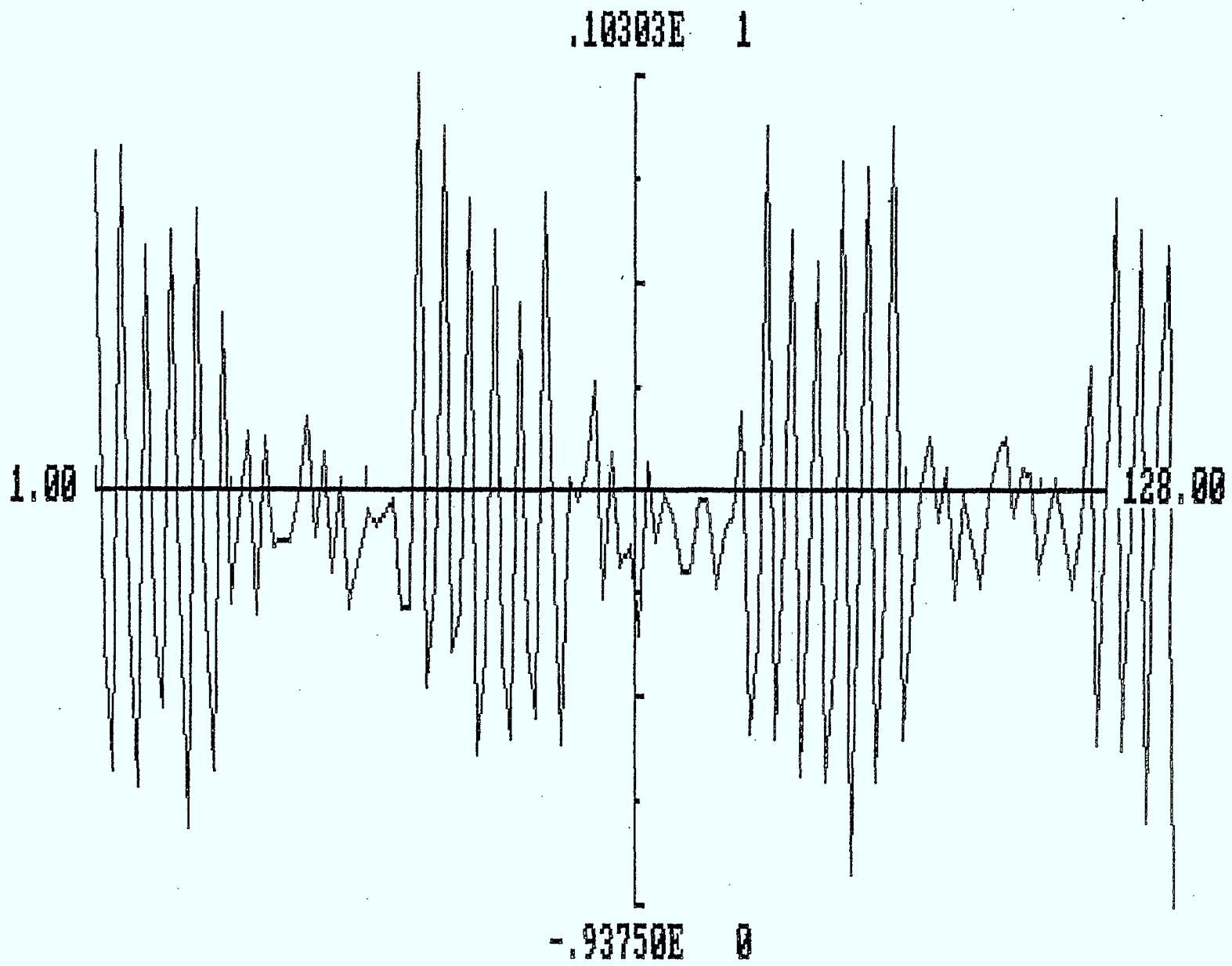

Fig. 3.13 A 2.5 ms segment of SARSAT signal illustrating a strong ELT signal.

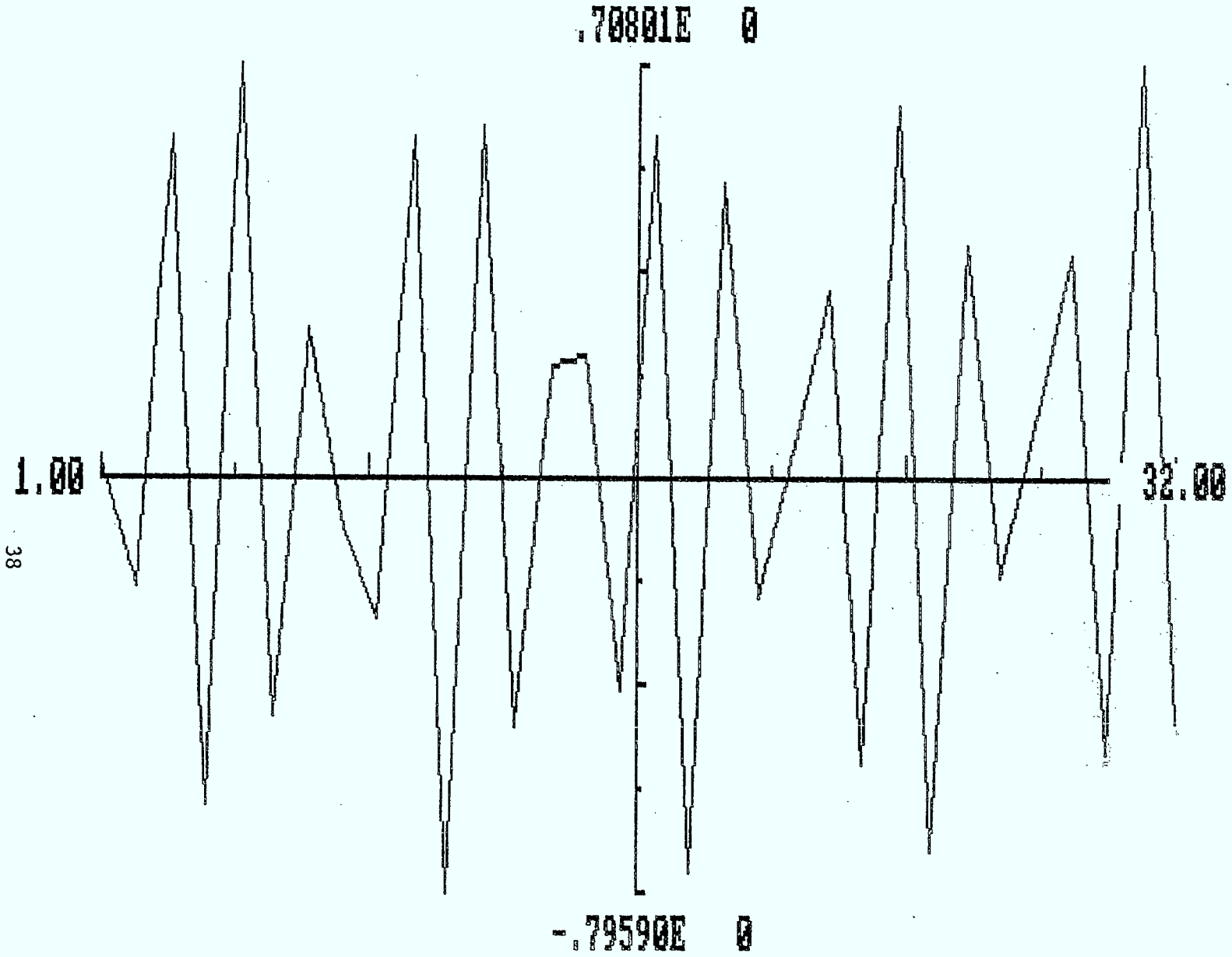

Fig. 3.14 A 1.125 ms duration of SARSAT signal illustrating a PSK data interfering source.

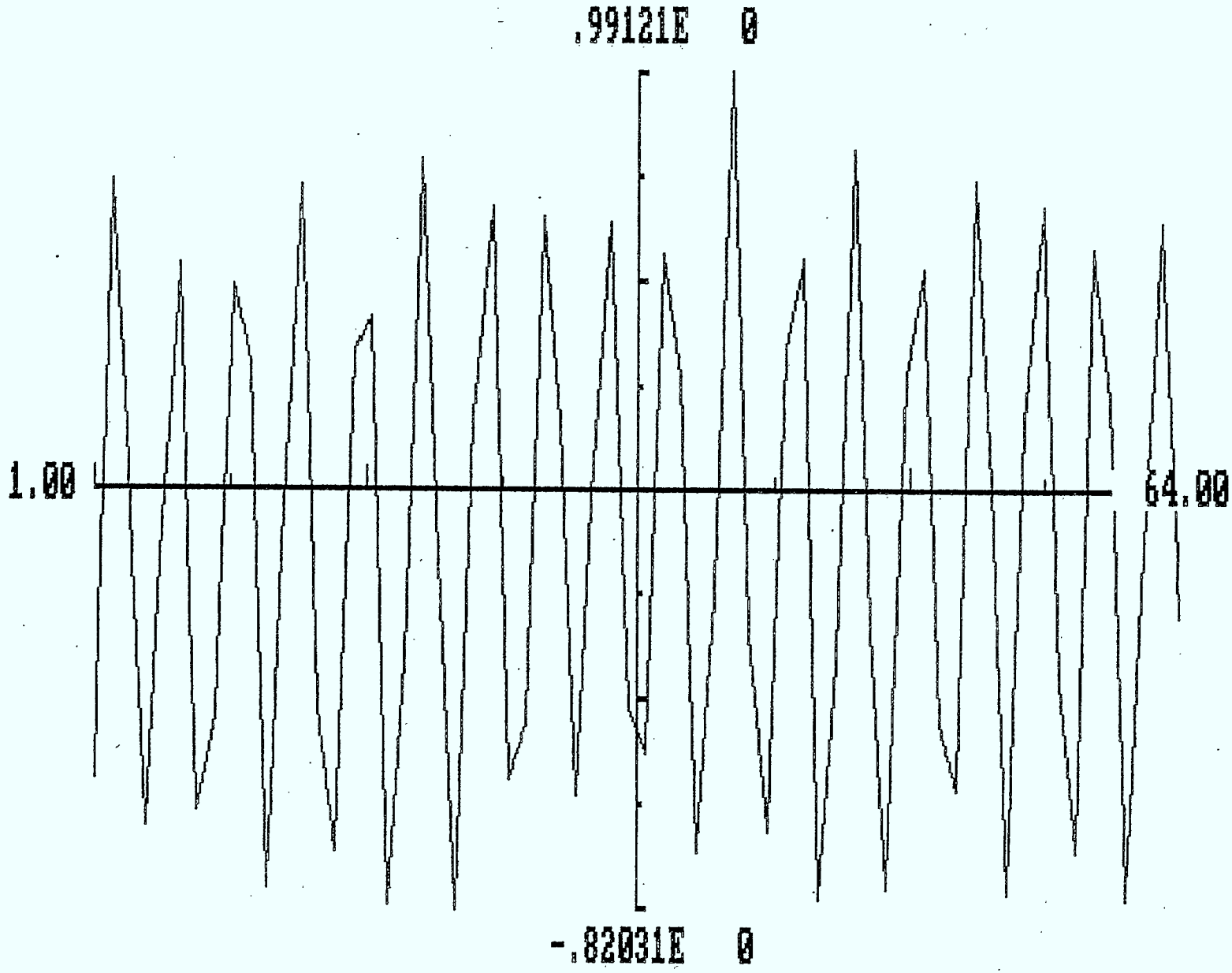

Fig. 3.15 A 1.125 ms duration of SARSAT signal illustrating a strong CW interferer.

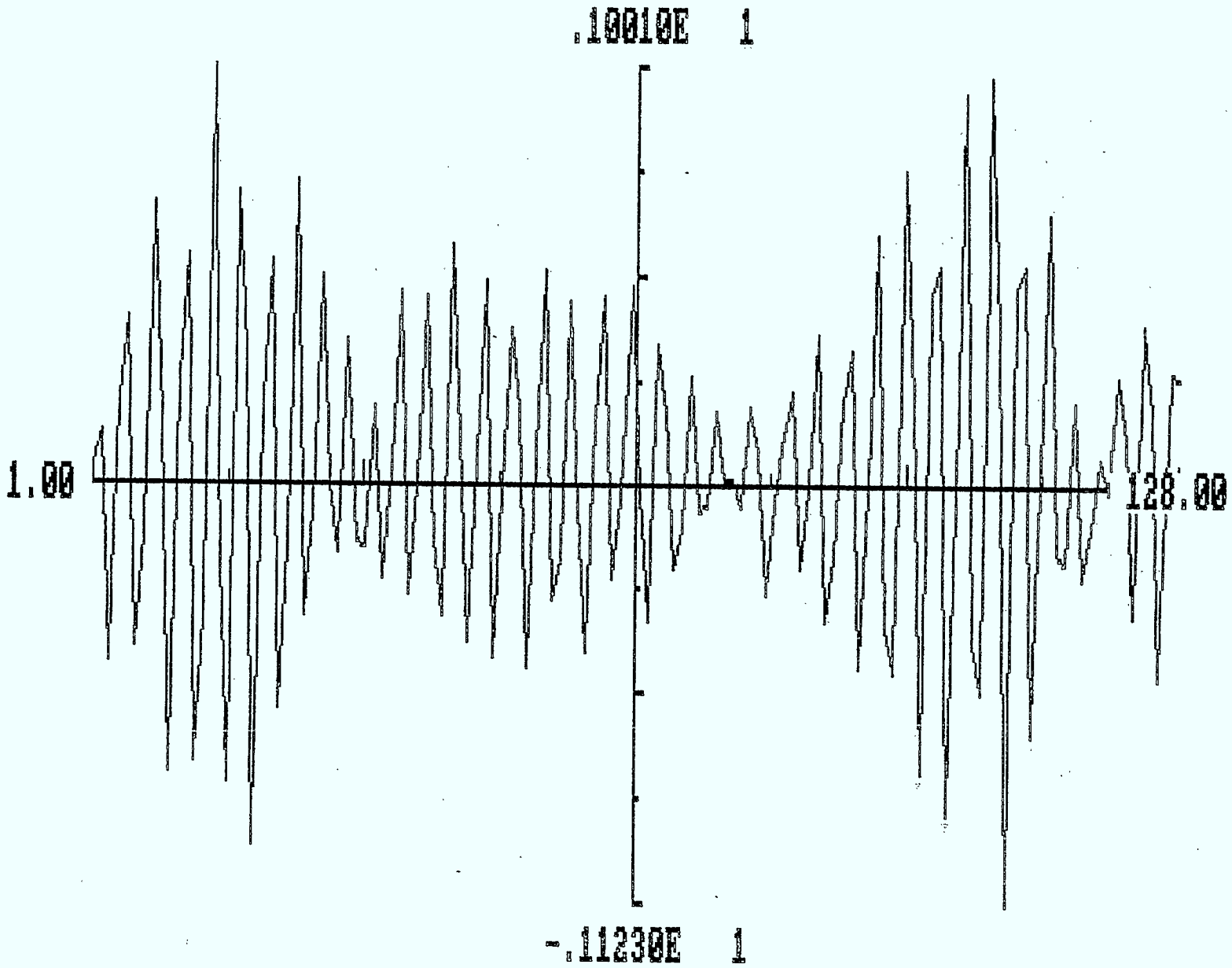

Fig. 3.16 A 2.5 ms duration of SARSAT signal illustrating possible voice interference.

very substantial amount. The amplitude peaks on Figs. 3.12 to 3.16 are all approximately the same amplitude; however, the signal of Fig. 3.12 is mainly noise whereas the signal of the last three traces is mainly interference. Thus, the digitizing circuitry of the data processor must have sufficient dynamic range to combat this change. Further, special precautions should be taken prior to the processing and interpretation of these signals.

In order to examine the existence of pulsed interference, an envelope detector was constructed. Figures 3.17 shows strong pulse which has entered and caused a transient in the AGC amplifier. Figure 3.18 illustrates a shorter duration pulses which occurred slightly later in time and indicates the leading edge of yet another pulse. These few traces were taken over a period of only a few seconds. Many other disturbances were observed in addition to these.

Based on these few observations, it is safe to say that a detailed study of the problem is in order. There are two possible temporal designations which can be used to advantage in assessing the activity of the pass. First, is the short term in which interference or signals are received over a short period in time. In this case, the time designation for short term could be durations less than or equal to the output of one averaged FFT estimate, namely 1 second. The second designation is the long term which would include all durations over 1 second. For the short term, interference would include bursts of signal or interference which would alter the individual FFT estimates comprising the averaged FFT output. For the long term, the interference would include sources more continuous in time which would affect many consecutive averaged FFT outputs.

3.7 THRESHOLD BASED ACTIVITY MEASURE

There are many independent variables which can be used to describe interference (amplitude, modulation, frequency sweep etc.) but only two which give a useful pictorial description in a narrow-band system such as COSPAS-SARSAT, namely length of time and bandwidth. The length of time specifies the duration that the interference is present in any one pass and may consist of many different contributions. The bandwidth of each of the

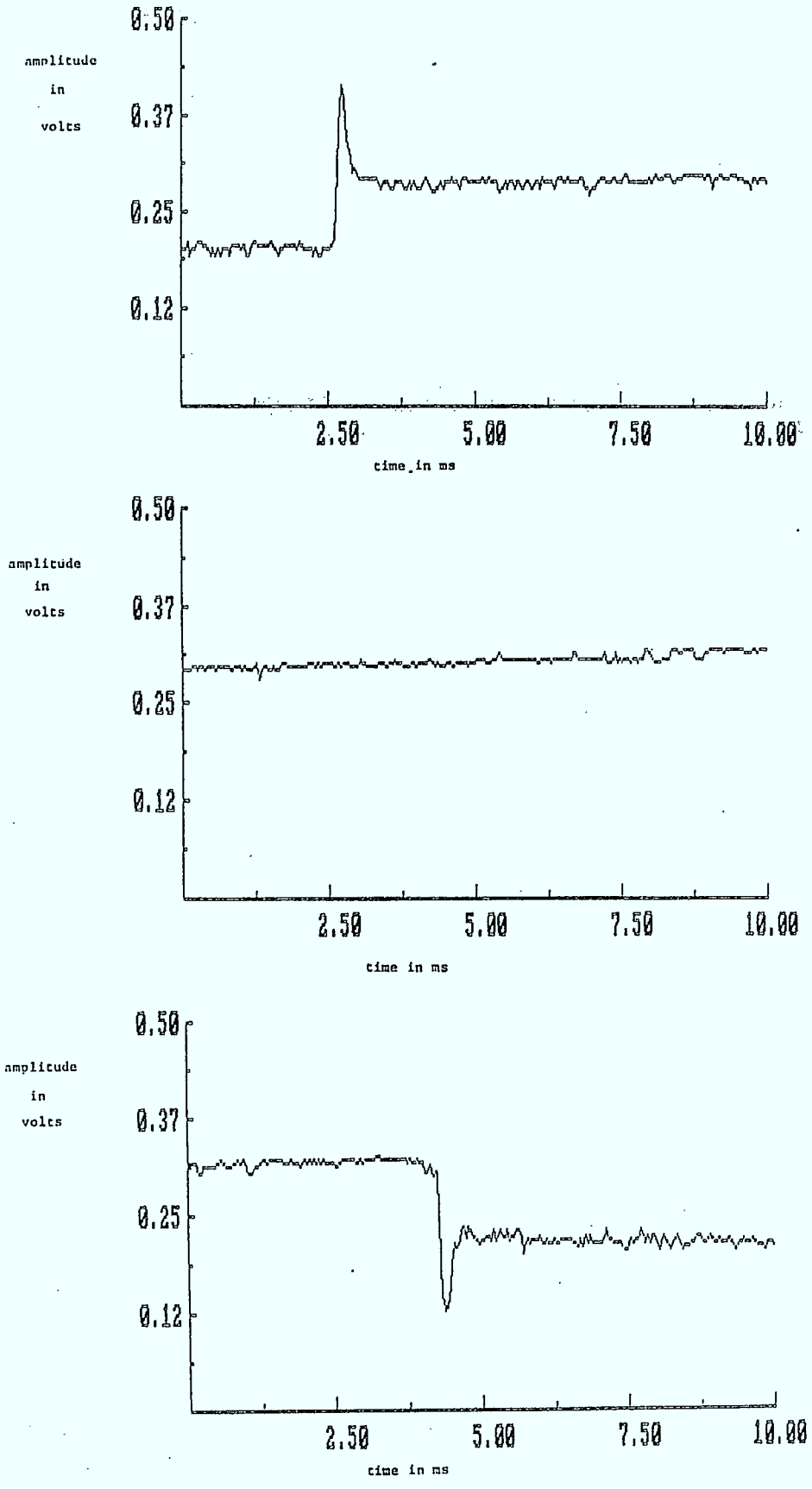

Fig. 3.17 A 30 ms segment of SARSAT signal illustrating a 23 ms long pulse detected by envelope detection.

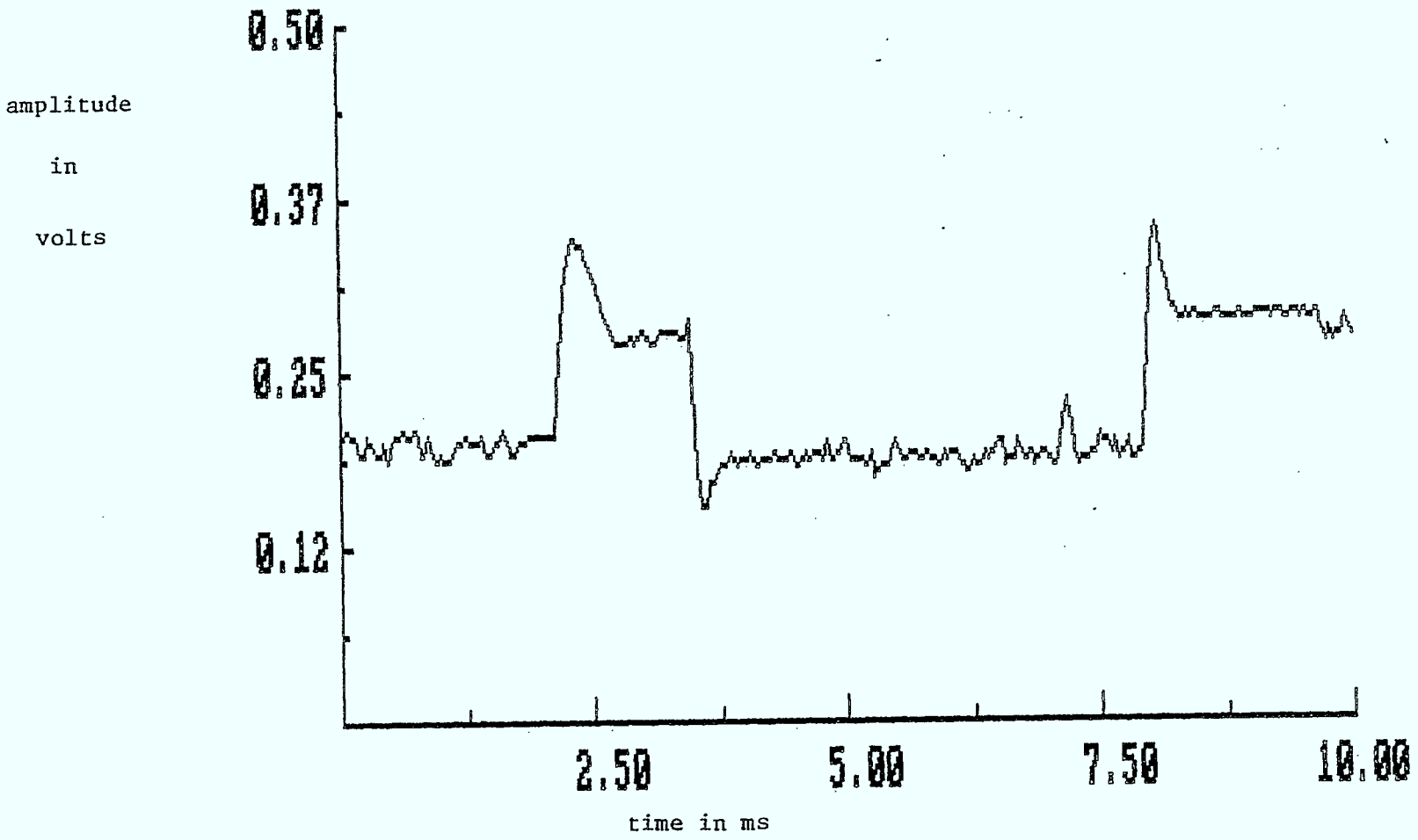

Fig. 3.18 A 10 ms segment of SARSAT signal showing a short duration pulse followed by a second pulse.

contributions is a measure of the amount of frequency band which is occupied by an interfering source. Thus, the interference for a given pass can be specified for N interfering sources by defining the time bandwidth product

$$TB = \sum_{n=1}^{N} T_n B_n \tag{3.7}$$

where

T_n = duration of interference from the n^{th} source

B_n = in-band bandwidth of interference from the n^{th} source

If the total duration for a pass is T (600 to 900 s typical) and the bandwidth of the receiver is B (25000 Hz), then the overall goodness of the pass data can be measured by calculating

$$GP = \frac{T*B - TB}{T*B} * 100\% \tag{3.8}$$

For a pass with no interference, GP = 100% and for a pass completely jammed GP = 0%. In practice, this can be implemented by simply setting several different thresholds in the power spectrum and counting the number of times the thresholds are exceeded.

3.8 SPECTRUM BASED ACTIVITY MEASURE

The averaged spectrum provides a useful means for measuring the activity of the pass since CW, narrowband and wideband interference can all be identified easily in the frequency domain.

We have seen that interference can range in bandwidth from very narrow (CW) occupying a few tens of Hz to very wide (wideband) covering thousands of Hz. In addition, the interference may be present for periods ranging from milliseconds to many tens or hundreds of seconds.

Frequency distributed interference can be described by considering the spectrum at the output of the receiver. If the input to the receiver is additive white Gaussian noise, then the output of the receiver has a flat spectrum, i.e. all components, x_i, for a given averaged FFT

have the same value. When ELT signals are present, there is an increase in the spectrum level in those locations where the coherent portions of the ELT signals contribute. This is mainly at the carrier peak since the sidebands are approximately 10 dB below the carrier peak (as is shown in Figure 4.20 to 4.22). Thus, the total contribution to the spectrum from ELT sources is small compared to receiver noise. Consequently, it is possible to compute a meaningful identifier for the detection of interference by calculating the mean and the variance of the averaged FFT spectral estimate components.

$$a = \frac{1}{N} \sum_{i=1}^{N} x_i$$

$$v = \frac{1}{N} \sum_{i=1}^{N} (x_i - a)^2 \tag{3.9}$$

Consider for example, the result of this computation for five different cases of output averaged spectrum with N = 1024.

Case 1 Receiver Noise Alone (Gaussian)

All values of x_i are constant since the output averaged spectrum is flat. Thus,

$$a = 1 \tag{3.10}$$

$$v = 0$$

Case 2 Few Coherent Sources (Fig. 3.2, for example)

A few values of x_i (say 10) have value 1 and the remaining have value 0.1 (–10 dB). Thus,

$$\begin{aligned} a &= \frac{1}{N}[10 + (N - 10)*0.1] \\ &= 0.109 \\ v &= \frac{1}{N}[(1 - 0.109)^2 + (0.1 - 0.109)^2] \\ &= 0.0078 \end{aligned} \tag{3.11}$$

Case 3 Single Strong CW Interferer (Fig. 3.3, for example)

All values of x are zero except for the point at the frequency of the interference. Thus,

$$\begin{aligned} a &= \frac{1}{N} \\ &= 0.00098 \\ v &= \frac{1}{N}(1-0.00098)^2 \\ &= 0.00098 \end{aligned} \tag{3.12}$$

Case 4 Strong Narrowband Interference

Assume, for example, that 10% of the points have a uniformly high value with the remaining points being negligible. Then,

$$\begin{aligned} a &= \frac{1}{10} = 0.1 \\ v &= \frac{1}{N}[0.1N^*(1-0.1)^2 + 0.9N^*0.1)^2] \\ &= 0.009 \end{aligned} \tag{3.13}$$

Case 5 Strong Wideband Interference

Assume that 75% of the points have uniformly high value with the remaining points being negligible. Then,

$$\begin{aligned} a &= 0.75 \\ v &= \frac{1}{N}[0.75N^*(1-0.75)^2 + 0.25N^*0.75)^2] \\ &= 0.1875 \end{aligned} \tag{3.14}$$

These five cases are plotted in a-v space as illustrated in Fig. 3.19. Cases 2 and 4 produce overlap; however, the remaining cases are quite distinct. Thus, the a-v measure provides a possible means for at least some determination of the activity of the pass. Note that the measure can be performed on the points provided by a single averaged FFT at a given

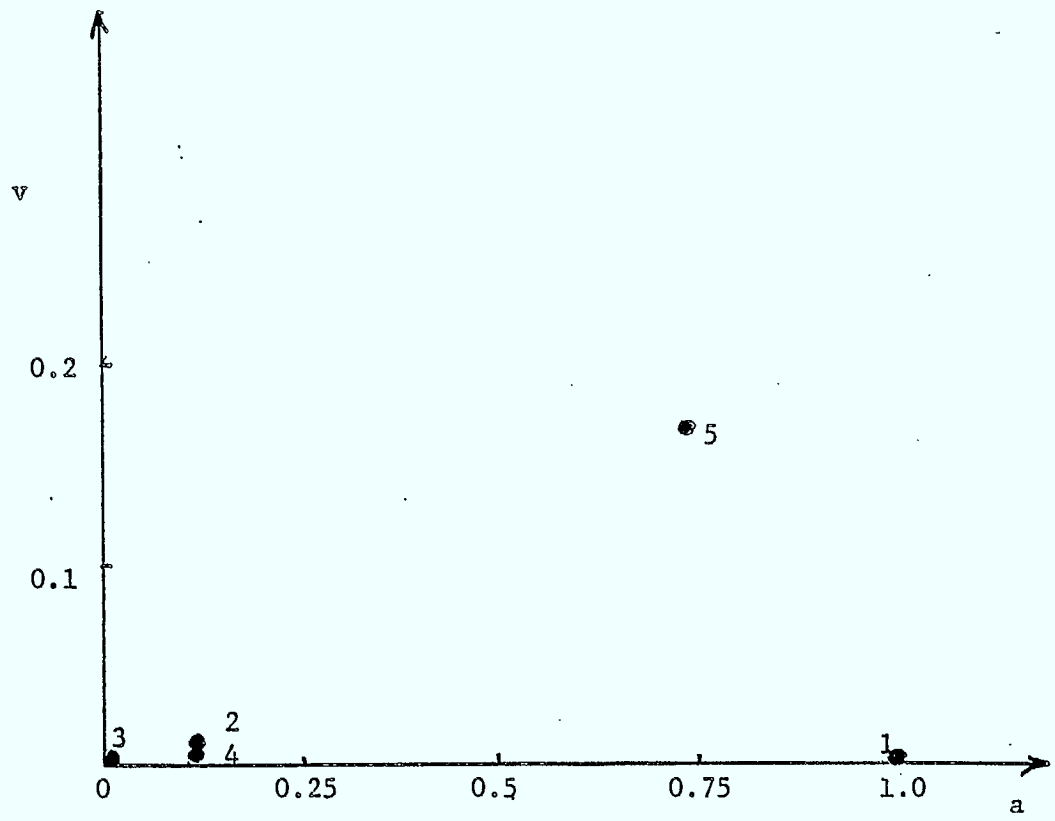

Fig. 3.19 Plot of five different cases of received signal in a-v space.

point in time or by the points provided by a set of averaged FFT points for a signal frequency. Further studies in this area are required, however.

3.9 ENVELOPE DETECTED ACTIVITY MEASURE

The remaining factor which can easily be measured is the strength, e, of interfering signals. Since it has been shown that pulsed interference enters the system in different forms, a convenient method of detecting this pulsed interference is by means of an envelope detector.

A particularly useful implementation is to combine the envelope detection with an FFT applied to longer records from the envelope detector. All detected signals are in baseband format which gives a measure of the content of the total signal. For example, detected noise alone has a spectrum which is Rayleigh while pulse modulated sine wave produces a spectrum described by Marcum's Q function. Monitoring the zero-frequency component of the spectrum gives a measure of the total received power while monitoring the bandwidth characteristics of the detected signal, b, provides an indication of the amount of modulated carrier in the signal.

3.10 CONCLUDING REMARKS

In this section, we have demonstrated that a wide variety of interfering signals enter the SARSAT system and compete with the ELT signals. Examples of narrowband and wideband interference have been presented through the use of dot charts. In addition, samples of recorded SARSAT receiver output have been examined and shown to contain CW interference, data modulated carrier, voice modulated carrier and pulse modulated carrier.

Three possible methods of evaluating the pass have been presented which can be used as interference classifiers:

1) I{GP= } which gives a measure for the whole pass;

2) I{a,v:t} which gives a spectrum measure of interference at time t;

3) I{e,b:t} which gives an amplitude measure of interference at time t.

Each method gives some useful information at to the activity of the pass; however, further study is required in order to fully evaluate the effectiveness of the methods with real data.

4. CHARACTERISTICS OF ELT SIGNALS

4.1 OVERVIEW

This section presents a detailed study of the spectra produced by emergency locator transmitter (ELT) signals and identifies some of the important characteristics which can be used to recognize ELT signals in a multi-signal environment. Typical ELT units use very simple circuits having in some cases poor short term carrier oscillator stability due, perhaps, to variation in the power supply voltage or loading of the carrier oscillator caused by the modulation being applied to the amplifier stages. This coupled with the modulation leads to a signature which can be associated with the individual ELT unit and used to provide an identifier.

In this section, three different models for ELT signal generation are developed. The first model, called the Ideal Coherent Model, produces a highly idealized spectrum which is not found to exist in practice. The second model, called the Non-Ideal Coherent Model is capable of producing a wide range of spectra and represents a large number of real ELT signals. Use of this model leads to a new design specification which should become mandatory. The third model, called the Non-Coherent Model, demonstrates the degradation caused by not providing continuous operation of the ELT carrier oscillator. Computer generated spectra for the Non-Ideal Coherent Model are compared with spectra from real ELT signals.

4.2 ELT SIGNALS

The typical ELT signal may be represented by a modulated carrier waveform, as illustrated in Fig. 4.1. Two different transmitter carrier frequencies may be used (either 121.5 MHz or 243 MHz). The modulation can be represented in an exponential manner as shown with the pulse-null duration T_1 being approximately 0.7 ms and the pulse-null duration T_M being about 1.6 ms. The total period of the signal may vary from 0.25 s to 0.5 s

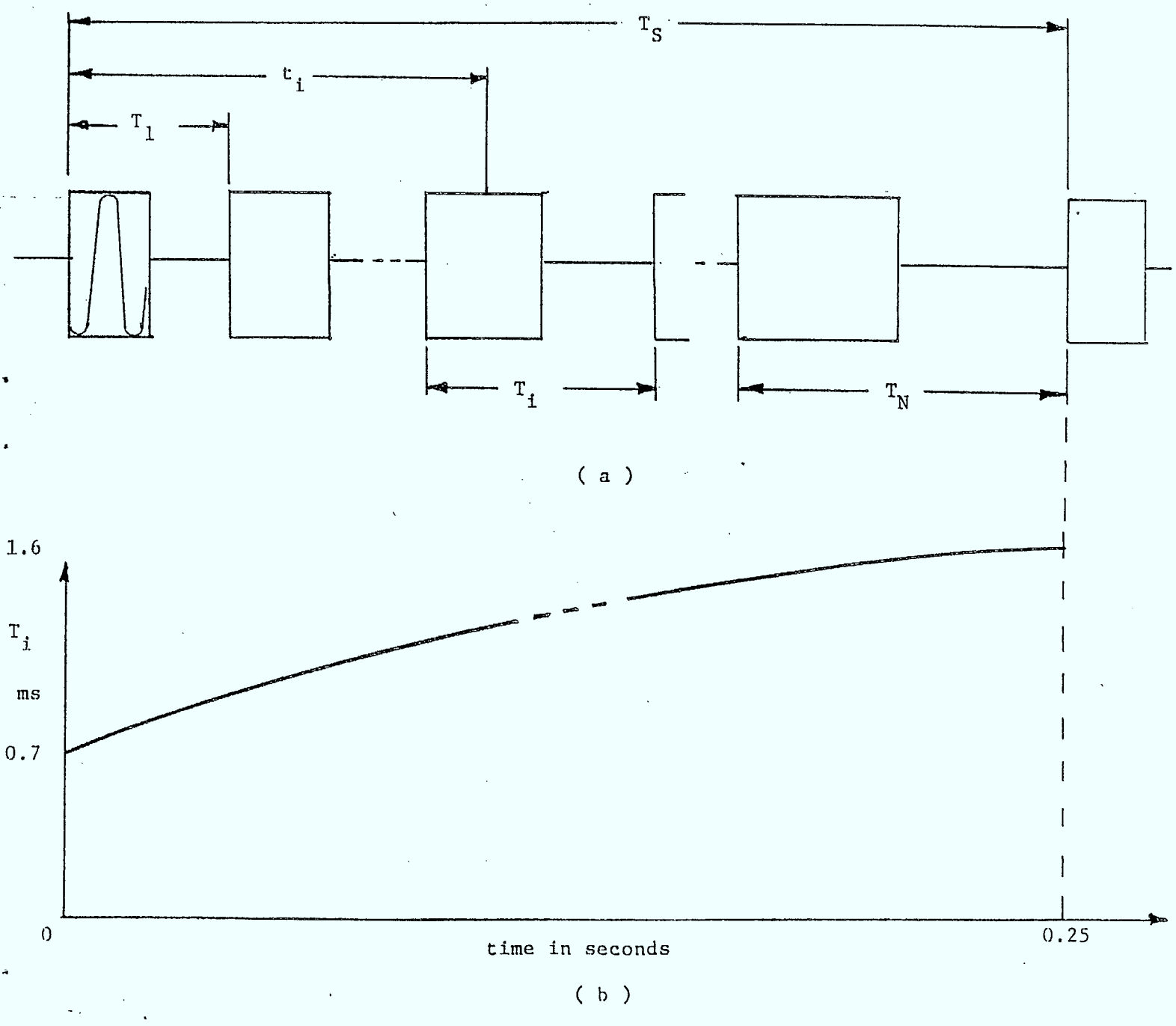

Fig. 4.1 (a) ELT signal comprising N pulse-null pairs of carrier.
(b) Variation in duration of the pulse-null pairs versus sweep time.

depending on the particular unit. A summary of the pertinent specifications is given in Table 4.1. We note that the long-term frequency tolerance is specified; however, the variation of frequency in the short-term is not.

In general, the ELT units can be divided into three models. The first model, called the Ideal Coherent Model, includes those units which can be represented by a constant-frequency oscillator that is switched to the power amplifier as illustrated in Fig. 4.2A. We see that in Fig. 4.2B, the phase from pulse to pulse is continuous. The second model, called the Non-Ideal Coherent Model, can also be represented by Fig. 4.2. However, it is possible that the frequency of the carrier oscillator during the ON time is slightly different from the value during the OFF time. This change can be caused by: 1) a variation in power supply voltage feeding the oscillator due to the change in load current supplied to the power amplifier, or 2) a variation in the input impedance to the switch as seen by the crystal oscillator as the switch is opened and closed.

The third model for ELT units, called the Non-Coherent Model, includes those ELT units which can be represented by an oscillator which is switched ON and OFF by the modulator, as shown in Fig. 4.3A. In this case, the phase from pulse to pulse is no longer related, as shown in Fig. 4.3B. This results in a very broad spectrum which is difficult to process using spectral estimation techniques.

For these three models, we now compute the resulting spectra for the transmitted ELT signals and compare these with the spectra of real signals.

4.3 SIGNAL SPECTRA FOR ELT SIGNALS

The ELT signal illustrated in Fig. 4.1 can be represented by a set of N pulse-null pairs in the time domain. Mathematically, we have

$$s(t) = \sum_{i=1}^{N} s_i(t) \tag{4.1}$$

where $s_i(t)$ is the signal for the ith pulse. Thus,

Table 4.1

carrier frequency	121.5 MHz (optional 243 MHz)
frequency tolerance	± 50 ppm
power output	approximately 100 mW
modulation type	pulse
pulse duration	33% to 55%
percentage modulation	> 85%
modulation frequency	downward swept
sweep rate	2 to 4 sweeps/second
modulation frequency change	700 Hz minimum
modulation frequency limits	300-1600 Hz

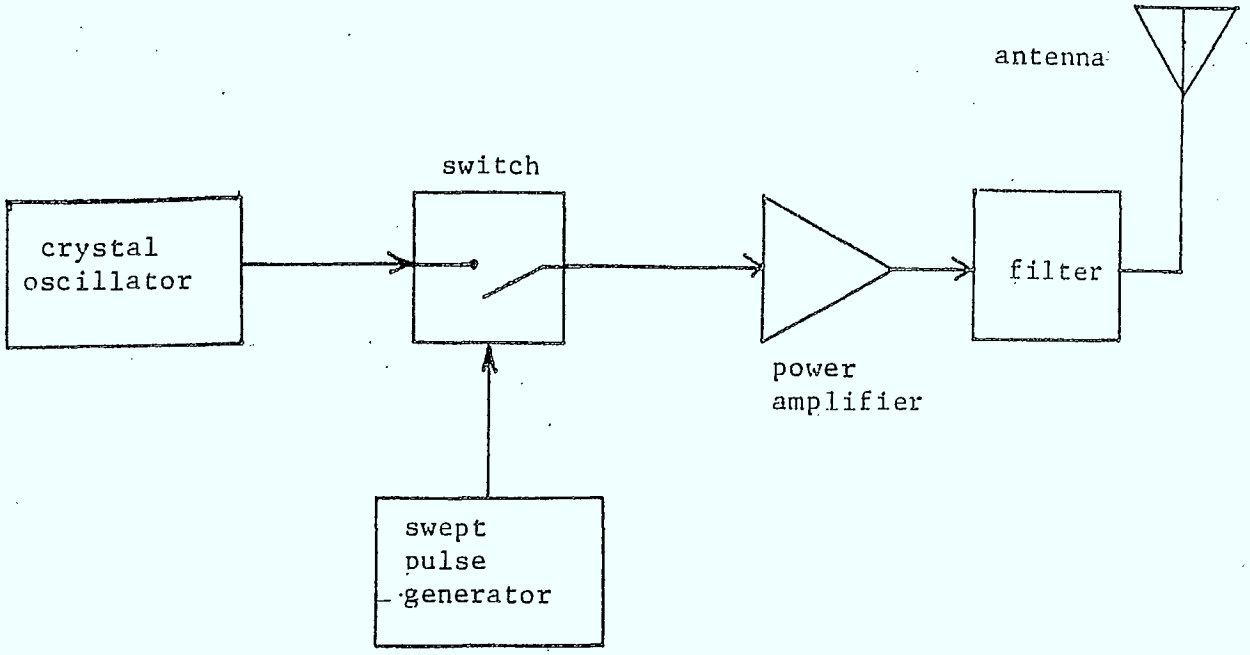

(a)

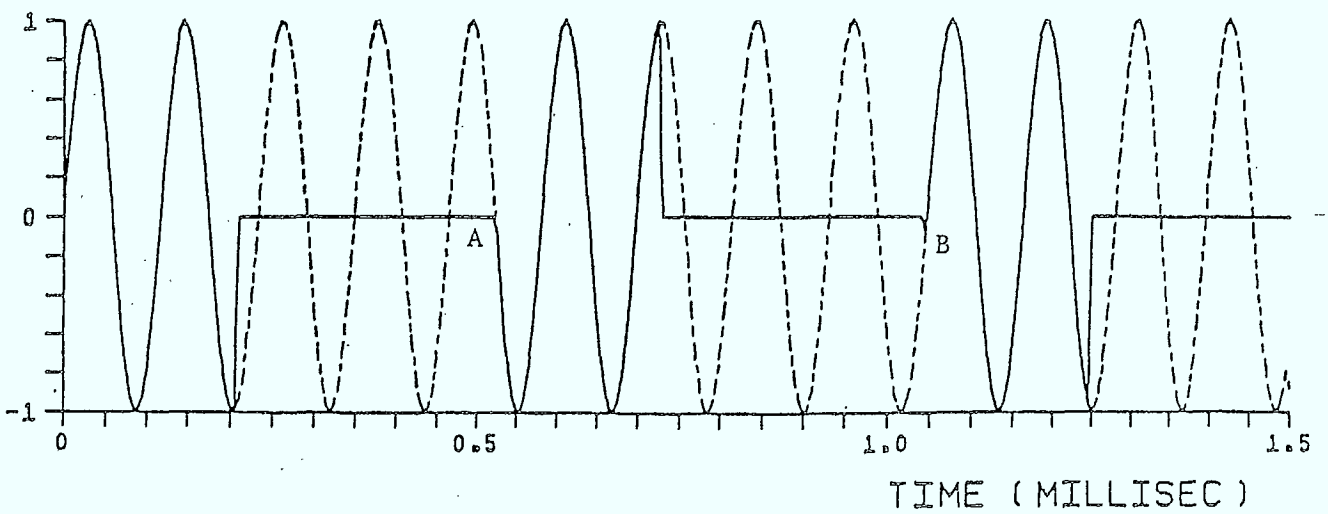

(b)

Fig. 4.2 (a) Block diagram for a coherent ELT.
(b) Portion of a coherent ELT signal with the ON time as a solid line and the OFF time dotted. Note the phase continuity at points A and B.

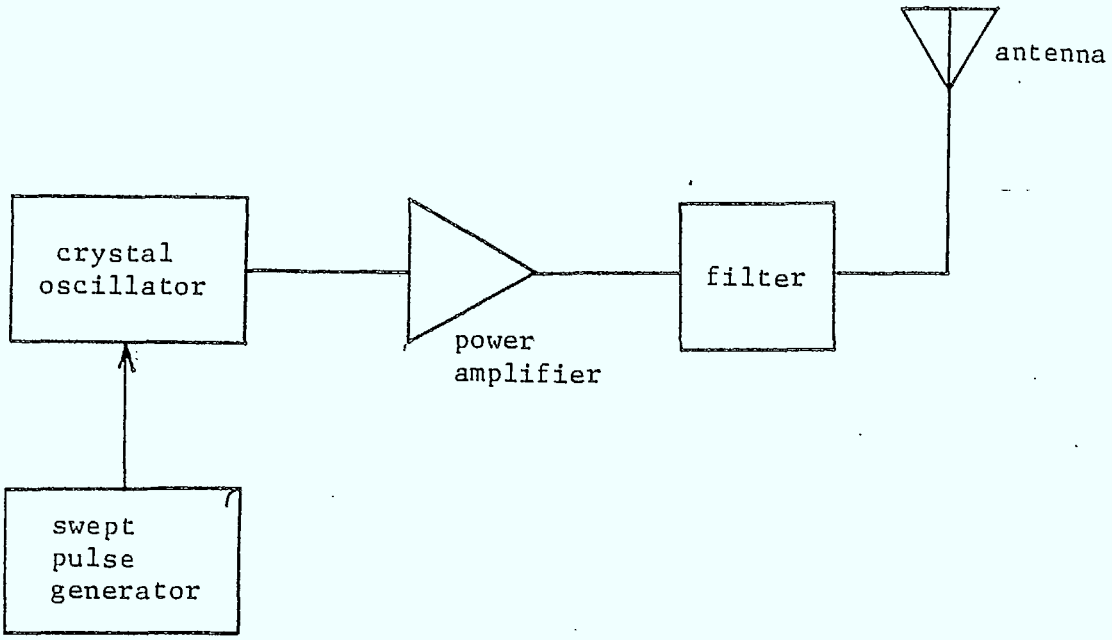

(a)

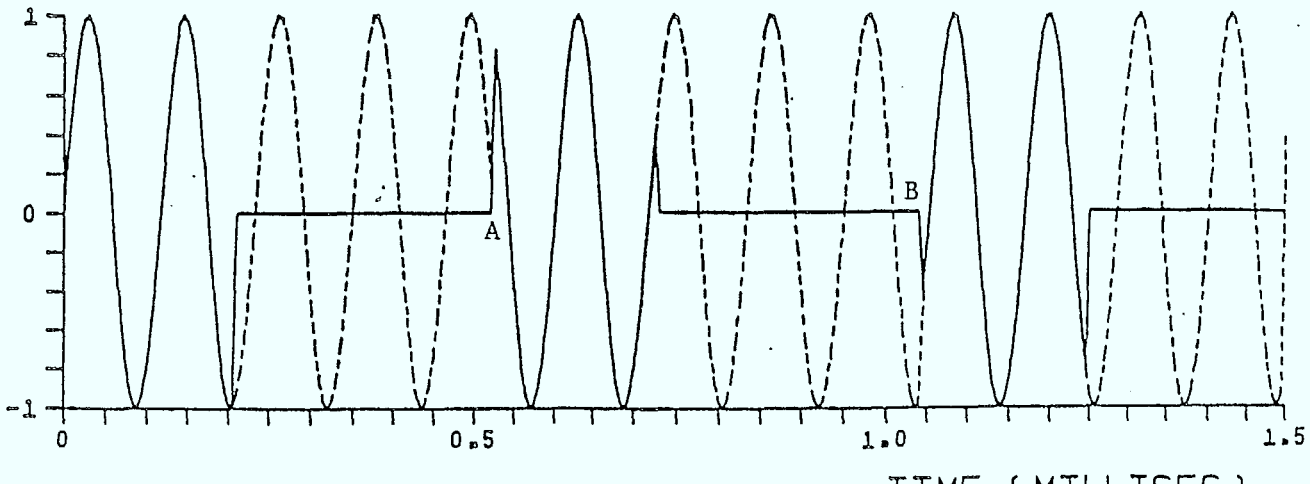

(b)

Fig. 4.3 (a) Block diagram for a non-coherent ELT.
(b) Portion of a non-coherent ELT signal with the ON time as a solid line and the OFF time dotted. Note the phase discontinuity at points A and B.

$$s_i(t) = A\cos[2\pi(f_c + f_d)t + \theta_i)] \qquad t_i - \frac{dT_i}{2} \le t \le t_i + \frac{dT_i}{2} \tag{4.2}$$

$$= 0 \text{ otherwise}$$

where

$A =$ amplitude of the signal

$f_c =$ carrier frequency of the pulse

$f_d =$ doppler shift caused by satellite motion

$t_i =$ time shift from the centre of the first pulse to the centre of the ith pulse

$T_i =$ the duration of the ith pulse-null pair

$d =$ duty cycle

$\theta_i =$ phase shift of the ith pulse described later in detail.

First, let us compute the spectrum for the case of constant doppler shift, i.e. $f_d = f_{do}$. Later, the effects of changing doppler shift will be taken into account.

The spectrum for this signal can be determined by summing the spectra from the individual components.

Thus, the spectrum of the first pulse can be easily calculated by noting that the Fourier transform is given by

$$F_1(f) = \frac{Ad\,T_1}{2}\,\text{sinc}[(f - f_c')\,dT_1] \tag{4.3}$$

where T_1 equals the duration of the first pulse-null pair, θ_1 is arbitrarily taken to be zero, and $f_c' = f_c + f_{do}$ which is the doppler shifted carrier frequency.

Using linearity and the shifting property, the Fourier transform for N pulses is simply

$$F_N(f) = \sum_{i=1}^{N} F_i'(f) \tag{4.4}$$

where

$$F_i'(f) = F_i(f)\exp[-j(2\pi f t_i - \theta_i)]$$

$$F_i(f) = \frac{Ad\,T_i}{2}\,\text{sinc}[(f - f_c')\,d\,T_i]$$

Hence, the Fourier transform of N pulses of signal is

$$F_N(f) = \sum_{i=1}^{N} \frac{Ad\,T_i}{2} \operatorname{sinc}[(f - f_c')\,dT_i] \cdot \exp[-j(2\pi f t_i - \theta_i)] \tag{4.5}$$

This relation can be used to determine the spectra produced by three different models, described next, which may arise in practice.

4.4 ELT MODELS WITH CONSTANT DOPPLER FREQUENCY SHIFT

4.4.1 Spectra for Ideal Coherent Model ELT

For this case, it is assumed that the crystal controlled oscillator has constant frequency over the entire signal. This would imply no short-term variation in carrier frequency. Consequently, it is noted that the exponential term in eq. (4.5) must be exactly unity when $f = f_c'$ Hence,

$$\theta_i = 2\pi f_c' t_i \tag{4.6}$$

Substituting this relation in eq. (4.5) produces

$$F_{IC}(f) = \frac{Ad}{2} \sum_{i=1}^{N} T_i \operatorname{sinc}[(f - f_c')\,dT_i] \cdot \exp[-j2\pi(f - f_c')\,t_i] \tag{4.7}$$

If the duration of signals processed is small compared to the total in a sweep, then T_i is nearly constant (i.e. $T_i = T$) and t_i for the first N pulses is very nearly given by

$$t_i = \frac{(i-1)}{N} T_D \tag{4.8}$$

where T_D = duration of N pulses or the window length of data.

With these simplifications, we have

$$F_{IC}(f) = \frac{AdT}{2} \operatorname{sinc}[(f - f_c')\,dT] \sum_{i=0}^{N-1} \exp[-j2\pi(f - f_c')\frac{i}{N} T_D] \tag{4.9}$$

The summation can be further simplified since

$$\sum_{i=0}^{N-1} \exp[-j2\pi(f - f_c')\frac{i}{N} T_D] = \frac{1 - \exp[-j2\pi(f - f_c')\,T_D]}{1 - \exp[-j2\pi(f - f_c')\,T_D/N]} \tag{4.10}$$

Computing the spectrum, we get

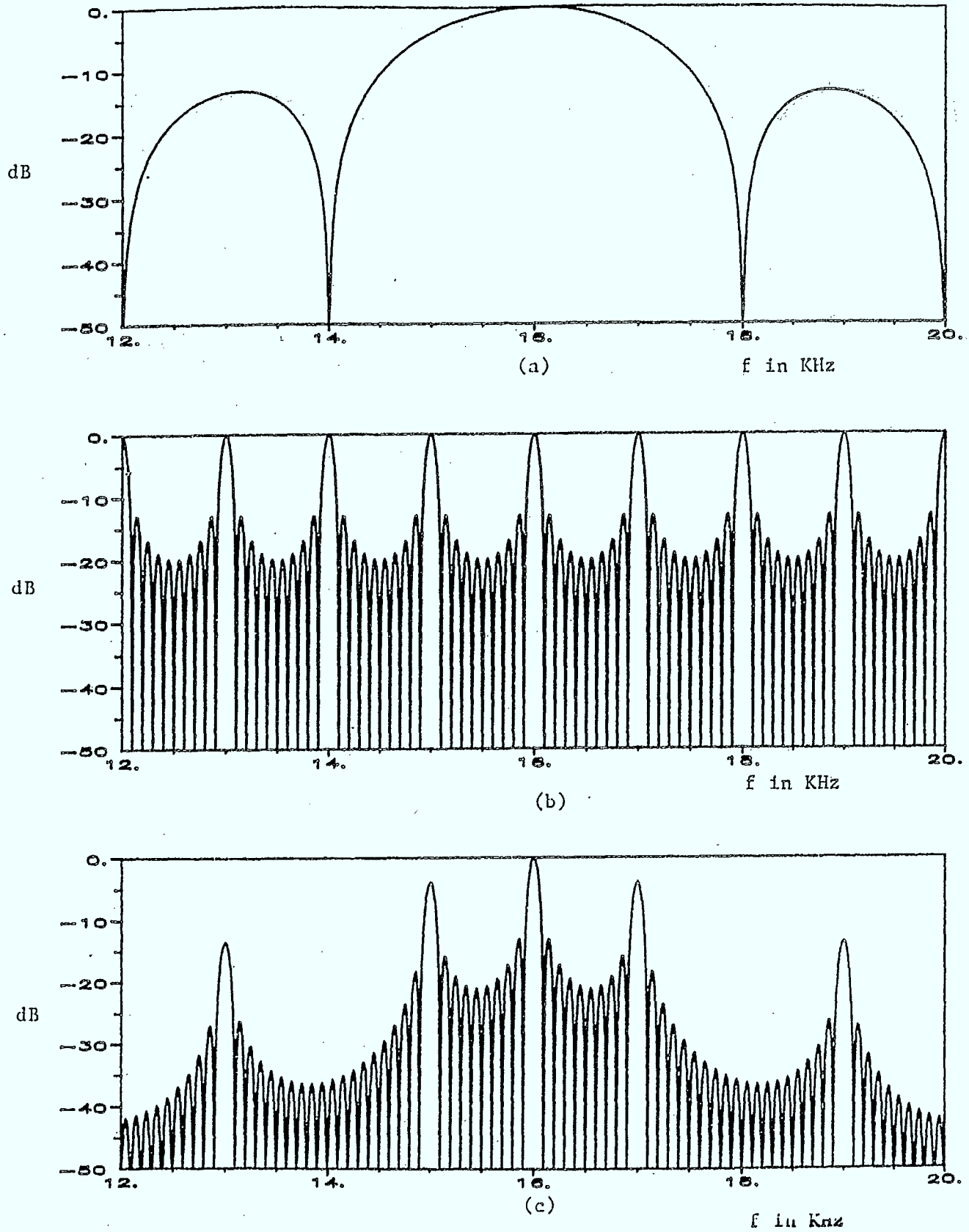

Fig. 4.4 (a) Plot of $\text{sinc}^2[(f - f_c')dT]$ for f_c' = 16 KHz, d = 0.5 and T = 1 ms.

(b) Plot of square of ratio of two sines for f_c' = 16 KHz, T_D = 10 ms and N = 10.

(c) Plot of $S_{IC}(f)$ for AdT/2 = 1.

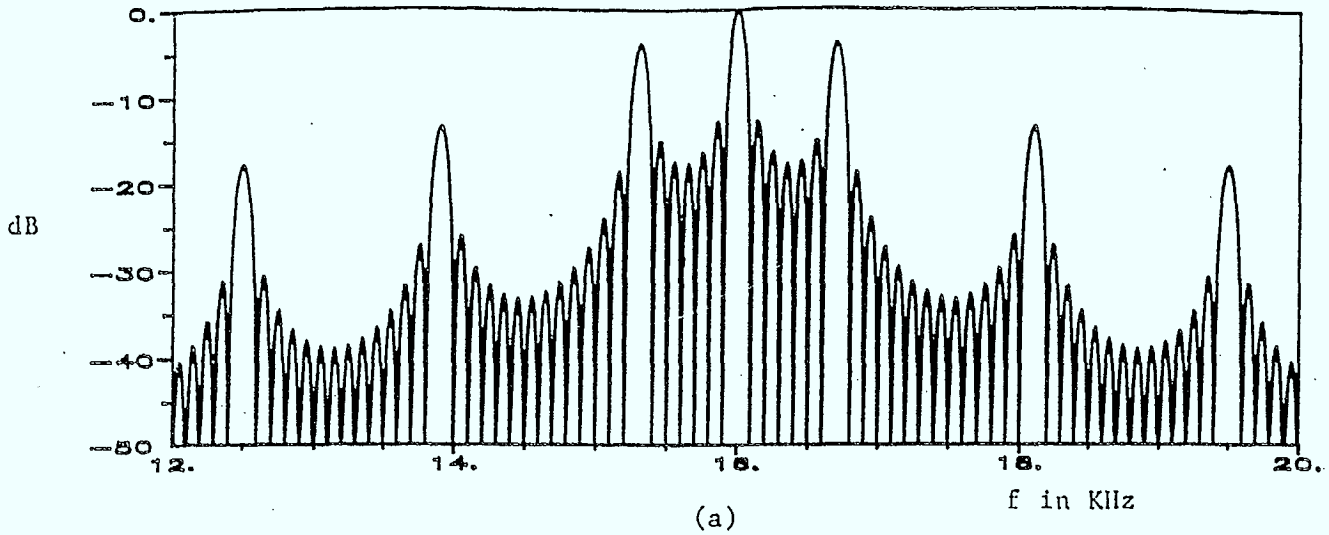

(a)

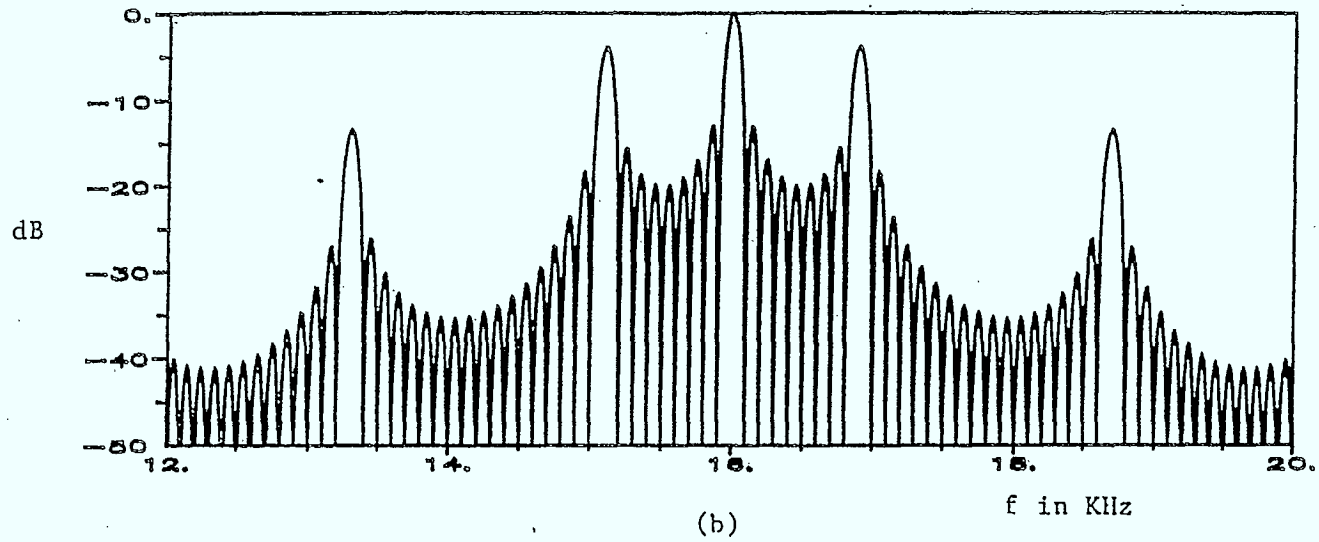

(b)

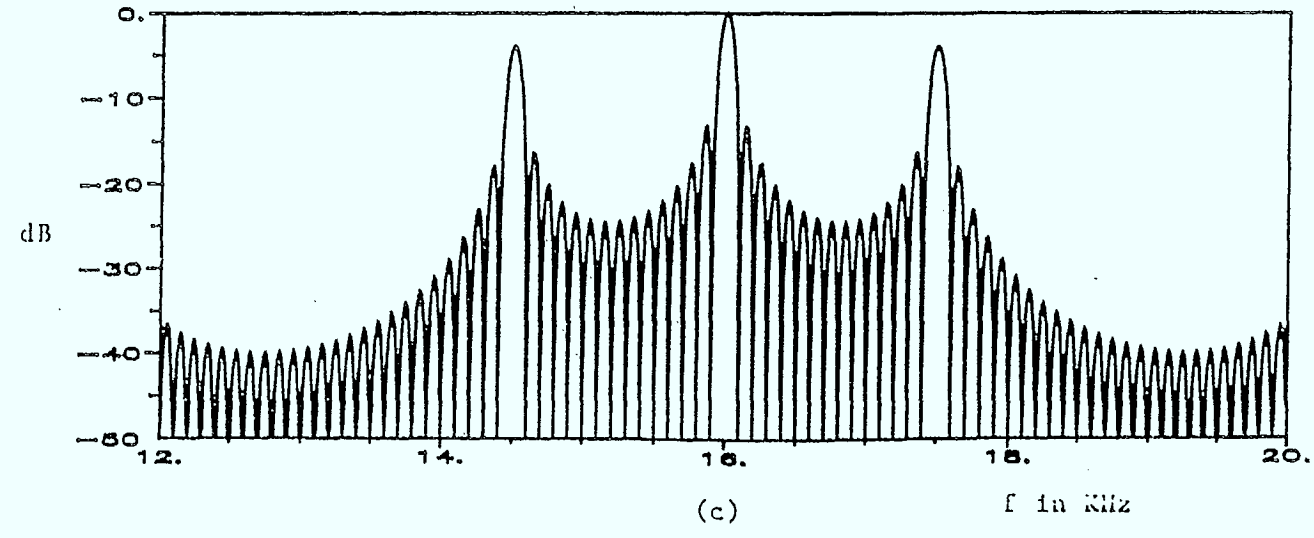

(c)

Fig. 4.5 Plot of $S_{IC}(f)$ for T = 1.42 ms (top), T = 1.11 ms (centre) and T = 0.67 ms (bottom) with d = 0.5, f_c' = 16 KHz, T_D = 10 ms and AdT/2 = 1.

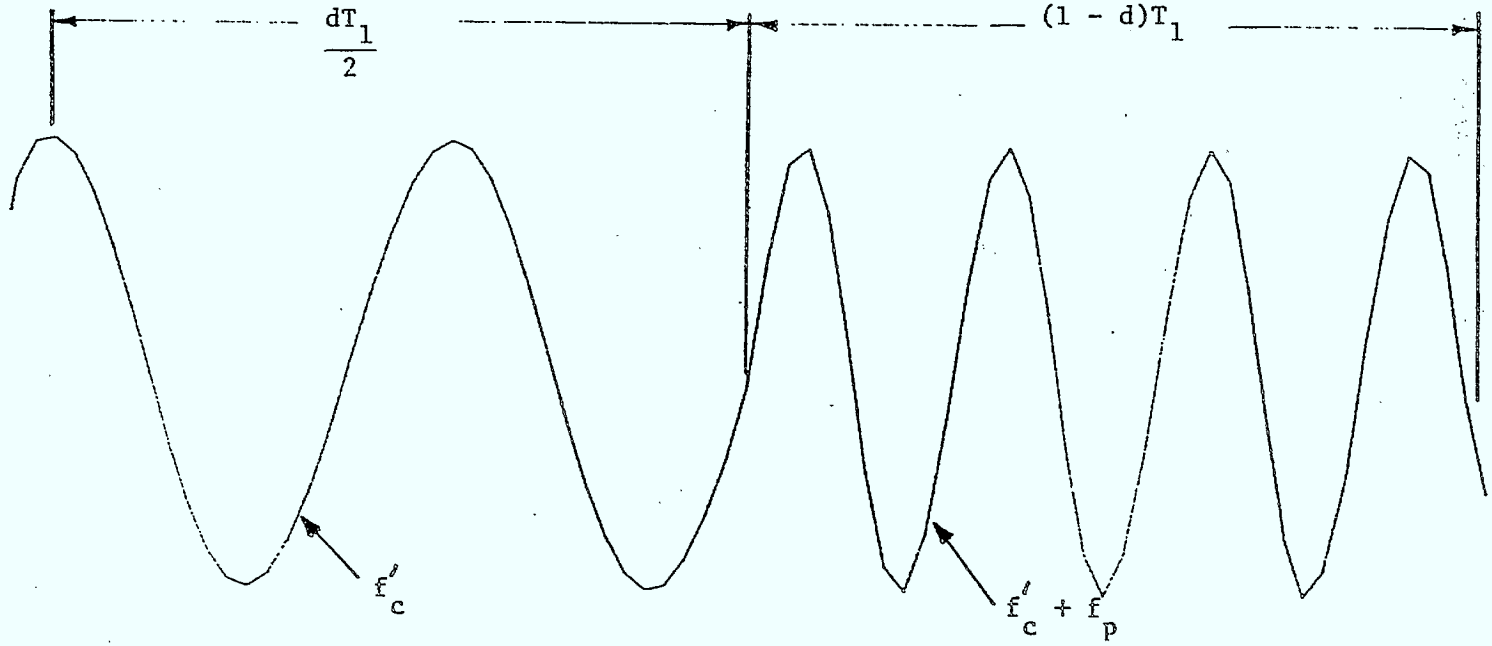

Fig 4.6 Phase shift produced by the two-frequency model.

$$S_{IC}(f) = \left[\frac{AdT}{2} \right]^2 \text{sinc}^2[(f - f_c')\, dT] \cdot \left\{ \frac{\sin\left(\pi(f - f_c')\, T_D\right)}{\sin\left(\frac{\pi(f - f_c')T_D}{N}\right)} \right\}^2 \tag{4.11}$$

From this expression, we see that the spectrum is the product of two relations, the first being the sinc function which has a peak at $f = f_c'$ and first nulls at $f_c' \pm 1/dT$. The second relation is the ratio of two sines which produces a multi-peak pattern with the peaks being located at $f = f_c' \pm (Nm/T_D)$, $m = 1, 2, 3, \ldots$. Figure 4.4 illustrates a plot of the two components and the overall relation for $(AdT/2) = 1$. Note that the bandwidth of the centre peak between nulls is $2/T_D$; thus, a more accurate measure of carrier frequency can be obtained simply by increasing the window length of data.

In Fig. 4.4c, we see that the peak at $f = f_c'$ is due to the carrier frequency while the peaks at other frequencies are due to the sidebands. This is demonstrated in Fig. 4.5 for three different values of T, which represent the beginning, middle and end of the frequency sweep of a typical ELT signal. In each case, the peak at $f = f_c'$ remains stationary while the sideband peaks move toward f_c' as T increases.

Unfortunately, this ideal spectrum does not accurately reflect the operation of actual ELT units since here the sidebands are symmetric in amplitude, while in practice, the sidebands are usually asymmetric. Thus, a modification to the model is required, which is discussed next.

4.4.2 Spectra for Non-Ideal Coherent Model ELT

For this case, it is assumed that the crystal controlled oscillator operates at frequency f_c' when the switch is closed and $f_c' + f_p$ when the switch is open, as illustrated in Fig. 4.6, due to the problems previously discussed. From eq. (4.2), the phase shift at the beginning of the second pulse when no frequency pulling is present is just

$$\theta_{2c} = 2\pi f_c' \left[\frac{dT_1}{2} + (1 - d)\, T_1 \right] \tag{4.12}$$

When frequency pulling occurs, the phase shift at the beginning of the second pulse is

$$\theta_{2p} = 2\pi f_c' \frac{dT_1}{2} + 2\pi (f_c' + f_p)(1-d)T_1 \tag{4.13}$$

Thus, the additional phase shift due to frequency-pulling is

$$\begin{aligned} \Delta\theta &= \theta_{2p} - \theta_{2c} \\ &= +2\pi f_p (1-d) T_1 \end{aligned} \tag{4.14}$$

Consequently, for the ith pulse, the total additional phase shift is

$$\Delta\theta_i = \sum_{j=1}^{i-1} 2\pi f_p (1-d) T_j; \qquad i = 2,3,4 \ldots N \tag{4.15}$$

Then,

$$F_{NC}(f) = \frac{Ad}{2} \sum_{i=1}^{N} T_i \, \mathrm{sinc}[(f-f_c')\, d\, T_i] \exp\{-j[2\pi (f-f_c')\, t_i - \Delta\theta_i]\} \tag{4.16}$$

If the duration of the signal processed is small compared to the total sweep, then T_i is nearly constant and eq. (4.8) applies. Thus, the simplified expression becomes

$$F_{NC}(f) = \frac{AdT}{2} \mathrm{sinc}[(f-f_c')\, dT] \cdot \sum_{i=0}^{N-1} \exp\left\{-j2\pi \left[(f-f_c')\frac{iT_D}{N} - f_p(1-d)\, iT\right]\right\} \tag{4.17}$$

Note $T = T_D/N$, define $f_s = f_p(1-d)$ to be the frequency shift and substitute into the summation in eq. (4.17). Thus,

$$F_{NC}(f) = \frac{AdT}{2} \cdot \mathrm{sinc}[(f-f_c')\, dT] \cdot \sum_{i=0}^{N-1} \exp\left\{-j\,2\pi \left[(f-f_c'-f_s)\frac{iT_D}{N}\right]\right\} \tag{4.18}$$

Computing the spectrum, we get

$$S_{NC} = \left[\frac{AdT}{2}\right]^2 \mathrm{sinc}^2[(f-f_c')dT] \cdot \left\{\frac{\sin[\pi(f-f_c'-f_s)T_D]}{\sin\left[\frac{\pi(f-f_c'-f_s)T_D}{N}\right]}\right\}^2 \tag{4.19}$$

Once again, we note that the spectrum is the product of two relations, the first being the sinc function and the second being the ratio of two sine functions. However, the sine functions now have a frequency shift f_s which shifts the multi-peak pattern, as illustrated in Fig. 4.7 for three different values of f_s.

Of considerable concern is the fact that the first nulls of the sinc function and the peaks of the sine relation can overlap as illustrated. The most serious occurrence of this takes place when

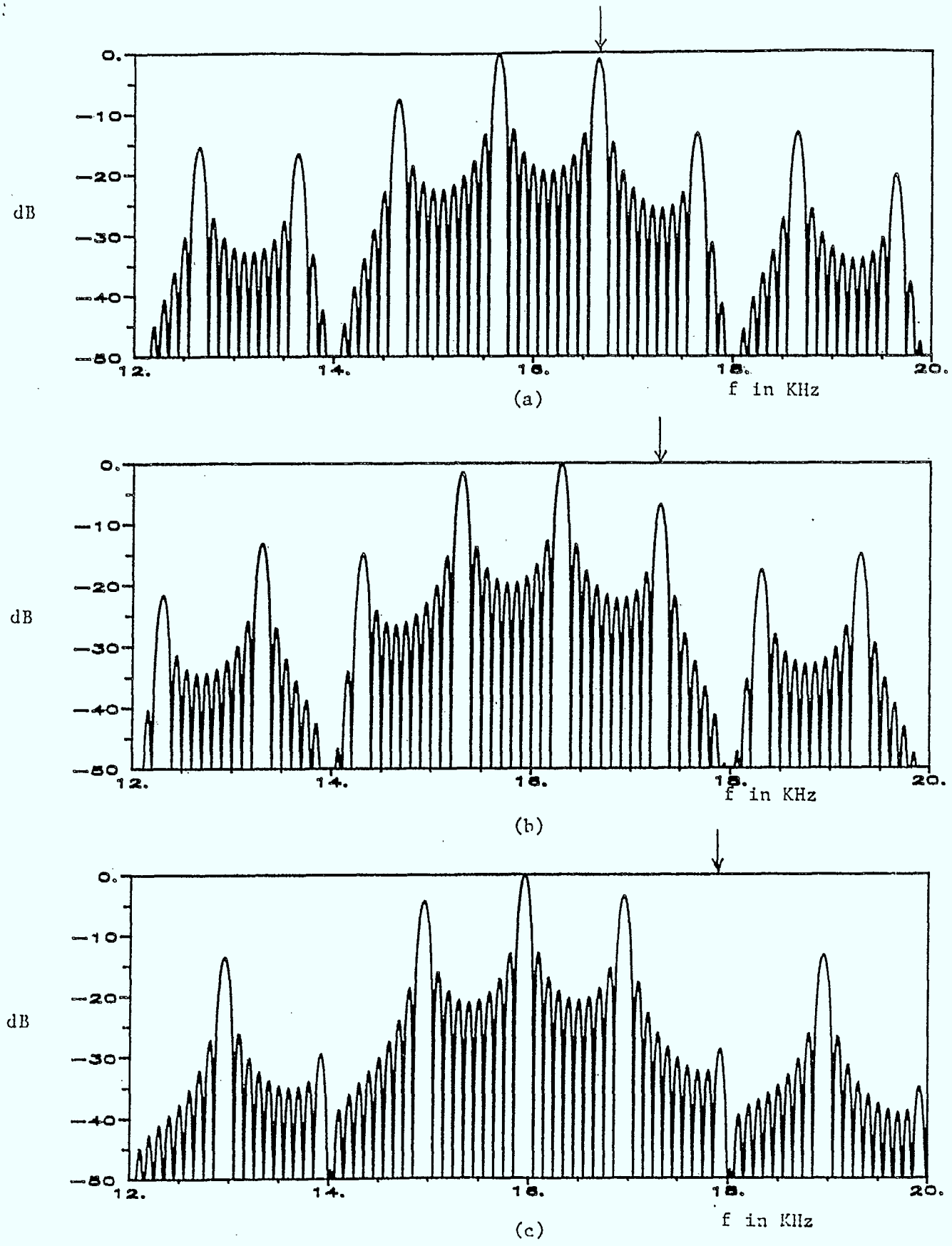

Fig. 4.7 Plot of $S_{NC}(f)$ for T = 1 ms, f_c' = 16 KHz, d = 0.5, T_D = 10 ms and f_s = 650 Hz (top), f_s = 1300 Hz (centre) and f_s = 1950 Hz (bottom). Note that the centre peak moves to the right as indicated by the arrow.

$$f - f_c' - f_s \Big|_{f = f_c' \pm \frac{1}{(dT)}} = 0 \tag{4.20}$$

since the carrier peak now coincides with the null of the sinc function. In this situation, carrier peaks are lost for a considerable portion of the sweep and one set of sidebands is enhanced while the other set is diminished.

Since $f_s = f_p(1-d)$, we find that the amount of frequency shift required to null the carrier peak is given by

$$f_p = \pm \frac{1}{d(1-d)T} \tag{4.21}$$

In order to evaluate the maximum permissible frequency shift for an actual ELT signal for nulling to occur, we evaluate eq. (4.21) using maximum values for both $d(1-d)$ and T. The first expression is maximum at $d = 0.5$ and, from Table 4.1, the maximum of T is $(1/300)\text{Hz}^{-1}$. This results in a value of $f_{p_{max}} = 1200$ Hz. Since, in practice, this value provides the upper bound, it is suggested that the total frequency change over the duration of the sweep be no more than 600 Hz (half the maximum or alternatively ± 300 Hz. Note that this is independent of carrier frequency.

4.4.3 Spectra for Non-Coherent Model

This model assumes the use of a crystal oscillator which is switched ON and OFF by the pulse modulation signal, as shown in Fig. 4.3. Note that this is completely different from the previous models in that here the oscillator is completely OFF between pulses; thus, there is absolutely no phase coherence between pulses.

In this case, the Fourier transform is given by

$$F_{NN}(f) = \sum_{i=1}^{N} \frac{Ad\,T_i}{2} \text{sinc}[(f - f_c')dT_i] \exp[-j(2\pi f t_i - \theta_i)]$$

where θ_i is assumed to be a uniformly distributed random variable between 0 and 2π. If the number of pulses is small, as before, the spectrum is

$$S_{NN}(f) = \left[\frac{AdT}{2}\right]^2 \text{sinc}^2[(f - f_c')dT] \sum_{i=1}^{N} \exp[-j(2\pi f t_i - \theta_i)] \tag{4.22}$$

which is not particularly useful. However, since θ_i is a random variable, we can evaluate the averaged spectrum through

$$S_{NA}(f) = E\{F_{NN}(f) \cdot F^*_{NN}(f)\}$$

$$= \left[\frac{AdT}{2} \right]^2 \text{sinc}^2[(f - f_c')dT] \cdot E \left\{ \sum_{i=1}^{N} \exp[-j(2\pi f t_i - \theta_i)] \sum_{k=1}^{N} \exp[-j(2\pi f t_k - \theta_k)] \right\}$$

$$= \left[\frac{AdT}{2} \right]^2 N \, \text{sinc}^2[(f - f_c')dT] \qquad (3.23)$$

since the expectation of the sum of all the products for $i \neq k$ is zero. We note here that the averaged spectrum has a shape which is $\text{sinc}^2[(f - f_c')dT]$, illustrated in Fig. 4.4a. This averaged spectrum is far broader than the previous spectra since the nulls are now at a frequency 1/(dT) above and below f_c. Thus, carrier frequency estimation for non-coherent ELT signals cannot easily be performed by use of a simple linear estimator such as Fourier transform.

4.5 COMPARISON OF REAL AND MODELLED ELT SPECTRA

Now that the ELT spectra are mathematically defined, it is useful to compute the spectra of computer generated ELT signals which represent the models developed and compare these spectra with those produced by real signals.

Using the Ideal Coherent Model ELT, an ELT signal with $d = 0.5$ has been generated with carrier frequency equal to $f_c' = 16.2$ KHz and the spectrum has been calculated by employing a set of 25 Blackman windowed 2048-point periodograms, as illustrated in Fig. 4.8. The dynamic range of each plot is 20 dB and approximately two sweeps of the ELT signal are provided. At the bottom of the plot is the averaged spectrum which is simply the normalized sum of the 25 periodograms.

This theoretical model can be compared with the actual spectra observed from two different manufactured ELT units. The first is a Pointer ELT which can be classed as coherent. Periodograms of the signal are plotted in Fig. 4.9 Again, the dynamic range is for

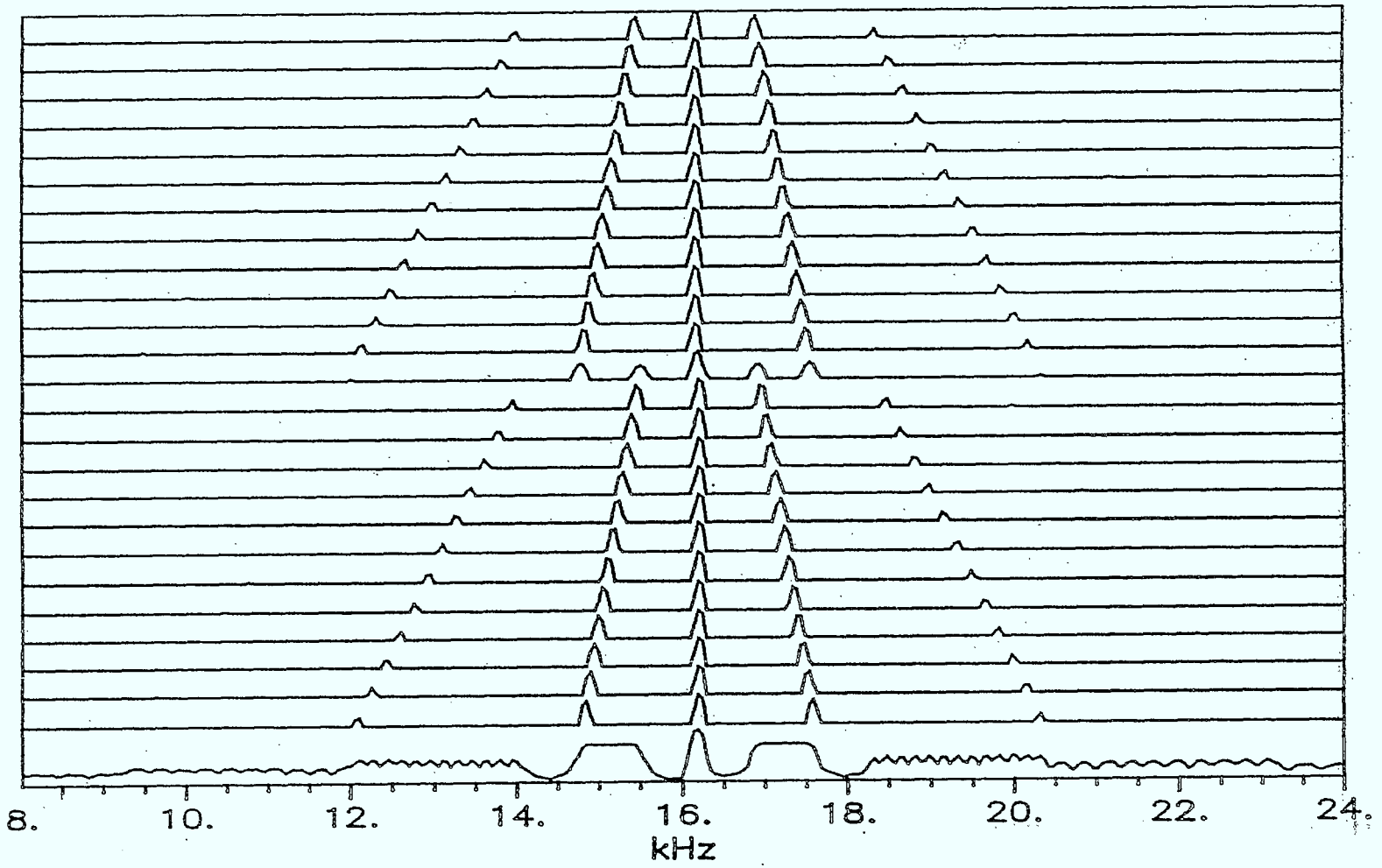

Fig. 4.8 Sequence of 25 consecutive Ideal Coherent ELT Model periodograms (bottom to top) with the averaged spectrum given at the bottom. For each of the 25 traces, T_D = 20 ms, d = 0.5 and f_c' = 16.2 KHz. Note the symmetry of the spectra around the 16.2 KHz centre frequency and the sweep of the modulation. The second upper and lower sidebands are reduced below the -20 dB threshold by the sinc^2 component of $S_{IC}(f)$.

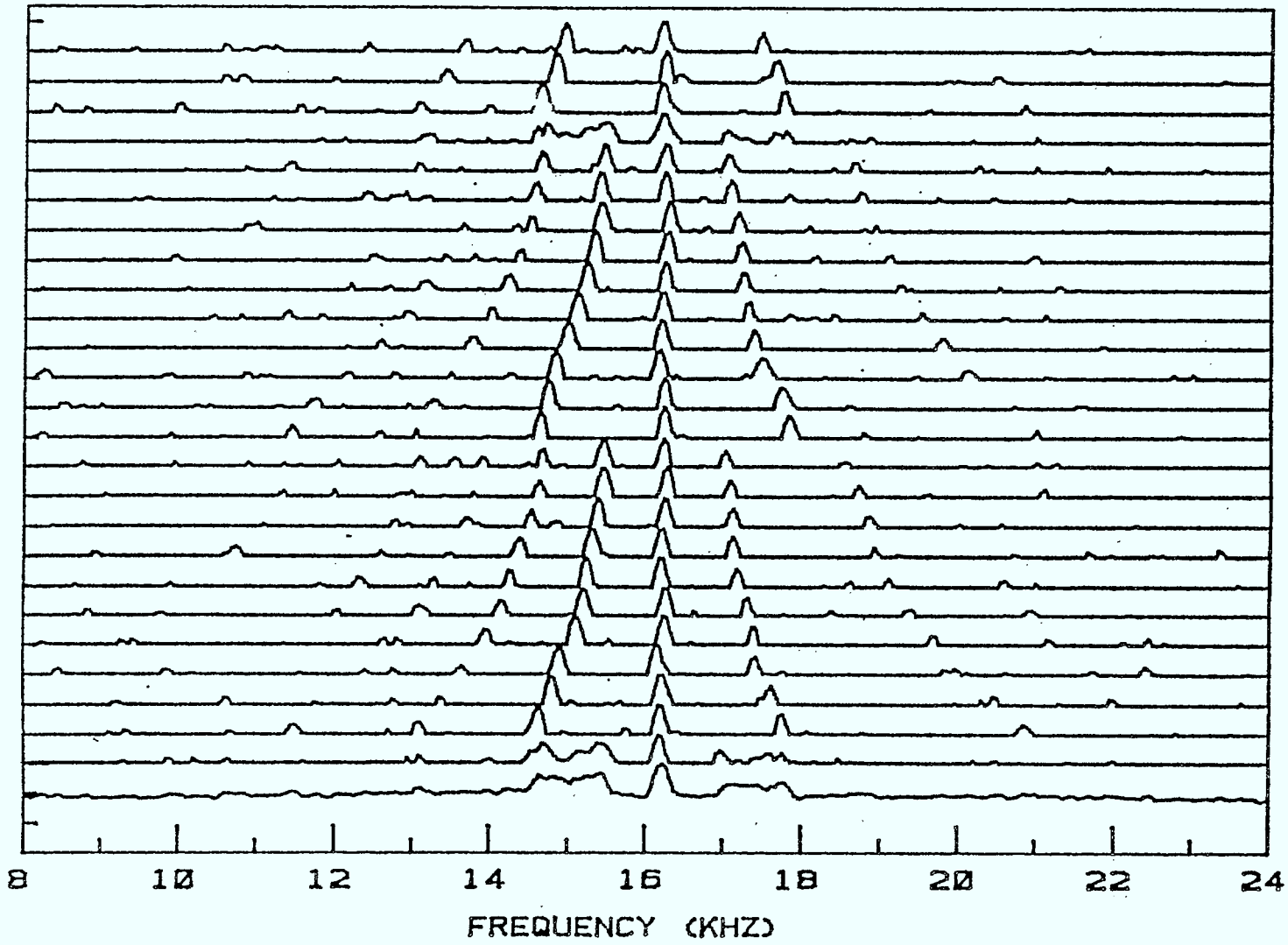

Fig 4.9 Sequence of 25 consecutive Pointer ELT periodograms with the averaged spectrum given at the bottom. Note the asymmetry of the sidebands around the 16.2 KHz centre frequency. For each trace T_D = 20 ms.

each plot is 20 dB and approximately two sweeps of the signal are present. We note that the amplitude of the sidebands of the Pointer ELT do not agree with the Ideal Coherent Model, however.

Using the Non-Ideal Coherent Model, we plot the spectra for $f_c' = 15.7$ KHz and $f_p = 1$ KHz with $d=0.5$, as shown in Fig. 4.10. Comparing with Fig. 4.9, we note that the agreement is remarkable in that the carrier is at constant frequency and the first upper and lower sidebands slide reasonably smoothly toward the carrier with time. In addition, the first lower sideband in both the modelled signal and the real signal is considerably stronger than the first upper sideband. The second upper sideband is nearly absent in both and the third upper sideband is quite prominent in both. The lower second and third also are in agreement. Finally, we note close agreement in the averaged spectra.

The second coherent ELT examined is the Garrett ELT. Periodograms for this ELT are given in Fig. 4.11. Since the amplitudes of the first sidebands are unequal, the Ideal Coherent Model is inadequate. However, by using the Non-Ideal Coherent Model with $f_c' = 16.75$ KHz, $f_p = -0.5$ KHz, and $d=0.36$, we obtain the plots of Fig. 4.12. Again, we see that the agreement is good in that the carrier remains constant and the first upper and lower sidebands are well defined. The upper second sidebands are both well defined and the lower second sidebands are both diminished. The averaged spectra are in good agreement.

We now examined the spectra for the Narco ELT in Fig. 4.13. In this case, it appears that carrier component of the spectrum is nulled at a frequency approximately two-thirds along the sweep. Using the Non-Ideal Coherent Model with $f_c' = 17.5$ KHz, $f_p = 4$ KHz, and $d=0.5$, we plot Fig. 4.14 and once again obtain excellent agreement with the actual signal. Note that the averaged spectra in both cases indicates a large amount of the power in the lower sideband while the carrier component is weakened. Clearly, this condition should be avoided if automated spectral estimation techniques are to be employed.

Finally, we generate a Non-Coherent Model ELT signal by using phase randomization for each of the signal pulses. The signal plot is given in Fig. 4.15 where we see

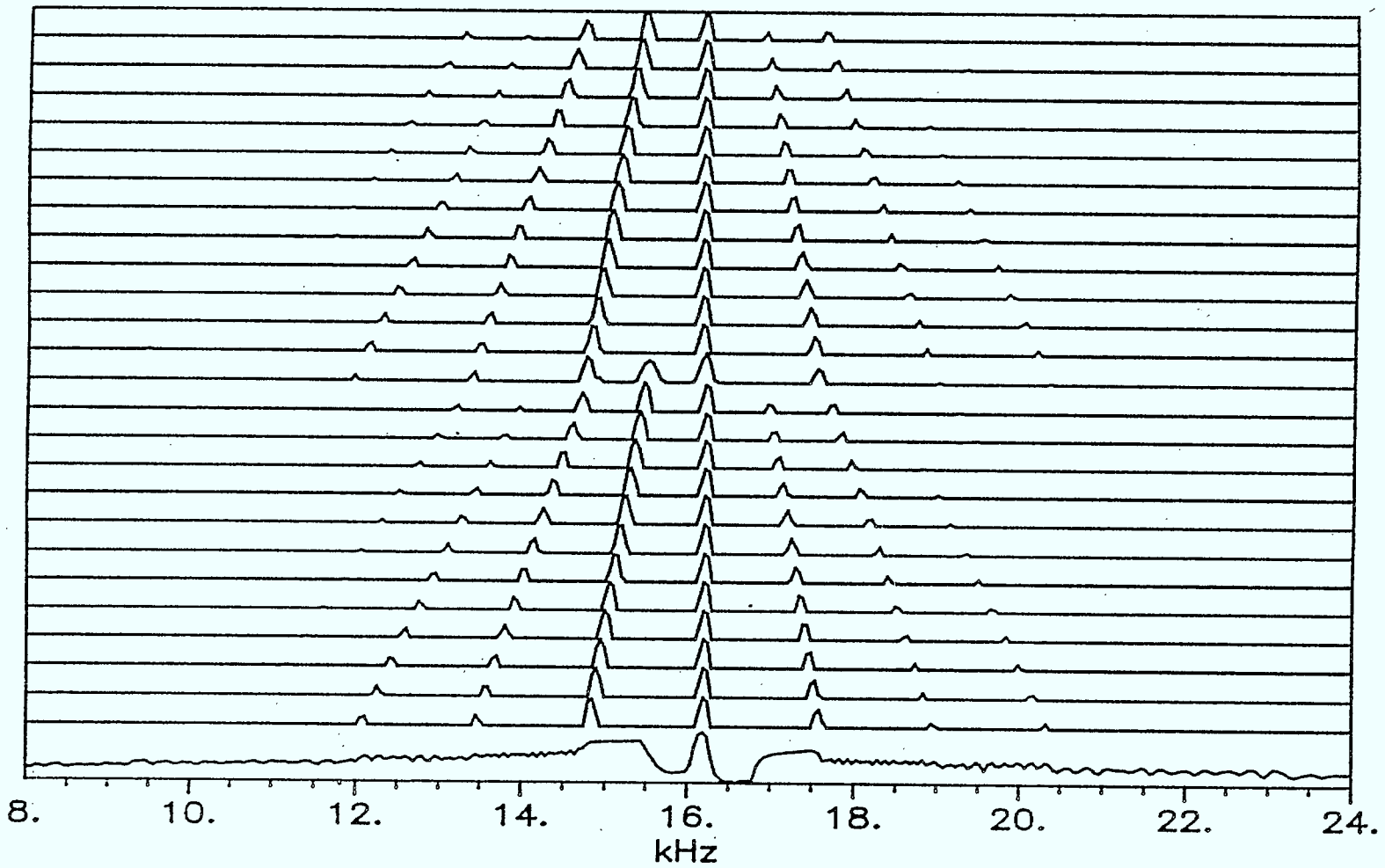

Fig. 4.10 Sequence of 25 consecutive Non-Ideal Coherent ELT Model periodograms with the averaged spectrum at the bottom. By choosing $f_c' = 15.7$ KHz and $f_p = 1$ KHz an asymmetry is produced which corresponds more closely to the observed Pointer ELT spectra. For each trace, $T_D = 20$ ms and $d = 0.5$.

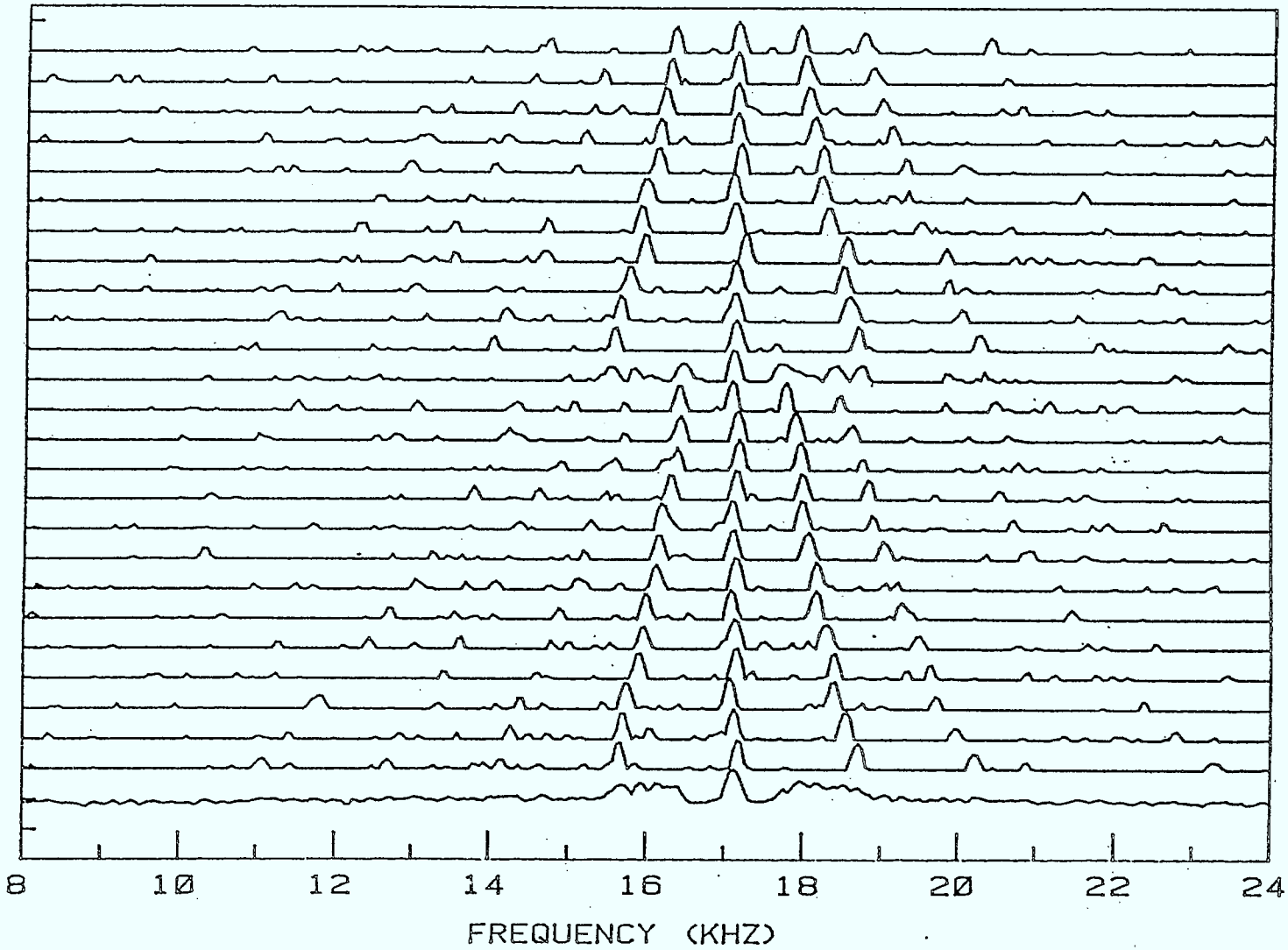

Fig. 4.11 Sequence of 25 consecutive Garrett ELT periodograms with the averaged spectrum given at the bottom. Note that the lower second sideband nearly disappears. For each trace, T_D = 20 ms.

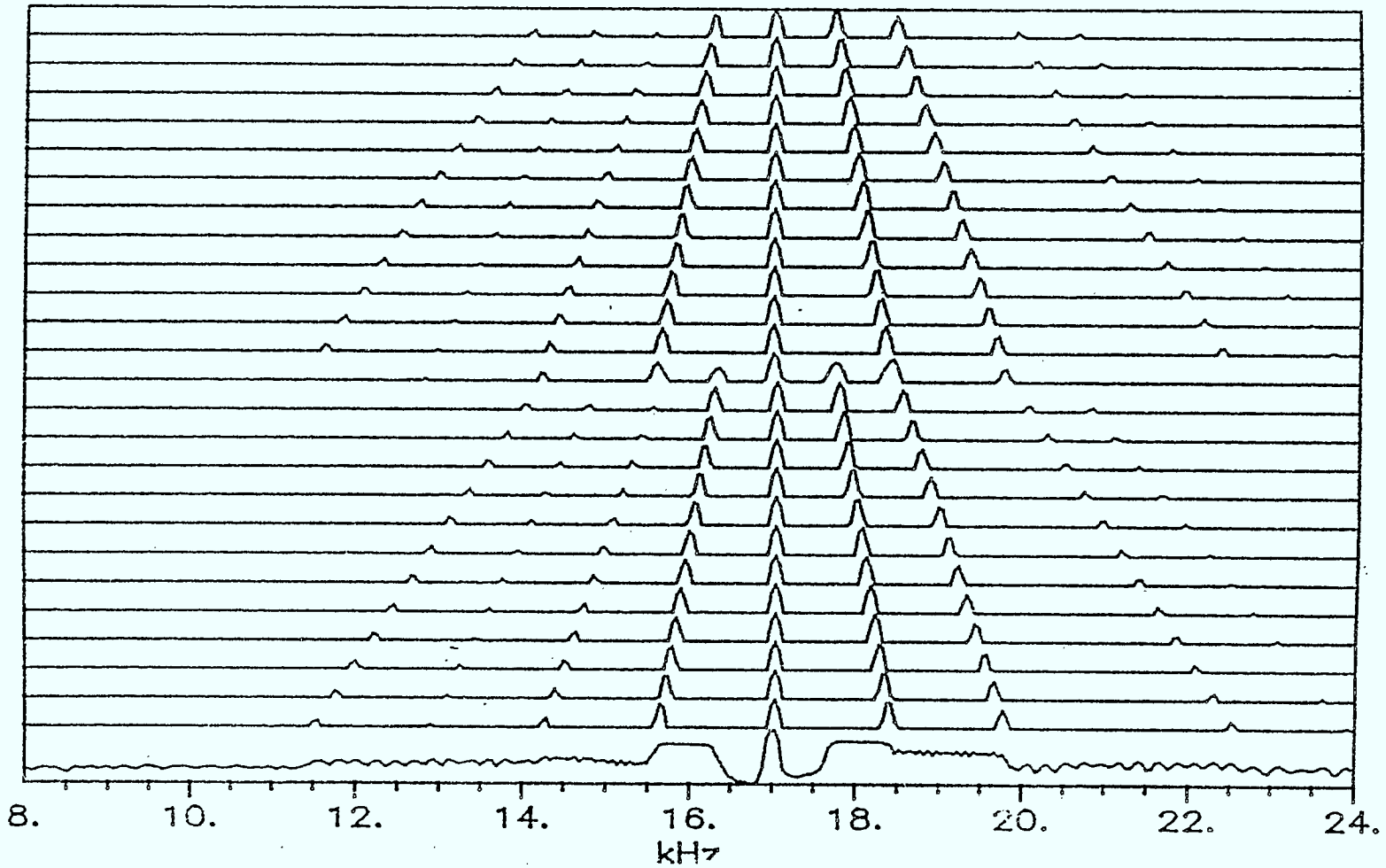

Fig. 4.12 Sequence of 25 consecutive Non-Ideal Coherent ELT Model periodograms with the averaged spectrum at the bottom. By choosing $f_c' = 17.35$ KHz, f_p = = −0.5 KHz and d = 0.36, the spectral waveforms are found to agree well with the observed Garrett spectra. For each trace, $T_D = 20$ ms.

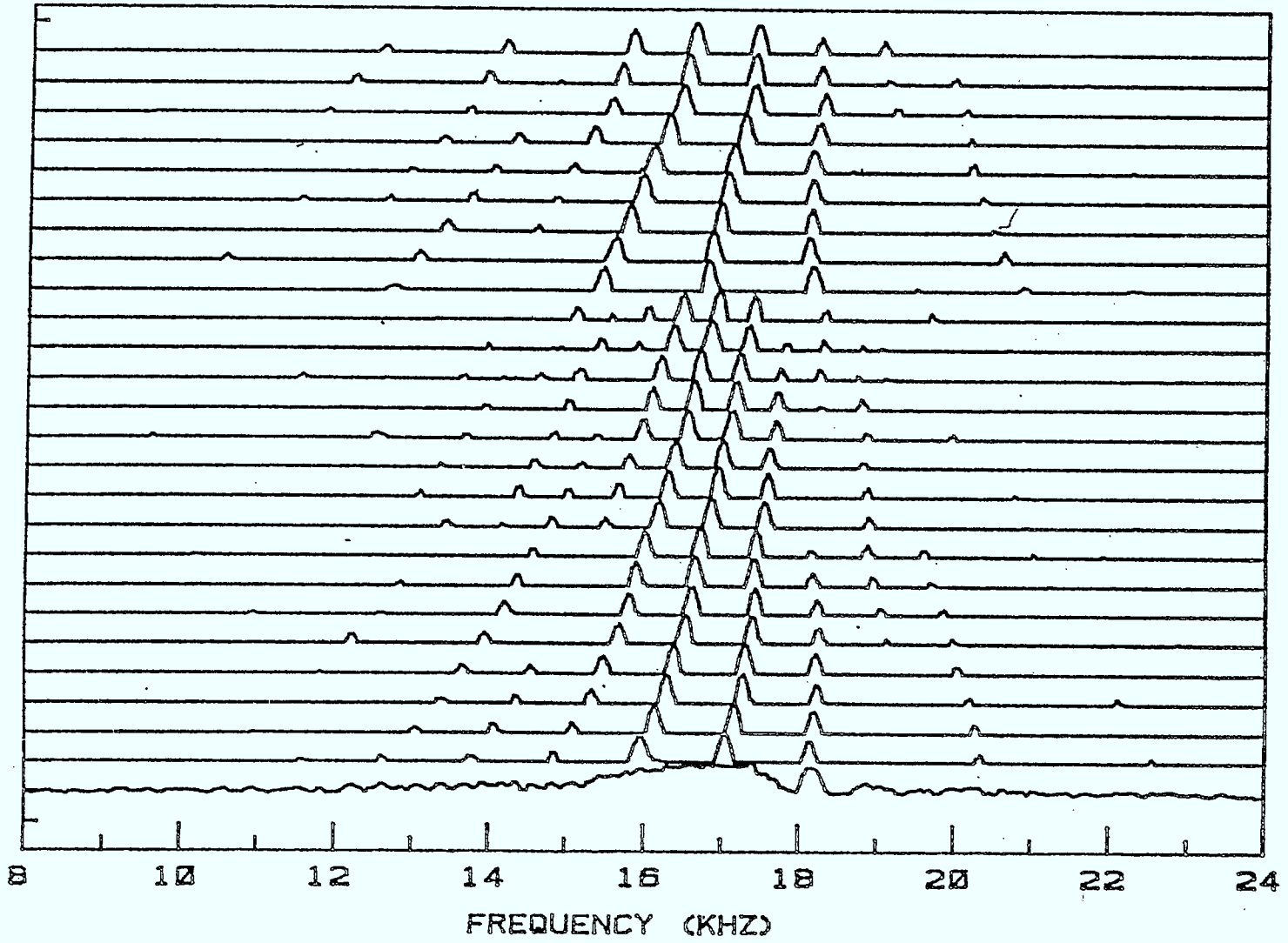

Fig. 4.13 Sequence of 25 consecutive Narco ELT periodograms with the averaged spectrum at the bottom. Note that the carrier peak at 18.1 KHz disappears for a considerable portion of the time. For each trace, T_D = 20 ms.

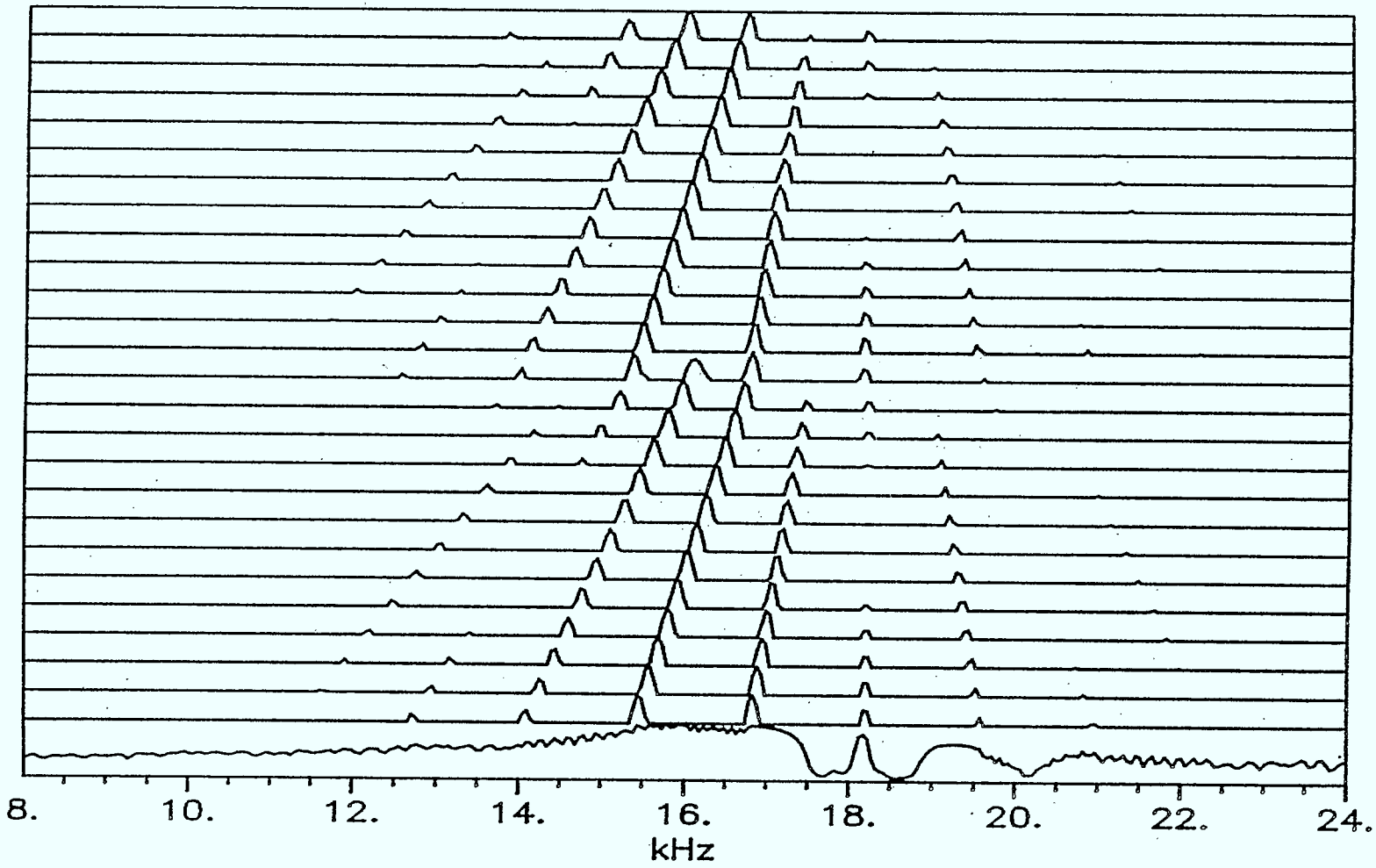

Fig. 4.14 Sequence of 25 consecutive Non-Ideal Coherent ELT Model periodograms with the averaged spectrum at the bottom. By choosing f_c = 16.2 KHz, f_p = 4 KHz and d = 0.5, the spectral waveforms produce a spectrum which closely represents the Narco spectrum. For each trace, T_D = 20 ms.

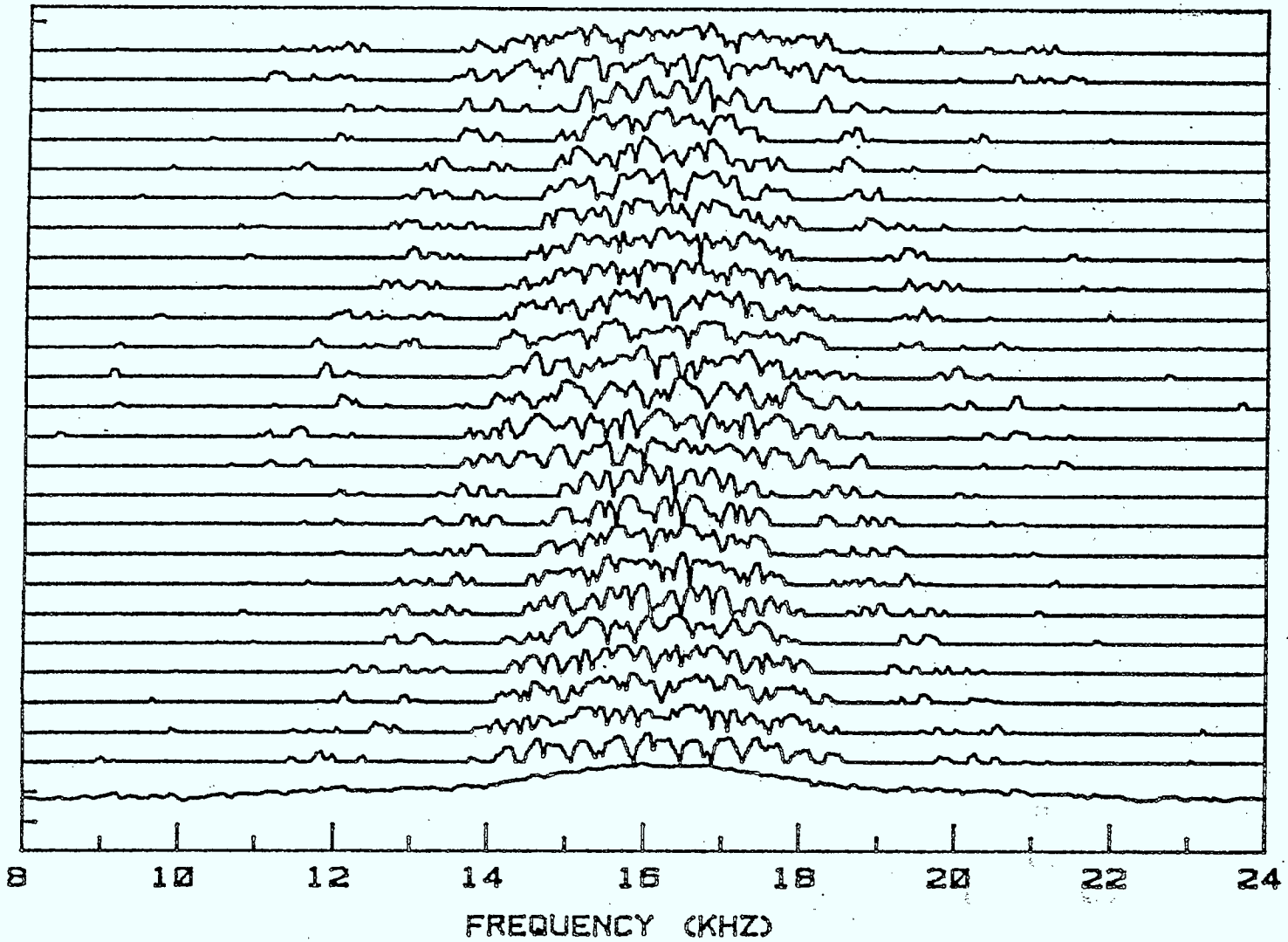

Fig. 4.15 Sequence of 25 consecutive Non-Coherent ELT Model periodograms with the averaged spectrum at the bottom. Here we see a very broad averaged spectrum which is difficult to process for carrier frequency measurement. For each case, T_D = 20 ms.

that the individual periodograms have a very wide bandwidth. Comparing the averaged spectrum with the prediction of Fig. 4.4a, we again find close agreement. Thus, if automatic spectral estimation techniques are to be employed, this design for ELT signals should be avoided at all costs.

4.6 EFFECTS OF DOPPLER SHIFT

The effect of changing doppler frequency shift can be calculated exactly; however, the analysis becomes involved as is now demonstrated.

We can assume the doppler shift over a short period of time (say 1 to 2 s) is a linear function of time given by

$$f_d = f_{do} + k \cdot t \tag{4.24}$$

where k is a constant.

Then substituting into equation (4.2), we obtain

$$\begin{aligned} s_i(t) &= A \cos[2\pi (f_c' t + k t^2) + \theta_i]; \quad t_i - \frac{dT_i}{2} \le t \le t_i + \frac{dT_i}{2} \\ &= 0 \qquad \text{otherwise}. \end{aligned} \tag{4.25}$$

The Fourier transform for the first pulse is then given by

$$\begin{aligned} F_1(f) &= \int_{-\frac{T_1}{2}}^{\frac{T_1}{2}} s_1(t)\, e^{-j2\pi ft} dt \\ &= \frac{A}{2} \int_{-\frac{T_1}{2}}^{\frac{T_1}{2}} \cos\left[2\pi ((f_c' - f)t + kt^2) + \theta_1\right] dt \\ &\quad + j\frac{A}{2} \int_{-\frac{T_1}{2}}^{\frac{T_1}{2}} \sin\left[2\pi ((f_c' - f)t + kt^2) + \theta_1\right] dt \end{aligned} \tag{4.26}$$

where the negative frequency axis terms have been discarded.

Now, from integral tables we have [40]

$$G(x) = \int \cos(ax^2 + bx + c)\,dx =$$

$$\sqrt{\frac{\pi}{2a}} \left\{ \cos\left(\frac{ac-b^2}{a}\right) \bullet C\left(\frac{ax+b}{\sqrt{a}}\right) - \sin\left(\frac{ac-b^2}{a}\right) \bullet S\left(\frac{ax+b}{\sqrt{a}}\right) \right\} \tag{4.27}$$

and

$$H(x) = \int \sin(ax^2 + bx + c)\,dx =$$

$$\sqrt{\frac{\pi}{2a}} \left\{ \cos\left(\frac{ac-b^2}{a}\right) \bullet S\left(\frac{ax+b}{\sqrt{a}}\right) + \sin\left(\frac{ac-b^2}{a}\right) \bullet C\left(\frac{ax+b}{\sqrt{a}}\right) \right\} \tag{4.28}$$

where

$$C(x) = \sqrt{\frac{2}{\pi}} \int \sin^2 x\,dx$$

$$= \text{Fresnel's cosine} - \text{integral}$$

$$S(x) = \sqrt{\frac{2}{\pi}} \int \cos^2 x\,dx$$

$$= \text{Fresnel's sine} - \text{integral}.$$

The spectrum for N pulses would then be computed by

$$S(f) = \left(\frac{A}{2}\right)^2 \left\{ \sum_{i=1}^{N} [G(x) + H(x)] \Bigg|_{-\frac{T_i}{2}}^{\frac{T_i}{2}} \right\}^2$$

with $a = 2\pi k$

$b = 2\pi (f_c' - f)$

$c = \theta_i$

At this point it is clear that no simple relationships exist which will provide further insight. Thus, we attempt another approach.

From equation (4.19), we note that the spectrum for a non-ideal coherent signal has a well defined carrier peak at frequency $f = f_c' + f_s$. To a first approximation, the sine

function is constant and the sine function in the denominator varies N times more slowly than the sine function in the numerator.

Thus, approximately,

$$S_{IN} = \left(\frac{AdT}{2}\right)^2 \sin^2 \pi (f - f_c' - f_s) T_D \tag{4.29}$$

For a set of L different doppler shifts, the averaged spectrum is given by

$$S_{AV} = \left(\frac{AdT}{2}\right)^2 \sum_{p=0}^{L-1} \sin^2 [\pi (f - f_c' - f_s - pf_d') T_D] \tag{4.30}$$

where f'_d = change in doppler frequency shift in Hz per second.

In this case we simply have a set of carrier peaks with each peak being shifted by an amount $f_d' T_D$, as illustrated in Fig. 4.16. For L separate doppler shifts, we see that the measured L_{3db} bandwidth is

$$B_3 = (L-1) f_d' T_D + \frac{1}{2T_D} \tag{4.31}$$

For an ELT with perfect carrier stability, the amount of doppler shift present in the measured 3dB bandwidth can thus be determined by simply measuring the averaged bandwidth over a duration LT_D and then computing f_d' from the relation

$$f_d' = \frac{B_3 - \frac{1}{2T_D}}{(L-1) T_D} \tag{4.32}$$

Note the T_D is the window duration for a single periodogram.

Since the ELT in practice does not possess perfect carrier stability, it is necessary to take account of this instability.

4.7 BANDWIDTH OF UNSTABLE CARRIER ELT

Originally, it was assumed that the carrier frequency of the ELT had perfect stability. In practice, the carrier frequency is given by

$$f_c = f_{co} + f_{cd} + f_{cj} \tag{4.33}$$

where f_{co} = constant frequency carrier term

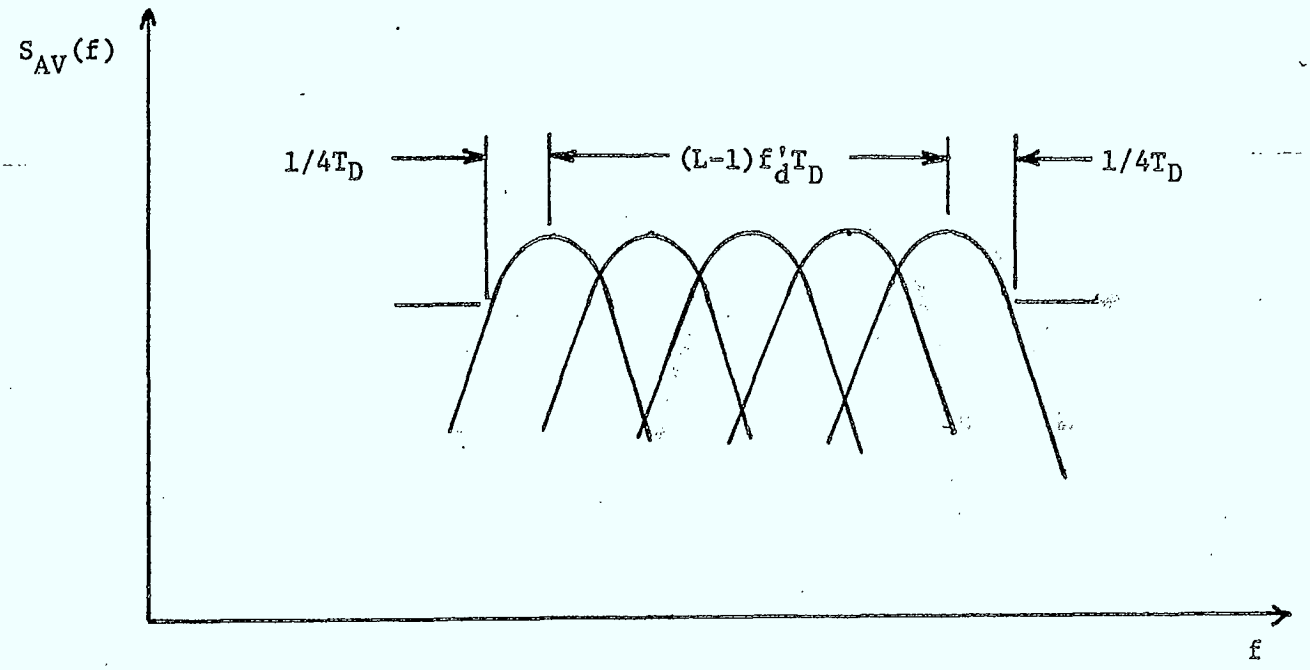

Fig. 4.16 3 dB bandwidth measurement of a coherent doppler shifted ELT signal for L separate intervals of T_D.

f_{cd} = frequency drift term

f_{cj} = frequency jitter term.

The spectrum produced with $f_c = f_{co}$ has already been computed exactly and the case when linear frequency shift occurs has been approximated by considering doppler shift.

For the case of frequency jitter, it is assumed that the long term variation is Gaussian. Consequently, for coherent ELT signals, we note he following:

1) By using long window lengths, the effects of window duration on the bandwidth becomes negligible.

2) Assuming window length does not contribute to the bandwidth, the measured bandwidth is proportional to the total duration of the measurement.

3) The effects of jitter on the carrier frequency of an ELT signal produce a constant valued increase to the total measured bandwidth which is independent of the duration of the measurement.

4) For identification to be possible, the effects of noise in these determinations must be negligible.

Thus, the overall bandwidth of the signal is given by

$$B_T = (L-1)\, f_d'' T + 1/2T_D + B_E \tag{4.34}$$

where

B_T = total 3 dB bandwidth of the measured signal.

B_E = bandwidth contribution produced by jitter.

f_d'' = total of the change in doppler shift and change in ELT carrier frequency due to drift, in Hz per second.

The value of B_E is a characteristic of the ELT signal itself and can be determined in a practical way by simply computing the averaged periodograms in two or more consecutive time intervals. We note that the change in centre frequency is a measure of the sum of the drift in the ELT frequency and the doppler shift which in turn provides f_d''. By computing the average 3 dB bandwidth of the two or more measurements, we obtain B_T. Thus, B_E can be

calculated using equation (4.34). From a practical standpoint, using long window lengths of data (larger values of T_D) given fixed total signal duration (LT_D), gives better results since the $1/2T_D$ term becomes negligible.

Three examples of this are given for real satellite pass data in Figure 4.17 for signals A, B and C. The average of 13 8K-periodograms is taken for three consecutive 1 s durations with the interval between the first two being 4 s and the interval for the last two being 5 s. For signal A, we find that the total 3 dB bandwidth is about 20 Hz and the frequency change from plot to plot is approximately 25 Hz with the average interval being 4.5 s ($f_d'' = 25/4{,}5$ Hz/s). Since there are 13 periodograms computed for each 1 s estimate, $T_D = 1/13$ s and $L = 13$. Substituting in eq. (4.34) we get:

$$B_T = 20 \text{ Hz} = (12 \times 25) / (4.5 \times 13) + 12/3 + B_E$$

or

$$B_T = 8.3 \text{ Hz}.$$

Thus, the bandwidth of signal A is 8.3 Hz and this is, to a first approximation, independent of doppler shift and ELT carrier drift.

For signals B and C, the same analysis can be applied resulting in bandwidths of 18.5 Hz and 88 Hz, respectively. We note that for signal B, the change in doppler shift and drift frequency are negligible and only the window effect remains. For signal C, the change in doppler frequency is slightly higher than for signal A, and the bandwidth is very much higher. Thus, using signal bandwidth, three different signals have been labeled and the differences between their bandwidths (8.4 Hz, 18.5 Hz and 88 Hz) are measurable.

4.8 ELT SIDEBAND RECOGNITION

There are several different possible methods for measuring the sidebands of ELT signals. These include one-shot sideband detection, matched filter sideband detection, and averaged sideband detection. Each method is described in detail with the associated advantages and disadvantages.

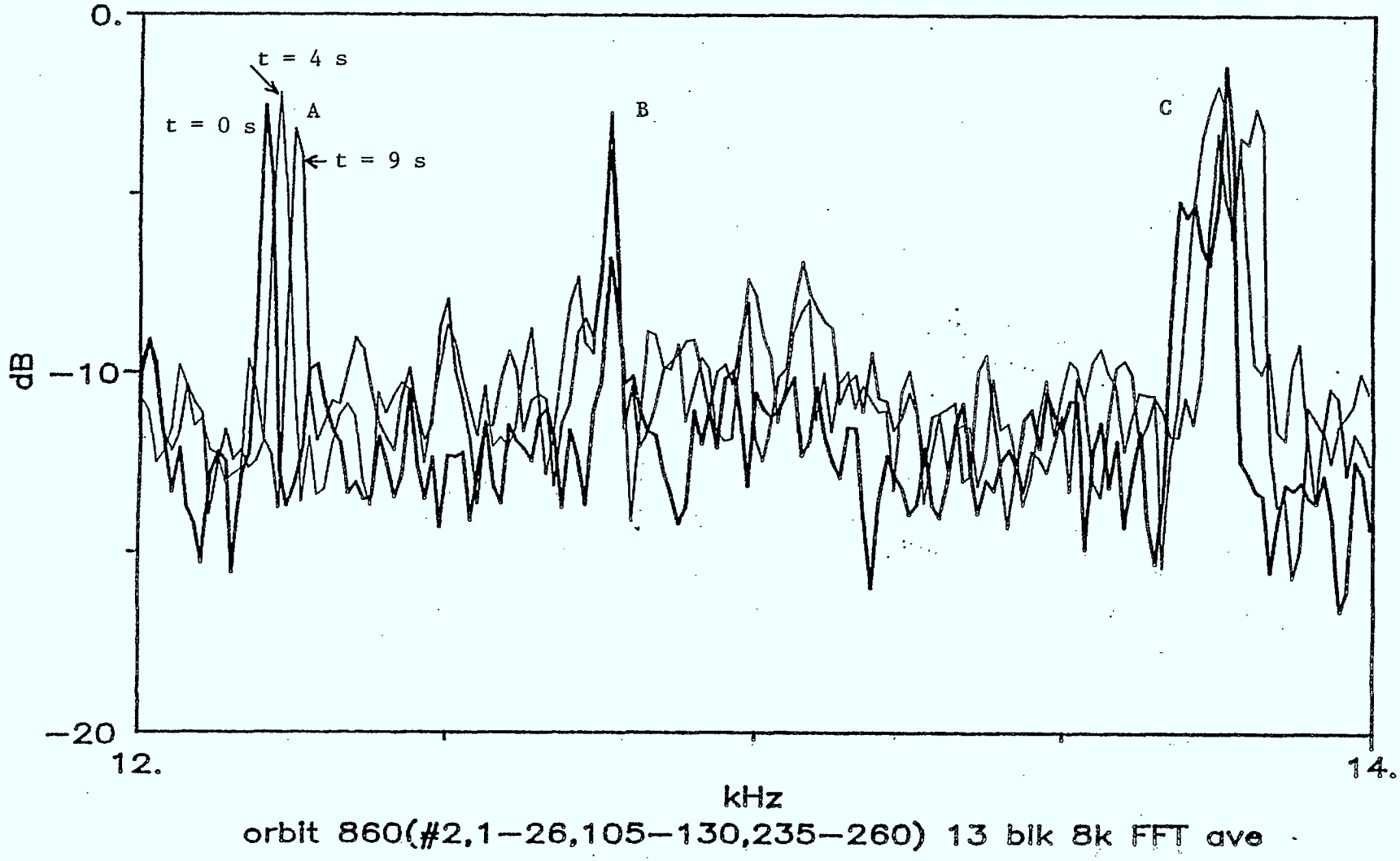

Fig. 4.17 Averaged spectra for three one-second durations separated in time as shown.

4.8.1 One-Shot Sideband Detection

One-shot sideband detection assumes the use of a periodogram or MEM spectral estimate. By applying a threshold to the spectral estimate, it is possible to locate the peaks of the spectrum, as illustrated in Fig. 4.18. The main advantage of this method is that detailed information of ELT sweep would be abailable. The actual characteristic of sweep frequency as a function of time would be deduced which would then lead to an extremely accurate identifier. However, the implementation is a major problem for this method since in the multi-peak environment, relating sideband peaks of carrier peaks appears to be nearly impossible in a practical sense. Furthermore, with the background noise, there is little chance of separating the sideband peaks from the noise peaks.

4.8.2 Matched Filter Sideband Detector

Matched filter sideband detection again assumes the use of a periodogram or MEM spectral estimate. This time, however, a search is made for a specific characteristic by using a replica correlator, as shown in Fig. 4.19. We note that theoretically, the sidebands of an ELT signal occur at regular multiples of N/T_D. Thus, a multiplying replica can be applied to any periodogram or MEM spectrum and the frequency offset, f_{OFF}, adjusted over the expected range of modulation frequencies. Peaks in the correlator output indicate sideband frequencies. Since sidebands due to other signals are unlikely to fall symmetrically about f_{OFF}, the method promises far better performance than the One-Shot Sideband Detector.

When noise is present, the noise peaks will pass through the correlator and provide an output which will compete with the actual sidebands. For strong signals, this may be serious and, consequently, a detailed record of the modulation characteristic would be obtained.

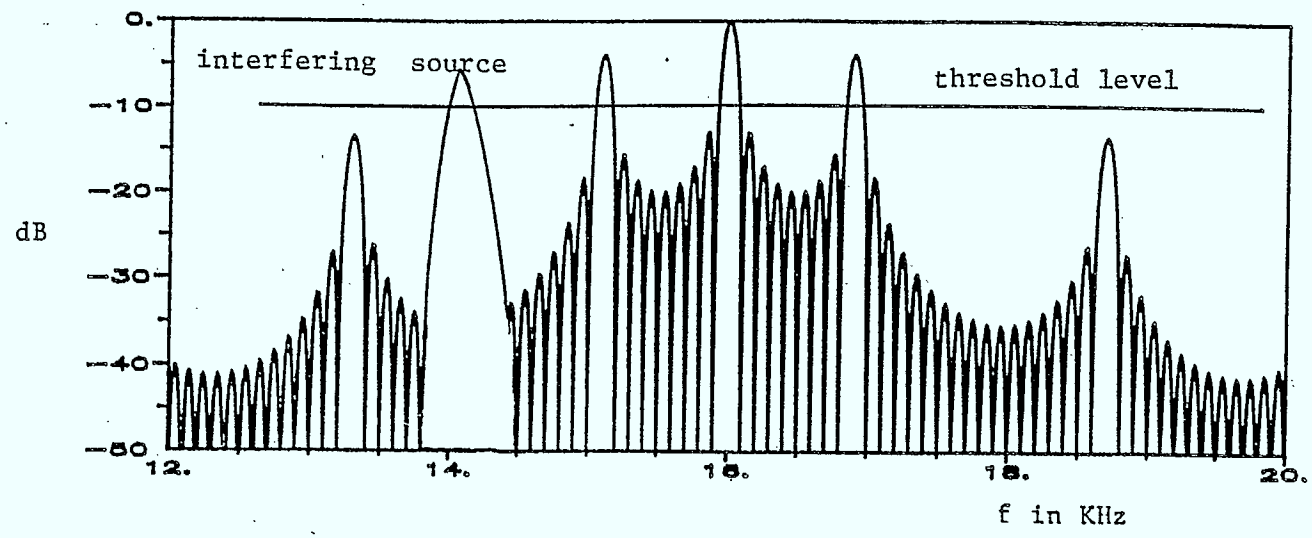

Fig. 4.18 One-shot sideband detection using a threshold. Note that the interfering source can cause errors in the measurement.

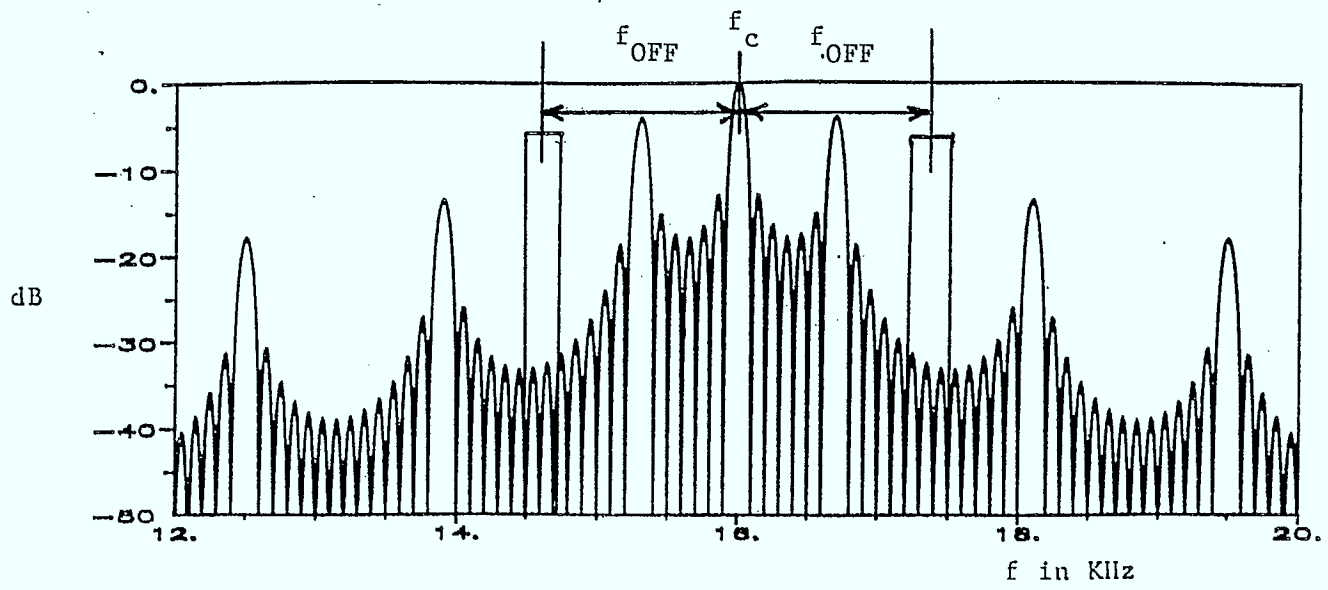

Fig. 4.19 Matched filter sideband detection. The sweeping gates are used to provide a correlation of sideband location.

4.8.3 Averaged Sideband Detection

Averaged sideband detection assumes the use of the average of a significant number of periodograms. The main advantage of this technique is that it gives useful information in a noisy background. The biggest disadvantage is that the information is incomplete since the sweep duration cannot be determined.

The averaged spectra have been computed for three different manufactured ELT unit signals. For the Pointer ELT, we see in Fig. 4.20, that the averaged sidebands are well defined and give an accurate estimate of the sweep width of the modulation. Since the lower and upper sweep bandwidths may be unequal, we designate them with B_1 and B_2. Furthermore, the combination of the carrier peak followed by deep nulls on both sides of the carrier and flat 'plateaus' should prove to be an effective identifier of an ELT signal. Signal identification is furthered by noting the relative amplitude between the carrier peak and the first sideband plateaus, R_1 and R_2.

The averaged spectra are obtained for the Garrett and Narco ELT signals, as shown in Fig. 4.21 and 4.22, respectively. For the Garrett, the spectrum is much like the Pointer in form although the relative heights of the sidebands with respect to the centre peak are different. The Narco demonstrates its own peculiar spectrum which is quite distinctive.

For comparison, the averaged specta are also computed for the modelled signals and given in Fig. 4.23 to 4.25 for the Pointer, Garrett and Narco, respectively. It is seen that the agreement is generally good. The averaged spectrum for the non-coherent ELT is plotted in Fig. 4.26 for completeness.

4.8.4 Correlated Sweep Duration

As mentioned in Section 4.8.3, sweep duration T cannot be measured by computing the averaged spectrum. However, an ingenious technique, first suggested by Mr. R. Renner of Canadian Astronautics Limited, has been tested and found to be highly effective. Essentially, the method is based on first locating a carrier peak in the averaged spectrum, as illustrated in

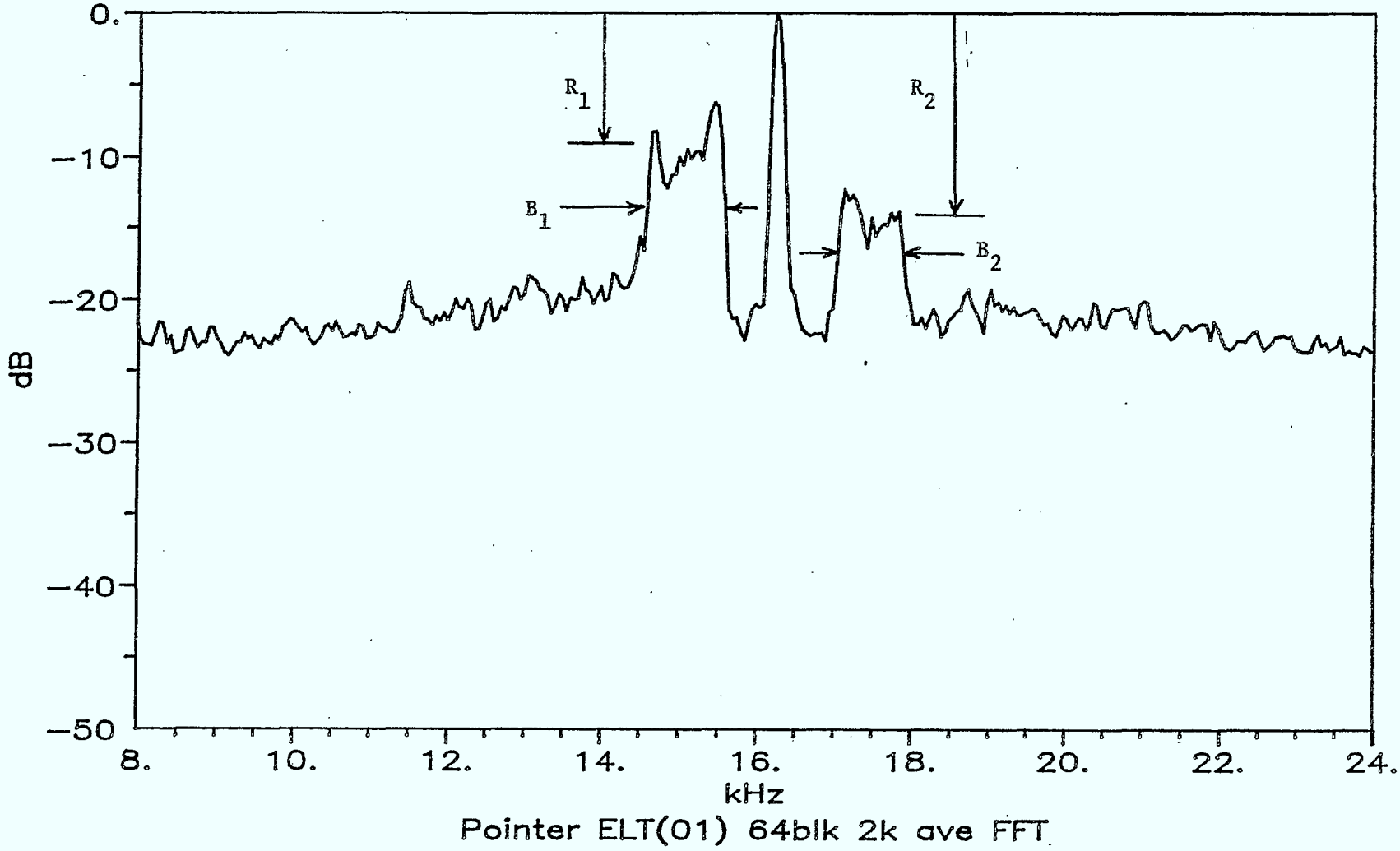

Fig. 4.20 Averaged spectrum for Pointer ELT illustrating B_1, B_2, R_1 and R_2 measures.

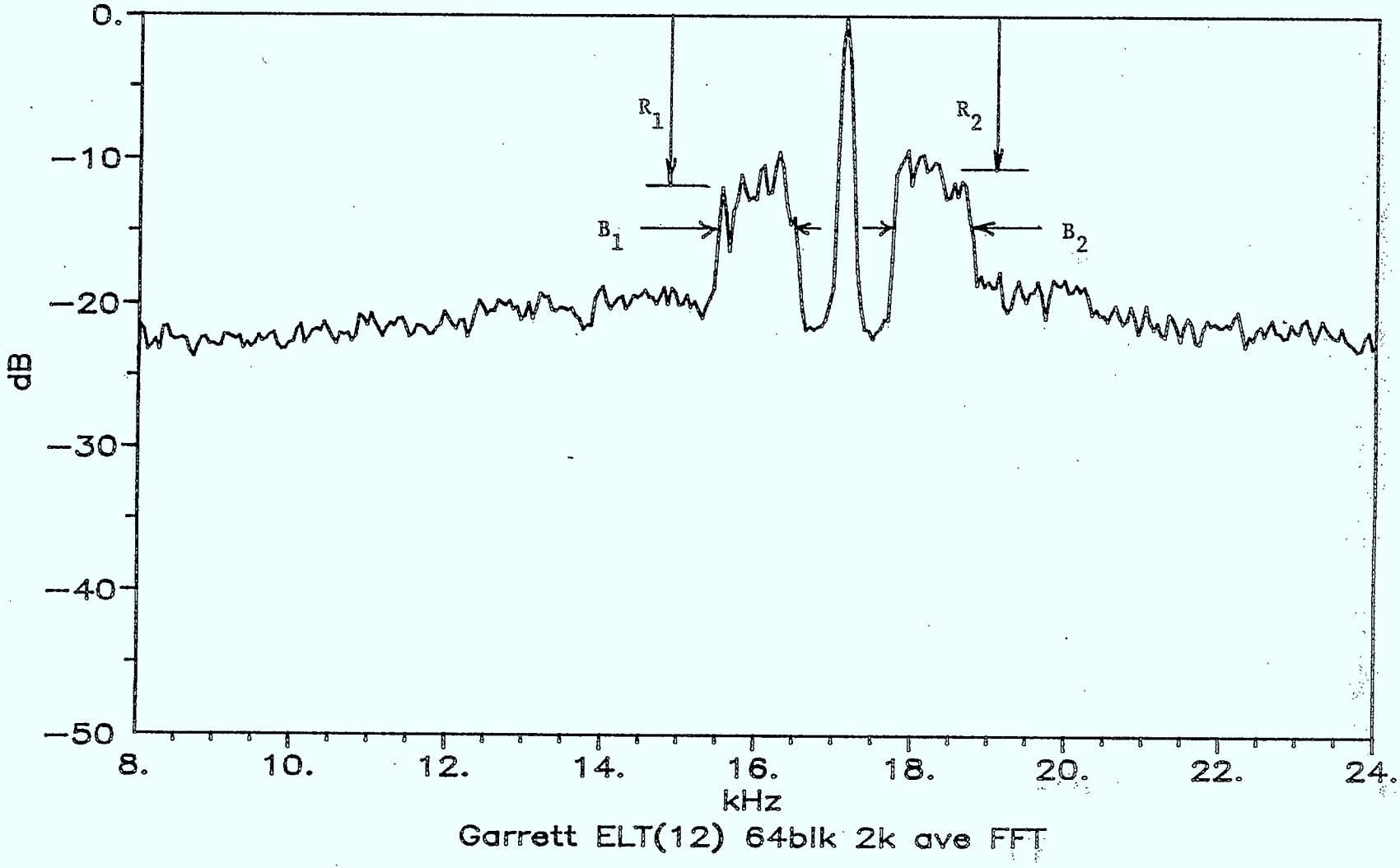

Fig. 4.21 Averaged spectrum for Garrett ELT illustrating B_1, B_2, R_1 and R_2 measures.

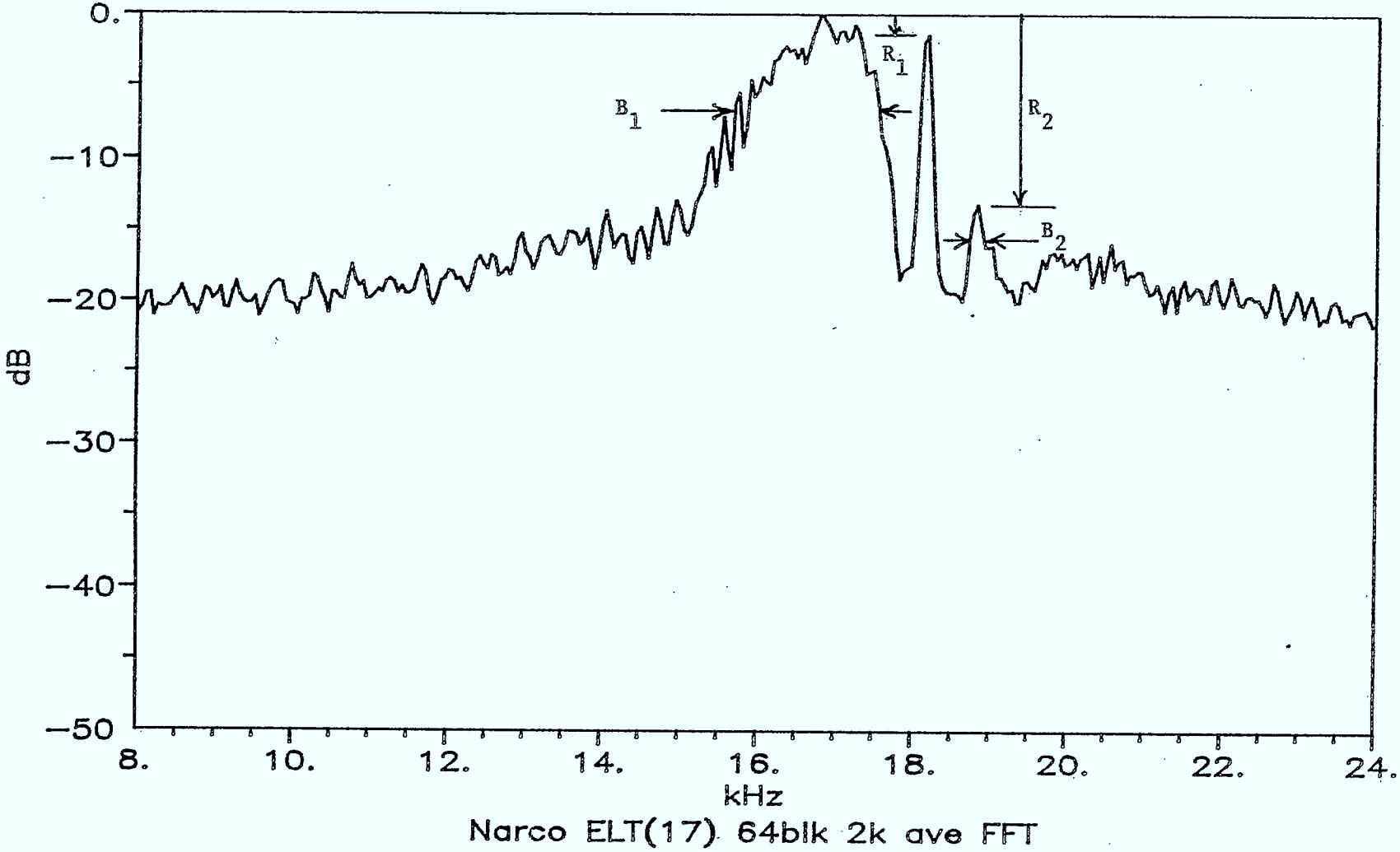

Fig. 4.22 Averaged spectrum for Narco ELT illustrating B_1, B_2, R_1 and R_2 measures.

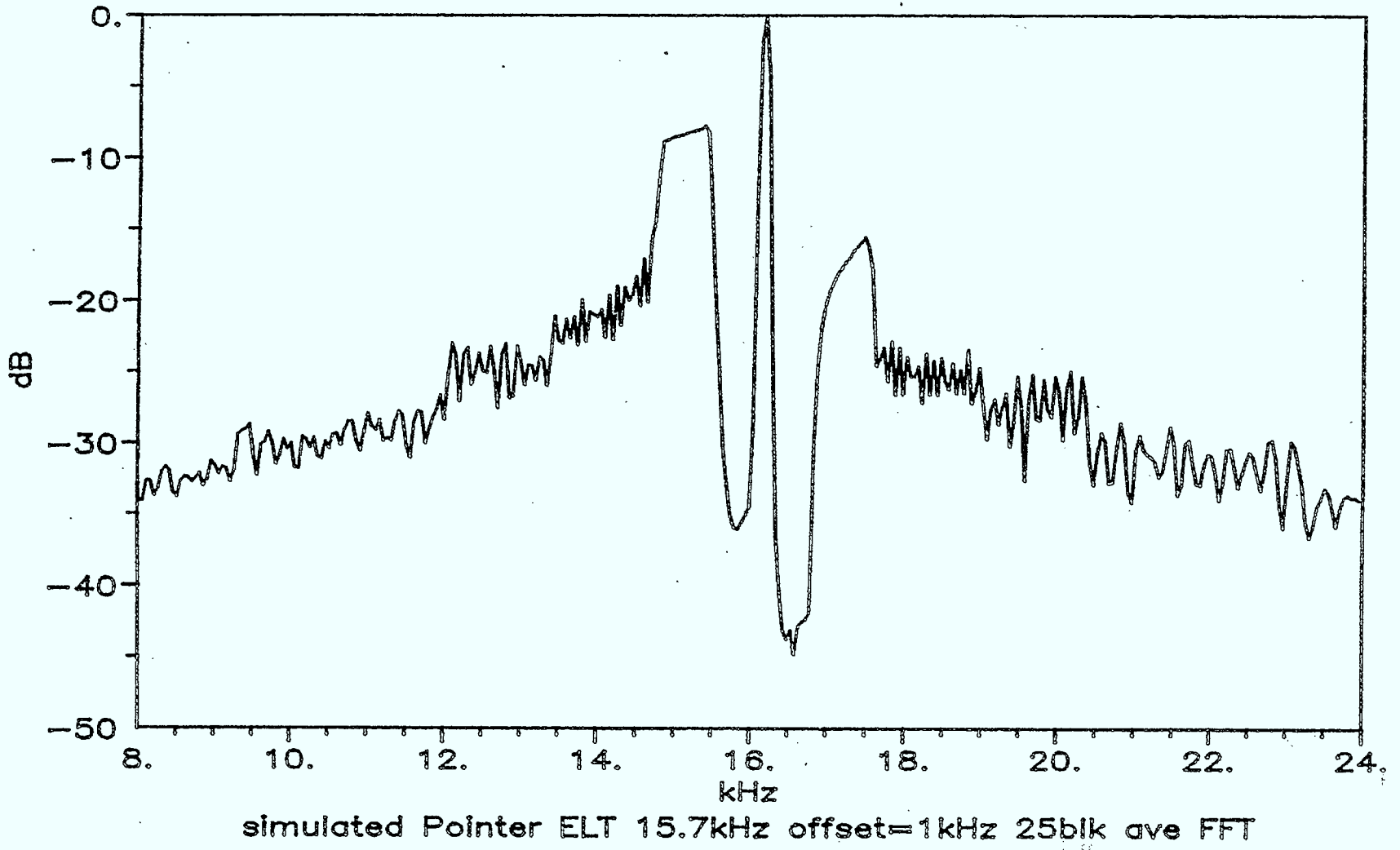

Fig. 4.23 Averaged spectrum for Pointer Model.

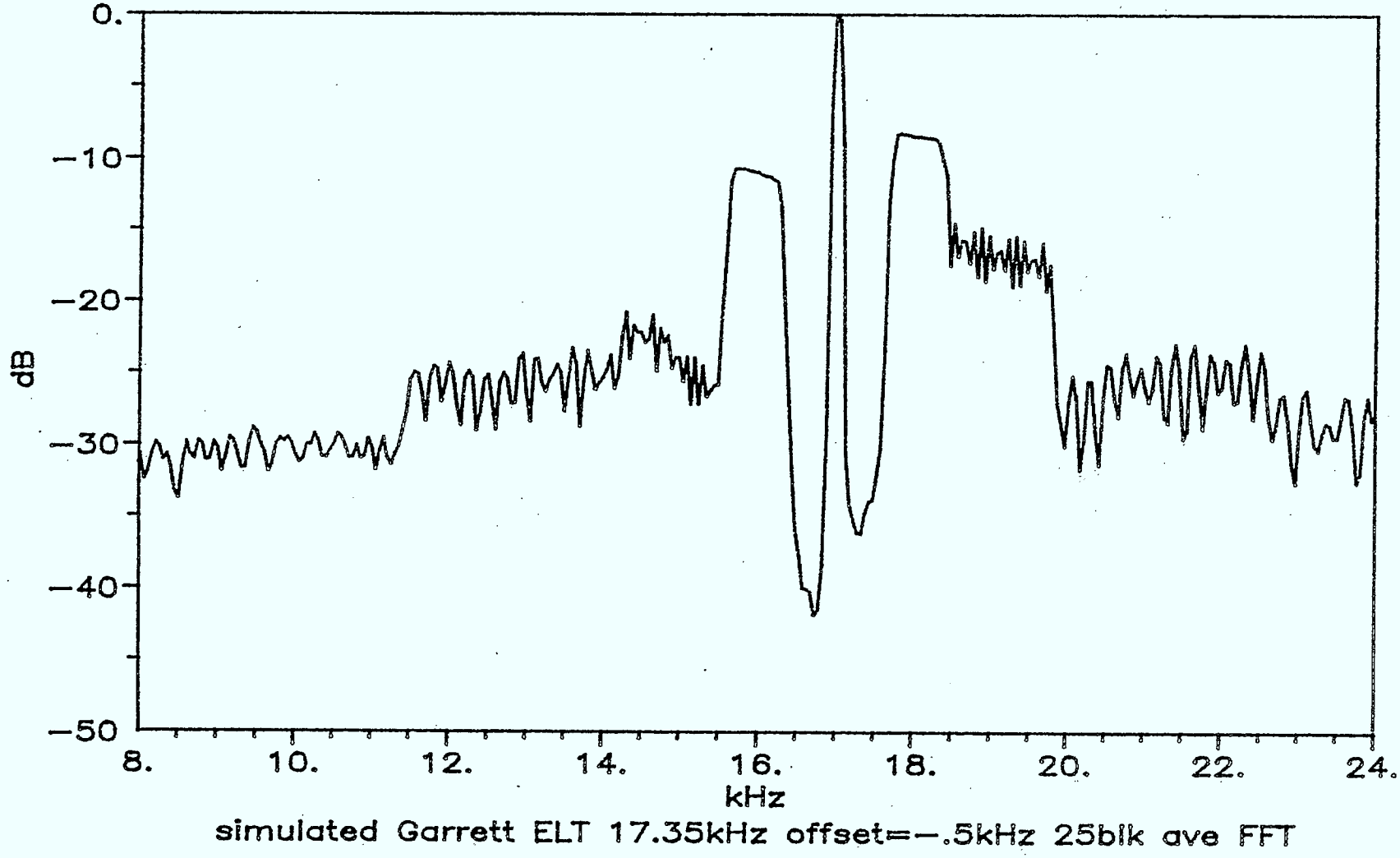

Fig. 4.24 Averaged spectrum for Garrett Model.

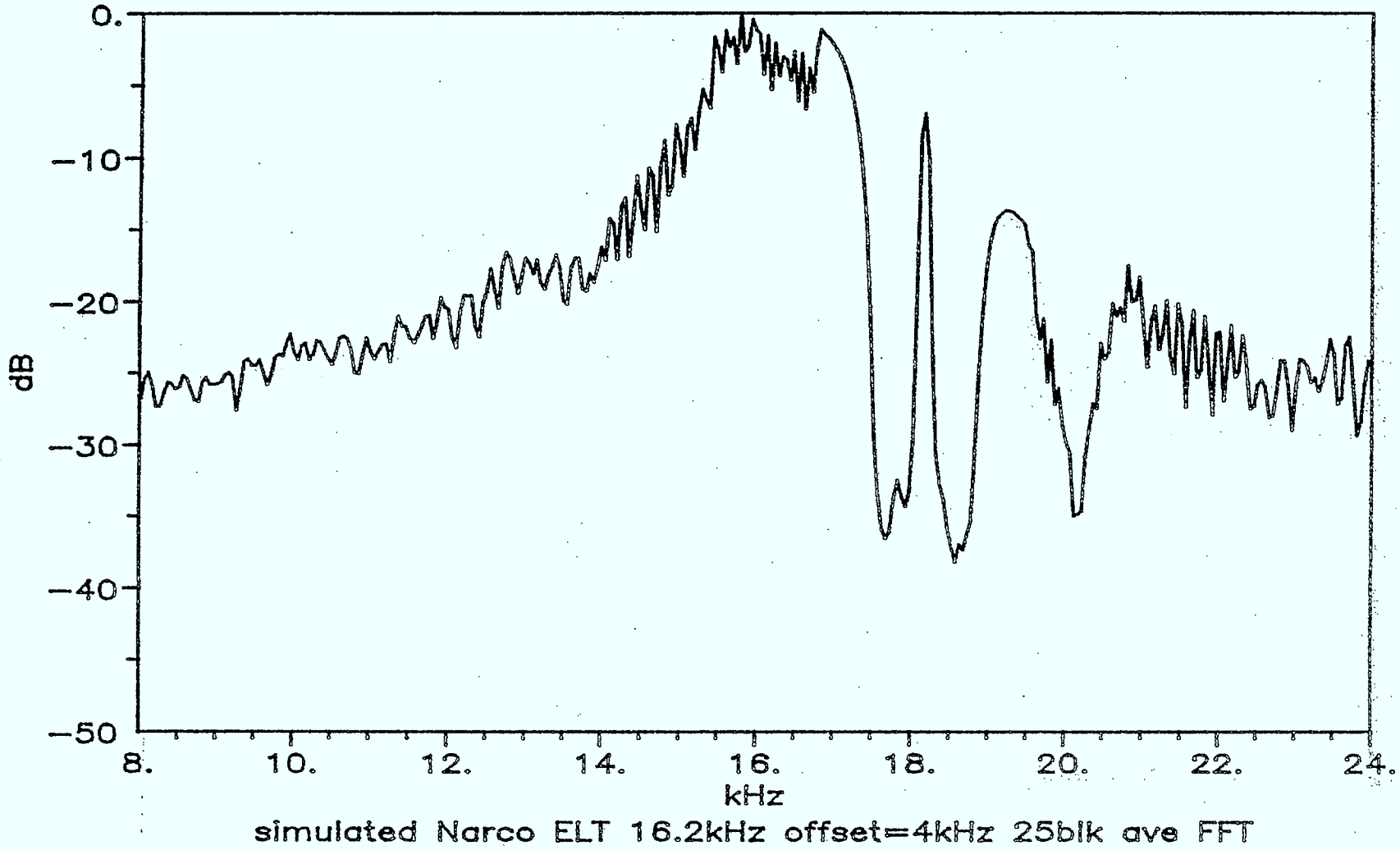

Fig. 4.25 Averaged spectrum for Narco Model.

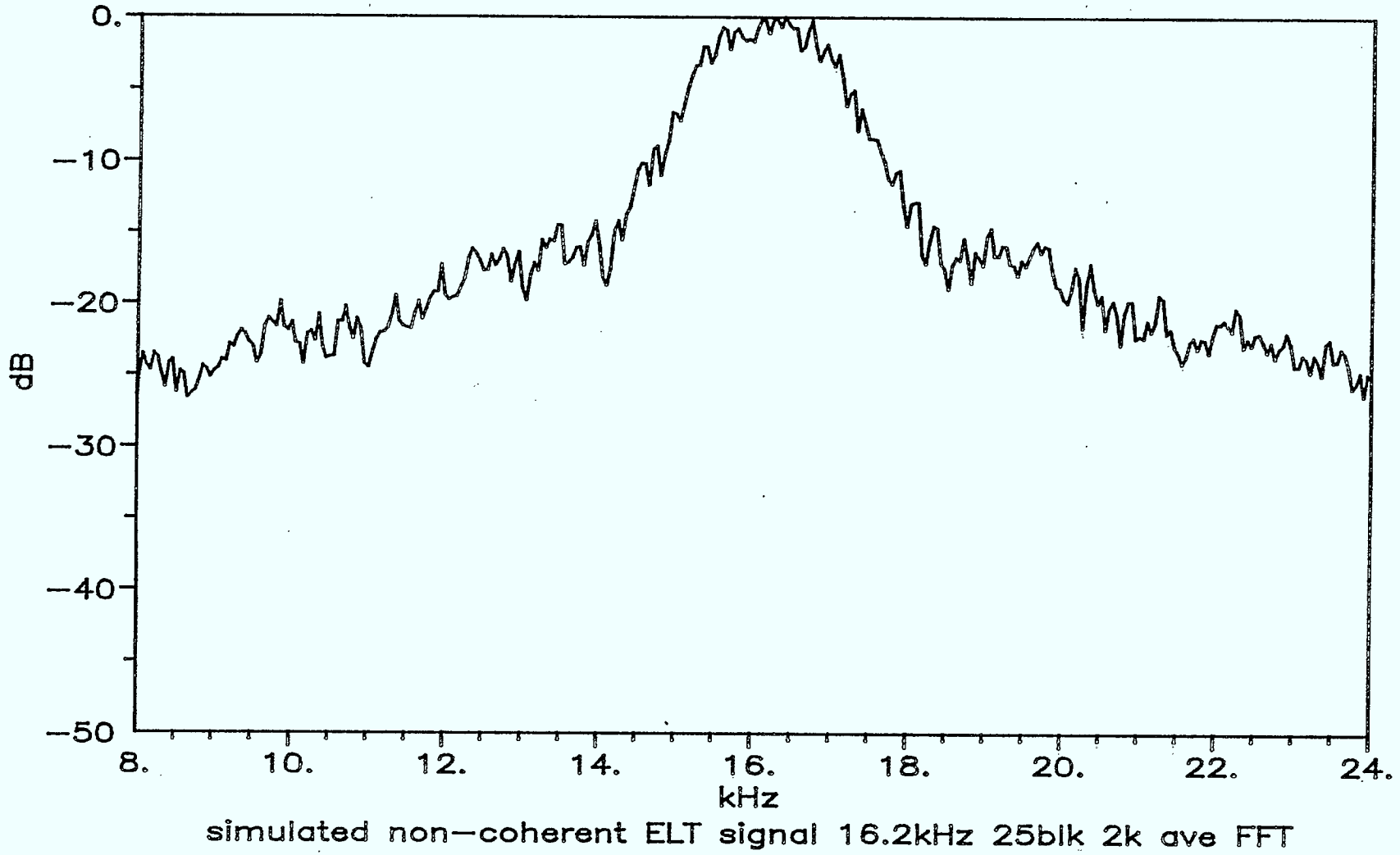

Fig. 4.26 Averaged spectrum for non-coherent ELT signal.

Fig. 4.27a. Then, a frequency band is selected around the carrier peak and the individual spectra (called the main set) comprising the averaged spectra in this frequency band are gated to a correlator, as shown in Fig. 27b. The correlator selects the first N records of individual spectra and performs a time correlation with the entire record. Wherever the N-record set matches the main set, a peak is produced at the output of the correlator. Otherwise, destructive interference occurs in the correlation and the output of the correlator is reduced.

The method has been tested by Mrs. S. El-Naga using the real data set from the Pointer, Garrett and Narco ELT units and the results are presented in Fig. 4.28 to 4.30. We see that the trace starts with sharp peak produced by the autocorrelation followed by other peaks with separation T, indicating a reasonably good cross-correlation response. Of considerable importance is the fact that the resulting signal does not rely on the quality of the ELT signal, but rather only that the signal is repetitive. Thus, the method provides a very effective means of detecting a modulated signal.

4.9 ELT IDENTIFIERS

It is now possible to select a set of signal identifiers for ELT signals. The first problem to be solved is the detection of a possibe ELT signal. By computing the averaged FFT, signal spectrum peaks will be produced for ELT signals having coherent spectra. (Little can be done for ELT units with non-coherent spectra if the FFT based spectral estimator is employed.) The frequencies of these peaks can easily be identified. Thus, detailed signal analysis can then be performed.

The most useful feature in detecting an ELT signal is the modulation. This is best determined using two measures; namely the Averaged Sideband Detection and the Correlated Sweep Detection. The first measure gives details of the relative levels of the two principal sidebands relative to the peak (R_1 and R_2) and the lower and upper sweep bandwidths (B_1 and B_2). The Correlated Sweep Detector gives the sweep duration (T).

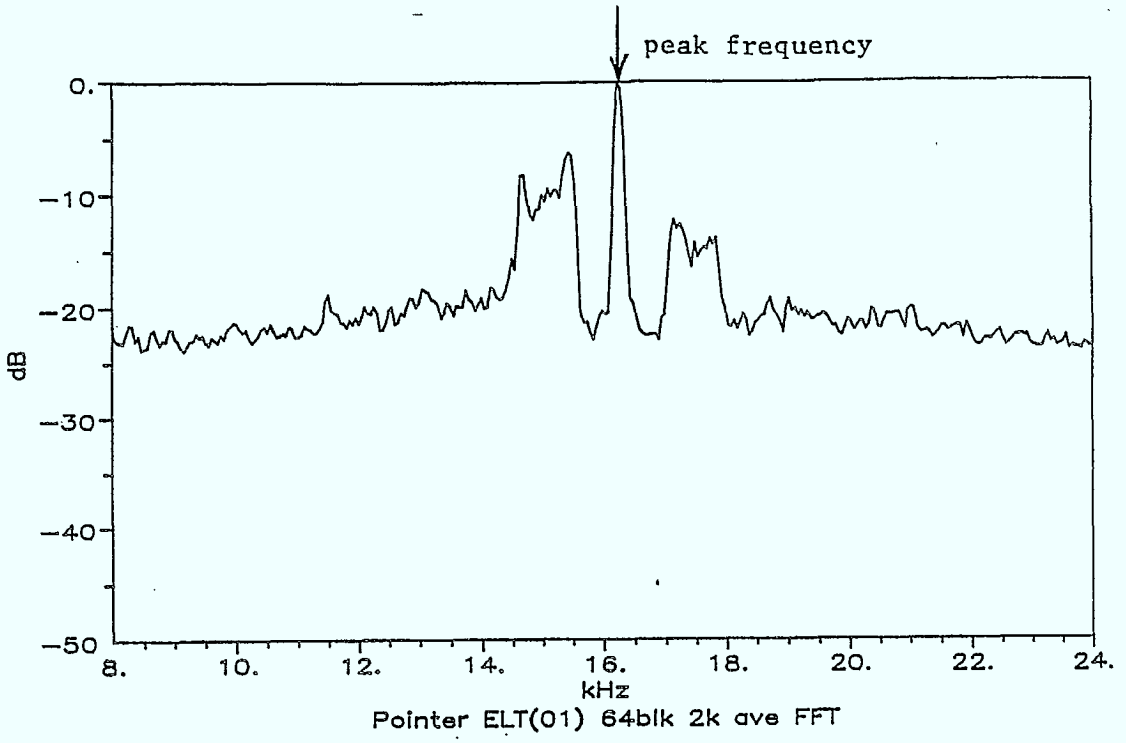

(a)

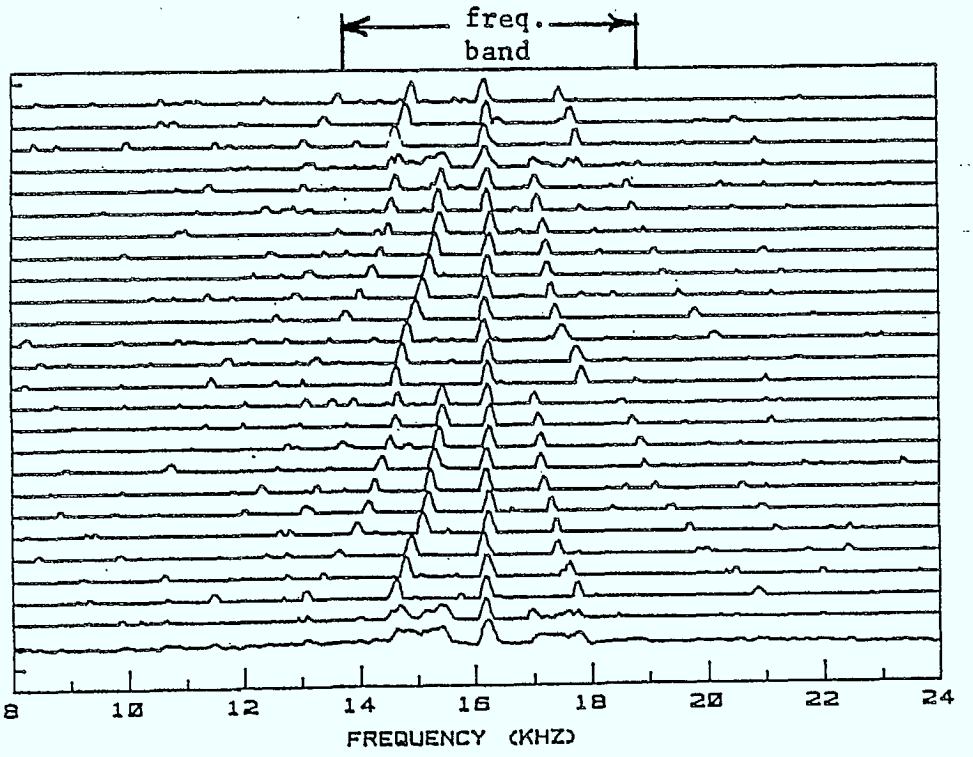

(b)

Fig. 4.27 (a) Locating the peak of averaged spectrum.
(b) Selecting the frequency band for the sweep measurement.

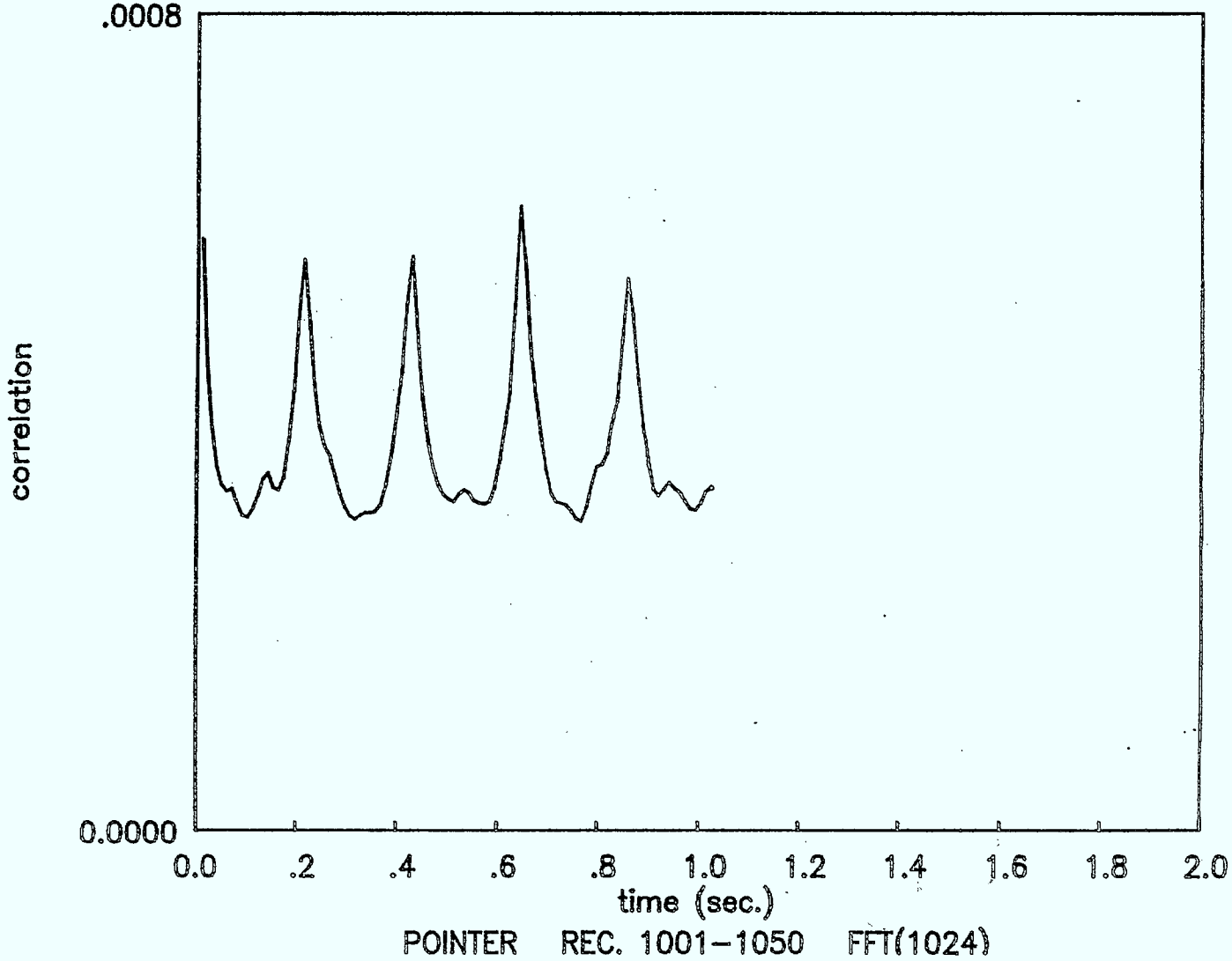

Fig. 4.28 Sweep duration for the Pointer ELT indicating T = 210 ms.
Compare with Fig. 4.9.

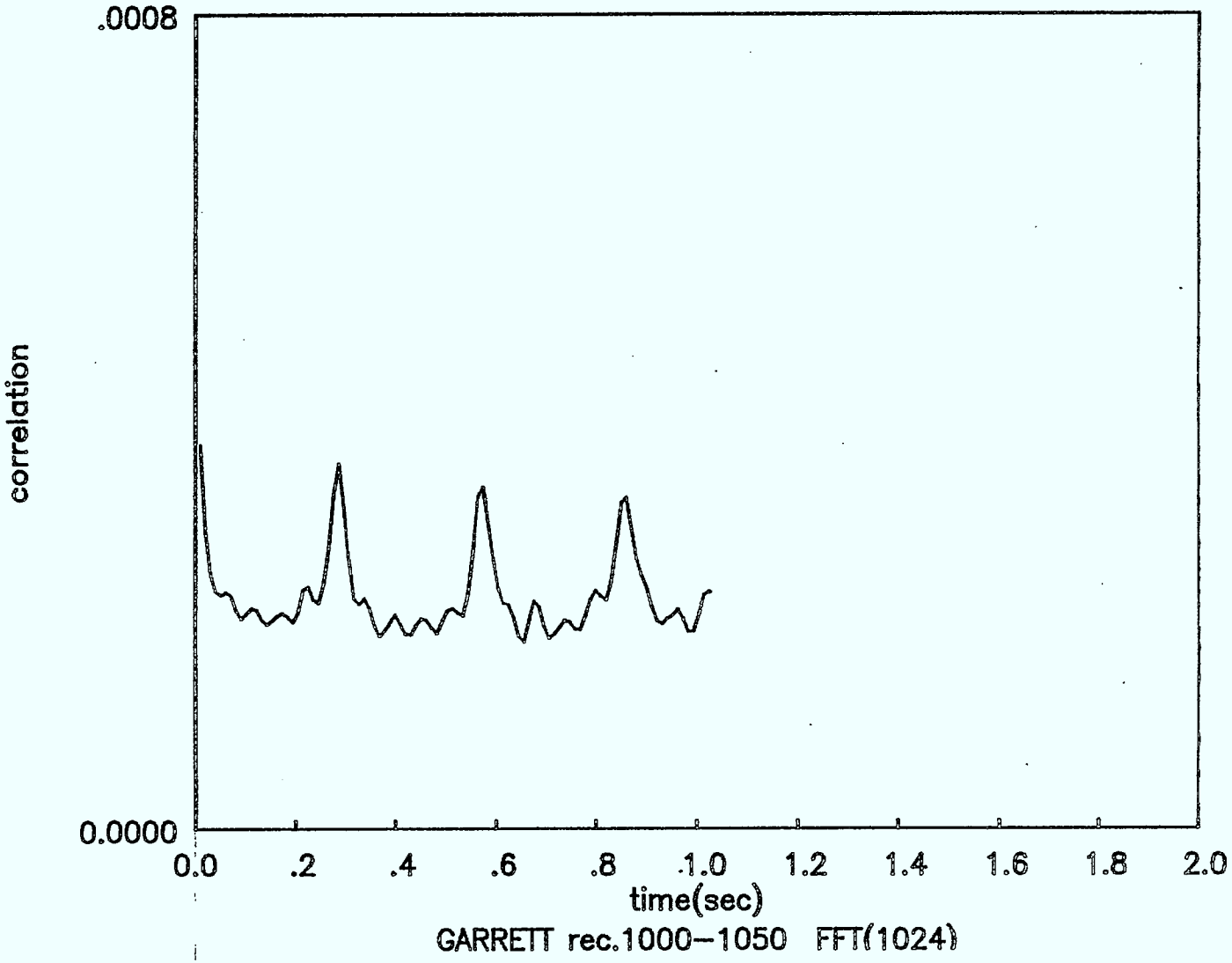

Fig. 4.29 Sweep duration for the Garrett ELT indicating T = 280 ms.
Compare with Fig. 4.11.

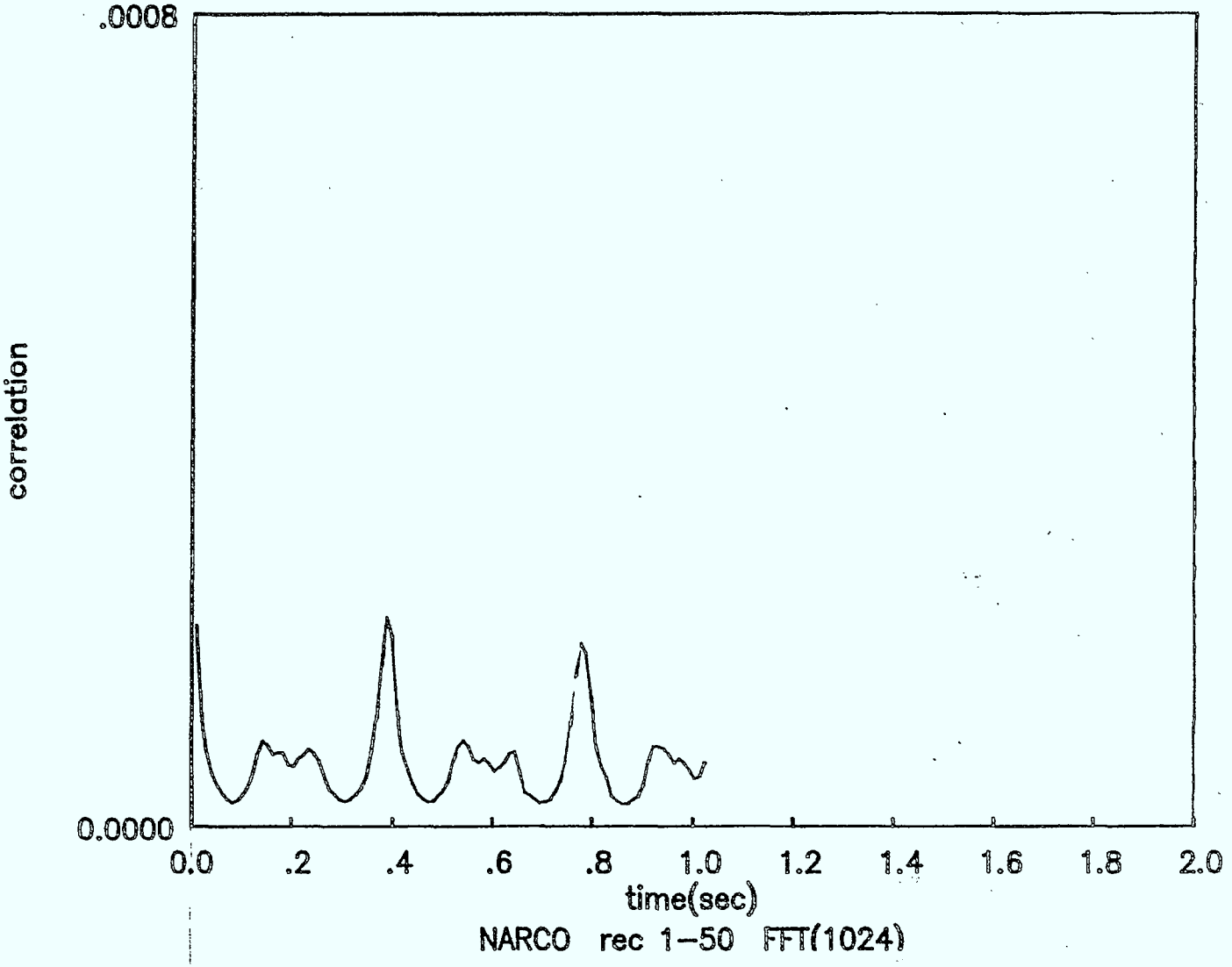

Fig. 4.30 Sweep duration for the NARCO ELT indicating T = 390 ms. Compare with Fig. 4.13.

In addition, it is possible to measure the frequency of the carrier peak (f), the combination of change in doppler shift and drift in carrier frequency with time f_d'' and the bandwidth of the carrier peak. With these three quantities, the ELT signal bandwidth (B_T) can be calculated which is useful for identifying any signal. Since the carrier frequency may be measured along the doppler curve, the ELT carrier frequency (F_E) can be deduced.

Due to the use of automatic gain control, it is not particularly easy to obtain an accurate measure of ELT signal strength especially in the presence of interference.

Hence, an ELT signal may be labelled in the following manner:

$$\text{ELT}\{f,t; f_d'', B_T, F_E; R_1, R_2, B_1, B_2, T\}$$

where

f = carrier peak value at time t

f_d'' = sum of change in doppler shift and carrier drift

B_T = ELT signal bandwidth

F_E = ELT carrier frequency

R_1 = height of lower sideband relative to carrier peak

R_2 = height of upper sideband relative to carrier peak

B_1 = sweep bandwidth of lower sideband

B_2 = sweep bandwidth of upper sideband

T = sweep period

There is also the possibility that a carrier peak could be correlated with the spectrum produced by the ELT model. In this case, an estimate of the parameters which relate directly to the model could be computed. Whether this technique is, in fact, feasible in the practical case has not been determined.

4.10 CONCLUDING REMARKS

In this section, a detailed study of ELT spectra has been presented. The analysis covers a wide range of different possible ELT signals and it is shown that the models developed accurately represent real ELT signals.

A set of parameters has been selected which can be used to characterise these ELT signals. The main feature of the parameter set is the ease with which they are measured in the noisy background.

5. DATA MANAGEMENT TECHNIQUES

There are two different requirements for the data management of ELT signals. First, is the problem of managing ELT signals received during a satellite pass referred to here as intrapass data management. The second requirement is the problem of managing ELT signals which result from the processing of different passes of the same satellite or passes of different satellites, referred to here as interpass data management.

5.1 INTRAPASS DATA MANAGEMENT

Intrapass data management is characterized by the following properties:

1) The ELT signal data will most likely be immersed in a background of interference from man-made sources. Thus, it is desirable to evaluate the influences of the interference.

2). The data are collected over a period of not more than approximately 900 s. As a result, changes in the characteristics of transmitted ELT signals received at the satellite should be relatively small. However, there may be significant changes in the interfering background.

3). The ELT signal data may not form a continuous doppler curve; thus, it is desirable to be able to relate the different segments of the data to a given ELT.

One particular approach to processing the pass data could be based on the following procedure:

A. Evaluate the Pass

The evaluation of the pass is based on the activity measure, discussed in Section 3. The activity measure can be evaluated by calculation:

1. Threshold Based Activity Measure

Using the averaged spectrum (computed once per second), set one or more fixed threshold levels and count the number of times the threshold is exceeded as compared to receiver noise alone. This results in a false alarm rate measure and is the simplest method for

determining interference level. In addition, the overhead is usually low for the implementation.

2. Spectrum Based Activity Measure

As the averaged FFT estimates are being computed, calculate the 'a' and 'v' values as a function of time along the pass. Thus, each averaged FFT data set now comprises the spectrum values and a two number set which evaluates the set. After the pass, the 'a' and 'v' values can be sorted in a-v space and analysed using cluster analysis to determine the characteristics of the resulting pattern. Note that it is also possible to compute 'a' and 'v' values along the pass for fixed values of frequency.

3. Envelope Detected Activity Measure

The output of an envelope detector is monitored and data points are stored at a rate of perhaps 1024 per second. The arithmetic sum of these points gives the strength e. For the bandwidth of the interference b, the FFT is performed on these data. (Since the FFT is already being called 100 times per second for spectral estimation, the overhead required for this technique is only about 1-2%). Thus, interference activity is now available in e-b space and the analysis can again proceed using cluster analysis.

B. Identify the ELT Signals

We note that in order to provide indentification of ELT signals, it is necessary to access both the averaged spectrum and the individual FFT estimates. However, since we assume that ELT signals are nearly always present for long durations (at least 10 s), it is necessary to process only once every 5 s which reduces the overhead by a factor of five. Thus, the following procedure can be employed:

1. For a 1 s segment of data, compute the 100 FFT estimates and the averaged spectrum and store all results.

2. Using the averaged spectrum, locate all the prominent peaks which may represent coherent ELT signals.

3. For each peak (in turn), compute the correlated sweep duration T using the individually stored FFT estimates and determine whether the T value lies in the proper range.

4. For each peak (in turn), evaluate the relative levels of the upper and lower sidebands relative to the peak (R1 and R2) and determine whether these values fall in the acceptable range (taking the background noise level into account). If the values fall into the proper range, compute the sweep bandwidths B1 and B2.

5. Repeat steps 1 to 4 at intervals of 5 s for the whole pass. Thus, there now exists a data base of up to 900/5 = 180 sets of values of possible ELT sources at times t_1,t_2, t_3, etc. At each time, a set consists of peaks at frequencies f_1, f_2, f_3, etc. with parameters R_1, R_2, B_1, B_2 and T. For example at time t_2, we have:

Signal at time t_2 and frequency f_1: $S\{t_2, f_1; R_1, R_2, B_1, B_2, T\}$

Signal at time t_2 and frequency f_2: $S\{t_2, f_2; R_1, R_2, B_1, B_2, T\}$

Signal at time t_2 and frequency f_3; $S\{t_2, f_3; R_1, R_2, B_1, B_2, T\}$ etc.

Note that these signal peaks are not necessarily ELT signals, but only possible candidates for being ELT signals.

6. After template matching has identified those portions of the curves which produce acceptable pass curves, call the data base of signal peaks using the values of time and frequency, eg. t_2 and f_3. This procedure would then test the various curves or segments of the curves to determine the properties of the signals using the methods outlined in steps 1 through 4. Complete curves, would then produce a label indicating the different parameters and the values of B_T (ELT signal bandwidth) and F_E (ELT carrier frequency).

For incomplete curves, the value of B_T could be calculated and the different segments could be matched to detemine whether they have the same parameter set. In some cases, this would also result in complete curves or parts where the value for F_E could be estimated.

7. Thus, at the end of the process, there would be a set of identified ELT signals, each with specific values for (B_T, F_E, R_1, R_2, B_1, B_2, T) which could be averaged over the doppler curve to improve accuracy.

8. Using the doppler data, the location of the ELT signal is established as one of two possible locations L_1 or L_2.

9. An additional parameter can be added to each member of the set to indicate the activity of the pass. This is important since a pass with high activity (interference) may contain a larger number of false ELT signal estimates. This parameter is referred to as I and could range from 0 to 7 as in Fig. 3.10.

10. Finally, the pass number and satellite (P/S) should be recorded in order to give an approximate time at which the ELT signal first appeared. This is useful for interpass data management. Thus, for every satellite pass, there is a set of ELT parameters produced with an averaged set of computed values and two possible locations, i.e. we have:

ELT1{P/S; B_T, F_e; R_1, R_2, B_1, B_2, T; I; L_1/L_2},

ELT2{P/S; B_T, F_E; R_1, R_2, B_2, T; I; L_1/L_2} etc.

These data would then be processed by the interpass data management procedure.

5.2 INTERPASS DATA MANAGEMENT

Interpass data management is characterised by the following properties:

1) Possible ELT locations accumulate as satellite passes continue.

2). The two different possible locations for each ELT results in a certain number of false indications. Consequently, there is a need for a consolidation process in order to minimize the data set.

3) For a given ELT location, the geometry between the ELT and the satellite has an effect on the calculation of the ELT parameters. Thus, it is possible to provide a measure based on relative loaction which would grade the location calculation.

One possible approach could be based on the following procedure:

1) Since there are many different possible locations, it appears quite likely that the data sets will cluster on either L_1 or L_2 loactions for ELT signals which are received on multiple passes.

2) Using the additional parameters available for ELT identification and the pass geometry, it appears that a 'best location' estimate could be devised to combine the data at the L_1 or L_2 locations and dispose of erroneous data.

3) As the data age, a time limit should be applied to delete all entries which exceed a certain limit. This would be based on the P/S parameters.

4) Known false indications should be removed from the data set as soon as possible.

6. CONCLUSIONS AND RECOMMENDATIONS FOR FURTHER RESEARCH

6.1 CONCLUSIONS

We conclude the following:

1) There is a significant number of interfering sources which affect the frequency bands of 121.5/243 MHz. These sources are mainly man-made and appear in the forms of impulsive interference and in-band interference. The former produces shock excitation of the receiver which effectively jams the reception of desired signals. The latter produces a competing background which may or may not mask the ELT signals.

2) It is possible to develop a set of parameters which can evaluate the amount of noise and interference in any satellite pass. These parameters can be based on a simple threshold test, or more advanced processes based on spectrum or envelope detection.

3) ELT signals have distinctive characteristics which can be evaluated by means of spectral estimation techniques and correlation. These parameters provide a signature which separates the individual ELT units in a single pass and may even provide some indication of ELT unit manufacture (especially if the unit has a peculiar characteristic).

4) It is possible to use the characteristics of interference background and ELT signal parameters to provide data management within a satellite pass (intrapass) and between satellite passes (interpass). The intrapass data management is capable of labelling complete pass curves and connecting segments of related pass curves. The interpass data management is capable of controlling the large amount of data collected by consolidating data using identified parameters.

6.2 RECOMMENDATIONS FOR FURTHER RESEARCH

Based on the findings outlined in this report, we recommend the following:

1) A study be made of the properties of interference in the real environment. At present, a tape containing 34 satellite passes is available. It is suggested that some of the more interesting interfering sources be examined to determine their properties.

2) The methods of evaluation as applied to activity of the pass be tested using real data in order to determine their effectiveness and relative complexity of implementation.

3) The methods outlined in section 4 for the identification of real ELT signals be tested using satellite pass data.

4) The data management techniques outlined in Section 5 for intrapass data management and interpass data management be tested using real data.

6.3 ACKNOWLEDGEMENT

The authors would like to thank the SARSAT Group at Communications Research Centre, Ottawa, for many useful suggestions and discussions. Also, we thank the DND for allowing use of the dot charts of satellite pass data.

REFERENCES

[1] E.N. Skomal: "Man-made Radio Noise", Van Nostrand Reinholt Publ. Co. (1978), New York.

[2] W.R. Vincent: "Examples of Signals and Noise in the Radio-Frequency Spectrum', IEEE Trans. on Electromagnetic Compatibility, vol. EMC-19, no. 3, August 1977, pp. 241-253.

[3] J.H. Herman: "The Radio Noise Environment in Near Space: A Review", IEEE International Symposium on Electromagnetic Compatibility, (Atlanta, GA, June 20-22, 1978), pp. 339-346.

[4] R.E. Taylor and J.S. Hill: "Aircraft measurement of radio frequency noise at 121.5 Hz, 243 MHz and 406 MHz", IEEE International Symposium on Electromagnetic Compatibility, (Montreux, Switzerland, June 28-30, 1977), pp. 353-356.

[5] R.E. Taylor and J.S. Hill: "Airborne Surveys of USA Urban Areas at 121.5/243 MHz", IEEE International Symposium on Electromagnetic Compatibility, (San Diego, CA, Oct. 9-11, 1979), pp. 245-251.

[6] R.E. Taylor and J.S. Hill: "Airborne Census Taker Using VHF Radio-Noise Techniques", IEEE International Symposium on Electromagnetic Compatibility, (Boulder, CO, August 18-20, 1981), pp. 521-524.

[7] R.E. Taylor and J.S. Hill: "Airborne Urban/Suburban Noise Measurements at 121.5/243 MHz", IEEE International Symposium on Electromagnetic Compatibility", (Seattle, WA, August 2-4, 1977), pp. 242-248.

[8] E.N. Skomal: "Analysis of Spaceborne VHF Incidental Noise Over the Western Hemisphere". IEEE International Symposium on Electromagnetic Compatibility, vol. EMC-25, n. 3, August 1983, pp. 321-328.

[9] R.M. Smith: "The Extent and Nature of Television Reception Difficulties Associated with CB Radio Transmissions", IEEE Trans. on Consumer Electronics, vol. CE-24, no. 1, Feb. 1978, pp. 6-15.

[10] R.M. Beeman: "Citizens Band Expansion and the Consumer Environment", IEEE Trans. on Consumer Electronics, vol. CE-24, no. 1, Feb. 1978, pp. 16- 23.

[11] W.L. Hand: "Personal Use Radio (CB) and its Effects on TV Reception", IEEE Trans. on Consumer Electronics, Feb. 1977, pp. 78-91.

[12] A.C.D. Whitehouse: "The Interference Effects of Citizens Band Radio", IERE Electromagnetic Compatibility, (University of Surrey, England, Sept. 21-23, 1982), pub. no. 56, pp. 9-22.

[13] Advertisement in Communications (USA), Feb. 1981, p. 46.

[14] Reference Data for Radio Engineers, Sixth Edition, Howard Sams (1975), Indianapolis, pp. 1-4 to 1-7 and 30-10.

[15] L. McCoy: "TVI – Here We Go Again", CQ, Oct. 1982, pp. 60-68.

[16] R.V.C. Dickinson: "CATV – A Multifacetted Problem", Second Annual Conference on CATV Reliability (Atlanta, GA, Feb. 23-24, 1977), pp. 50-56.

[17] W. Welsh: "Cable Television Interference, Part I of II", CQ, March 1984, pp. 86-88.

[18] R.A. Shepherd and J.C. Gaddie: "Ignition Noise of Foreign and Domestic Vehicles in Use in the United States", 1979 IEEE International Symposium on Electromagnetic Compatibility, (Oct. 9-11, 1979), pp. 232-238.

[19] M. Brain and A.N. Kent: "Characterization of Impulsive VHF Radio Interference in Motor Vehicles", Conference on Electromagnetic Compatibility (London, England, April 4-7, 1978), pp. 261-269.

[20] R.A. Shepherd, J.W. Engles and G.H. Hagn: "Automobile Ignition Noise and the Supernoisy Vehicle", IEEE International Symposium on Electromagnetic Compatibility" (Washington, DC, July 13-15, 1976), pp. 403-412.

[21] C. Egidi, P.G. Galliano and E. Nano: "R.F. Emission from Motor Vehicles - Review of Results", Alta Frequenza, vol. 49, no. 1, April 1980, pp. 179-185.

[22] D.E. Baran: "Prediction of Relative Available Noise Power for Vehicular Ignition Noise", IEEE International Symposium on Electromagnetic Compatibility, (Atlanta, GA, June 20-22, 1978), pp. 358-364.

[23] R.M. Morris, A.R. Morse, J.B. Griffin, O.C. Norris-Elye, C.V. Thio and J.S. Goodman: "The Corona and Radio Interference Performance of the Nelson River HVDC Transmission Lines", IEEE Trans. on Power Apparatus and Systems, vol. PAS-98, no. 6, Nov./Dec. 1979, pp. 1924-1932.

[24] P.S. Maruvada, R.D. Dallaire, O.C. Norris-Elye, C.V. Thio and J.S. Goodman: "Environmental Effects of the Nelson River HVDC Transmission Lines - RI, AN, Electric Field Induced Voltage, and Ion Current Distribution Tests", IEEE Trans. on Power Apparatus and Systems, vol. PAS-101, no. 4, April 1982, pp. 951-959.

[25] A.R. Morse: "Field Measurements of Station-Generated RI on the Nelson River HVDC Line in 1976", International Electrical, Electronics Conference and Exposition (Toronto, Sept. 26-28, 1977), pp. 78-79.

[26] M. Fukushima, Y. Sunaga, T. Sasano and Y. Sawada: "AN, RI and TVI from Single Unit Flashover of HVDC Suspension Insulator Strings", IEEE Trans. on Power and Systems, vol. PAS-96, no. 4, July/August 1977, pp. 1233-1241.

[27] E.R. Schroeder and R.V. DeVore: "Radio Interference on DC Lines from HVDC Converter Stations", IEE Proc., vol. 129, Part C, no. 5, Sept. 1982, pp. 221-227.

[28] D.M. LeVine: "The Spectrum of Radiation from Lightning", IEEE International Symposium on Electromagnetic Compatibility (Baltimore, MD, Oct. 7-9, 1980), pp. 249-253.

[29] J. Rai: "On the Origin of UHF Atmospherics", Journal of Atmospheric and Terrestrial Physics", vol. 40, 1978, pp. 475-478.

[30] S.V.C. Aiya: "Atmospheric Noise Data for Tropical Regions", Radio Science, vol. 14, no. 6, Nov.-Dec. 1979, pp. 1001-1010.

[31] E.K. Smith: "A Natural Radio Noise Source Environment", IEEE International Symposium on Electromagnetic Compatibility (Santa Clara, CA, Sept. 8-10, 1982), pp. 266-277.

[32] R.K. Crane: "Ionospheric Scintillation", Proc. IEEE, vol. 65, no. 2, Feb. 1977, pp. 180-199.

[33] R.G. Rastogi, M.R. Deshpande, H.O. Vats, K. Davies, R.N. Grubb and J.E. Jones: "Amplitude Scintillations of ATS-6 Radio Beacon Signals Within the Equatorial Electrojet Region (Ootacamund, dip 4°N)", Pramana, vol. 8, n. 1, 1977, pp. 1-13.

[34] G.F. Lyon: "Ionospheric Effects on the SARSAT System", Canadian Aeronautics and Space Journal, vol. 27, no. 4, Dec. 1981, pp. 327-335.

[35] R.K. Profitt: "Microcomputers and RF Interference", Australian Journal of Instrumentation and Control, Feb. 1983, pp. 18-19.

[36] R.R. Goulette and S.K. Xavier: "Control of Electromagnetic Emissions in Digital Circuits", IEEE International Symposium on Circuits and Systems (Newport Beach, CA, May 2-4, 1983), pp. 958-961.

[37] M. Mardiguian and D. White: "Prediction of EMI Radiation from PCBs", RF Design (USA), July-August 1983, pp. 26-36.

[38] R. Colley: "Industrial Process Heating Equipment – Its Environmental Effect in the Frequency Range from 100 KHz to 100 MHz", IERE Proceedings of the Conference on Electromagnetic Compatibility (Guildford, England, Apr. 4-7, 1982), pp. 175-182.

[39] H. Martin: "A Generalized Model of Man Made Electrical Noise", IEEE Symposium on Electromagnetic Compatibility (June 20-22, 1978, Atlanta, GA), pp. 347-357.

[40] I.S. Gradshteyn and I.M. Ryzhik: Table of Integrals, Series and Products, Academic Press (New York), 1965, p. 147.


ΤΑ ΠΑΝΤΑ ΕΝ ΧΡΙΣΤΩΙ ΣΥΝΕΣΤΗΚΕΝ